

University of Nebraska - Lincoln

DigitalCommons@University of Nebraska - Lincoln

Mechanical (and Materials) Engineering --
Dissertations, Theses, and Student Research

Mechanical & Materials Engineering, Department
of

Spring 4-21-2018

Modeling Residual Stress Development in Hybrid Processing by Additive Manufacturing and Laser Shock Peening

Guru Charan Reddy Madireddy

University of Nebraska - Lincoln, gmadireddy2@huskers.unl.edu

Follow this and additional works at: <https://digitalcommons.unl.edu/mechengdiss>



Part of the [Heat Transfer, Combustion Commons](#), [Manufacturing Commons](#), and the [Tribology Commons](#)

Madireddy, Guru Charan Reddy, "Modeling Residual Stress Development in Hybrid Processing by Additive Manufacturing and Laser Shock Peening" (2018). *Mechanical (and Materials) Engineering -- Dissertations, Theses, and Student Research*. 137.
<https://digitalcommons.unl.edu/mechengdiss/137>

This Article is brought to you for free and open access by the Mechanical & Materials Engineering, Department of at DigitalCommons@University of Nebraska - Lincoln. It has been accepted for inclusion in Mechanical (and Materials) Engineering -- Dissertations, Theses, and Student Research by an authorized administrator of DigitalCommons@University of Nebraska - Lincoln.

MODELING RESIDUAL STRESS DEVELOPMENT IN HYBRID PROCESSING BY
ADDITIVE MANUFACTURING AND LASER SHOCK PEENING

by

Guru Charan Reddy Madireddy

A THESIS

Presented to the Faculty of

The Graduate College at the University of Nebraska

In Partial Fulfillment of Requirements

For the Degree of Master of Science

Major: Mechanical Engineering and Applied Mechanics

Under the Supervision of Professor Michael P. Sealy

Lincoln, Nebraska

March, 2018

MODELING RESIDUAL STRESS DEVELOPMENT IN HYBRID PROCESSING BY
ADDITIVE MANUFACTURING AND LASER SHOCK PEENING

Guru Charan Reddy Madireddy, M.S.

University of Nebraska, 2018

Advisor: Michael P. Sealy

The term “hybrid” has been widely applied to many areas of manufacturing. Naturally, that term has found a home in additive manufacturing as well. Hybrid additive manufacturing or hybrid-AM has been used to describe multi-material printing, combined machines (*e.g.*, deposition printing and milling machine center), and combined processes (*e.g.*, printing and interlayer laser re-melting). The capabilities afforded by hybrid-AM are rewriting the design rules for materials and adding a new dimension in the design for additive manufacturing paradigm. This work focuses on hybrid-AM processes, which are defined as the use of additive manufacturing (AM) with one or more secondary processes or energy sources that are fully coupled and synergistically affect part quality, functionality, and/or process performance. Secondary processes and energy sources include subtractive and transformative manufacturing technologies, such as machining, re-melting, peening, rolling, and friction stir processing. Of particular interest to this research is combining additive manufacturing with laser shock peening (LSP) in a cyclic process chain to print 3D mechanical properties. Additive manufacturing of metals often results in parts with unfavorable mechanical properties. Laser shock peening is a high strain rate mechanical surface treatment that hammers a work piece and induces favorable mechanical properties. Peening strain hardens a surface and imparts compressive residual stresses improving the mechanical properties of material. The overarching objective of

this work is to investigate the role LSP has on layer-by-layer processing of 3D printed metals. As a first study in this field, this thesis primarily focuses on the following:

(1) defining hybrid-AM in relation to hybrid manufacturing and classifying hybrid-AM processes and (2) modeling hybrid-AM by LSP to understand the role of hybrid process parameters on temporal and spatial residual stress development. A finite element model was developed to help understand thermal and mechanical cancellation of residual stress when cyclically coupling printing and peening. Results indicate layer peening frequency is a critical process parameter and highly interdependent on the heat generated by the printing laser source. Optimum hybrid process conditions were found to exist that favorably enhance mechanical properties. With this demonstration, hybrid-AM has ushered in the next evolutionary step in additive manufacturing and has the potential to profoundly change the way high value metal goods are manufactured.

DEDICATION

Dedicated to my family.

LIST OF ABBREVIATIONS AND SYMBOLS

HM	Hybrid manufacturing
EDM	Electric discharge machining
AM	Additive manufacturing
Hybrid-AM	Hybrid additive manufacturing
DED	Directed energy deposition
PBF	Powder bed fusion
R_a	Surface roughness (arithmetic mean)
LENS	Laser engineered net shaping
CRS	Compressive residual stresses
UP	Ultrasonic peening
FPSP	Fine particle shot peening
PLD	Pulsed laser deposition
FSAM	Friction stir additive manufacturing
FSW	Friction stir welding
FSP	Friction stir processing
GPa	Gigapascal
MPa	Megapascal
σ_D	Fatigue limit (a.k.a. endurance limit)
N	Number of fatigue cycles
R	Corrosion rate
CPE4	4-node bilinear plane strain
JC	Johnson-Cook

T	Temperature
ISV	Internal state variable
$P(t)$	Magnitude of pressure at any time
r	Radial distance
R	Spot size
P_{\max}	Peak pressure
SRT	Short rise time
ns	Nano-second
mm	Millimeter
S11	Normal stress component in 1-direction
DLMD	Direct laser metal deposition
SMD	Shape metal deposition
Q	Heat flux
P	Laser power
DC2D4	4-node linear diffusive heat transfer
h_{1-3}	Convective heat transfer coefficients
ϵ	Radiation heat transfer coefficient
SLS	Selective laser sintering
EBM	Electron beam melting
U	Displacement
NT11	Nodal temperatures
SA	Stress analysis
HT	Heat transfer analysis
L1-20	Layers 1 to 20

ACKNOWLEDGEMENTS

I would like to convey my gratitude to my advisor, Michael Sealy, for giving me the opportunity to work with him. I thank him for his support, guidance, and teachings at every step of my research that helped me move forward with the research. I would also like to thank Chao Li who helped me learn Abaqus software and answering the questions and doubts I had during the initial stages of my research. I thank Dr. Ryan Pedrigi and his graduate student Caleb Berggren for helping me on how to use the supercomputer on campus for Abaqus simulations. I thank the staff at Holland Computing Center for their facilities and their help during the Abaqus setup process.

I would like to use this opportunity to thank Dr. Kamlakar Rajurkar and Dr. Joseph Turner for being a part of my committee and for their valuable feedback. Finally, I would like to thank my lab mates who have given their inputs during the course of this research and my friends in Lincoln for their continuous care and support.

CONTENTS

DEDICATION	iv
LIST OF ABBREVIATIONS AND SYMBOLS	v
ACKNOWLEDGEMENTS	vii
LIST OF TABLES	xi
LIST OF FIGURES	xii
PREFACE	xv
1. HYBRID PROCESSES IN ADDITIVE MANUFACTURING.....	1
1.1 Introduction	1
1.2 Hybrid Manufacturing.....	2
1.3 Hybrid Manufacturing Processes	4
1.4 Hybrid Additive Manufacturing (Hybrid-AM) Processes.....	5
1.4.1 Fully coupled processes.....	6
1.4.2 Synergy.....	6
1.4.3 Part and/or process improvement	7
1.5 Classification of Hybrid-AM processes	8
1.5.1 Hybrid-AM by machining	9
1.5.2 Hybrid-AM by ablation or erosion.....	11
1.5.3 Hybrid-AM by re-melting	12
1.5.4 Hybrid-AM by laser assisted plasma deposition.....	14
1.5.5 Hybrid-AM by peening	15
(a) <i>Laser shock peening</i>	15
(b) <i>Ultrasonic peening</i>	18
(c) <i>Shot peening</i>	19
(d) <i>Pulsed laser deposition</i>	21
1.5.6 Hybrid-AM by rolling & burnishing.....	22
1.5.7 Hybrid-AM by friction stir processing (FSP).....	25
2. LITERATURE REVIEW	29
2.1 Introduction to Laser Shock Peening	27
2.2 Process Mechanism of Laser Shock Peening.....	28
2.3 Literature Review on Laser Shock Peening	29
2.3.1 Effect of LSP on surface integrity	29
(a) <i>Topography</i>	30

(b) <i>Microhardness</i>	31
(c) <i>Residual stresses</i>	32
2.3.2 Effect of LSP on performance	33
(a) <i>Fatigue</i>	33
(b) <i>Corrosion</i>	34
2.3.3 Modeling LSP	35
(a) <i>Solver</i>	35
(b) <i>Material model</i>	37
(c) <i>LSP Loading</i>	40
2.4 Introduction to Directed Energy Deposition	43
2.5 Process Mechanism of Directed Energy Deposition	43
2.6 Literature Review on Modeling DED	45
2.6.1 Heat flux	45
2.6.2 Material deposition	46
2.6.3 Boundary conditions	47
2.6.4 Material properties	47
3. EFFECT OF LAYER THICKNESS AND PEENING PRESSURE ON RESIDUAL STRESSES IN HYBRID PROCESSING BY LASER SHOCK PEENING	51
3.1 Introduction	49
3.2 Finite Element Modeling	50
3.2.1 Model geometry	50
3.2.2 Material model	51
3.2.3 Thermal and mechanical loading	52
3.2.4 Initial and boundary conditions	53
3.3 Results and Discussion	53
3.3.1 Displacement	54
3.3.2 Nodal temperatures	55
3.3.3 Residual stress after LSP	56
3.4 Summary and Conclusions	58
4. EFFECT OF LAYER PEENING FREQUENCY ON RESIDUAL STRESSES DEVELOPMENT IN HYBRID PROCESSING BY LASER SHOCK PEENING	62
4.1 Introduction	60
4.2 Finite Element Modeling	63
4.2.1 Model geometry	63
4.2.2 Material model	65
4.2.3 Loading and boundary conditions	65
4.2.4 Simulation procedure	67
4.3 Results	70

4.3.1	Final residual stresses from different layer peening frequencies	70
4.3.2	Residual stress evolution	72
	(a) <i>LSP every 10 layers</i>	72
	(b) <i>LSP every 5 layers</i>	75
	(c) <i>LSP every 3 layers</i>	76
	(d) <i>LSP every layer</i>	77
4.3.3	Step history evolution of stresses	78
	(a) <i>LSP every 10 layers</i>	78
	(b) <i>LSP every 5 layers</i>	79
	(c) <i>LSP every 3 layers</i>	80
	(d) <i>LSP every layer</i>	81
5.	SUMMARY, CONCLUSIONS, AND FUTURE WORK.....	86
	APPENDIX.....	89
	Material properties of AISI 52100	89
	Material properties of Ti-6Al-4V	93
	REFERENCES	94

LIST OF TABLES

1.1	Classification of Hybrid-AM Machining Processes	10
2.1	Heat Flux (Q) Models	46
3.1	Heat Flux Process Parameters during Selective Laser Melting	52
4.1	Heat Flux Process Parameters.....	66
4.2	LSP Process Parameters.....	67
4.1	Width and Depth of Compressive Residual Stress Region Greater than -650 MPa.....	72

LIST OF FIGURES

1.1	Hybrid manufacturing methodologies	2
1.2	Hybrid manufacturing (HM) processes: (a) assisted HM processes and (b) mixed or combined HM processes	5
1.3	Schematic of hybrid-AM machining process on (a) side surface and (b) top surface	11
1.4	Selective laser erosion of SLM printed part	12
1.5	Selective laser re-melting of SLM printed part.....	13
1.6	Cross-sectional optical microscopy image of (a) only-SLM part (b) SLM with laser re-melting	14
1.7	Laser-assisted plasma deposition.....	14
1.8	Hybrid-AM by laser shock peening (LSP)	16
1.9	Experimentally measured residual stress (hole drilling technique) on austenitic SS 316L after hybrid-AM by laser shock peening using M2 PBF printer; (a) 40% and (b) 80% overlap ratios. Circles indicate depth at laser peened layers	18
1.10	Hybrid-AM using ultrasonic peening	19
1.11	Hybrid-AM using shot peening (SP)	21
1.12	Hybrid-AM using pulsed laser deposition (PLD) that combines printing and peening using a single laser source	21
1.13	Microstructural grain refinement during hybrid-AM by rolling.....	22
1.14	Comparison of microstructure for (a) non-rolled sample, (b) rolled sample with a 50 kN rolling force, and (c) rolled sample with a 75kN rolling force; (d) grain size as a function of rolling force.....	23
1.15	Micro-hardness as a function of rolling force profiled and slotted rollers	23
1.16	Intra-layer friction stir additive manufacturing (iFSAM).....	25
2.1	Schematic representation of laser shock peening	28

2.2	Change in roughness of laser peened AL6061-T6 alloy at 1.2 J laser pulse with increase in overlap ratio	31
2.3	Vickers micro-hardness along the surface from laser shock peening Ti-6Al-4V with single and double pulses	32
2.4	Residual stresses in Ti-6Al-4V alloy due to LSP with different number of shocks	33
2.5	σ_{\max} -N curves for unshocked and shock peened aluminum alloys	34
2.6	Corrosion rate and corrosion potentials of MgCa samples	35
2.7	LSP analysis procedure using Abaqus	36
2.8	LSP analysis procedure using LS-DYNA and ANSYS	37
2.9	Pressure-time profile of single LSP	41
2.10	Effect of laser intensity on residual stresses in AISI 52100 shock peened For 40 ns with 9 μm spot size	42
2.11	Schematic representation of LENS TM process	44
3.1	Two-dimensional model of hybrid additive manufacturing by SLM and LSP	51
3.2	Pressure-time history of a single pressure pulse from LSP	53
3.3	Magnitude of deformation in a 100 μm , 300 μm , 600 μm layer thickness model exposed to a 1 GPa and 2 GPa peening pressure	54
3.4	Nodal temperatures (NT11) along the depth direction below applied heat flux for a (a) 100 μm , (b) 300 μm , and (c) 600 μm layer thickness	55
3.5	S11 along the depth direction after laser peening with a pressure of 1 GPa for (a) 100 μm , (b) 300 μm , and (c) 600 μm layer thickness	57
3.6	S11 along the depth direction after laser peening with a pressure of 2 GPa for (a) 100 μm , (b) 300 μm , and (c) 600 μm layer thickness	57
4.1	Schematic representation of hybrid-AM by laser peening	61
4.2	Schematic representation of (a) thermal cancellation and (b) mechanical cancellation	62

4.3	Schematic of hybrid-AM model with thermal and mechanical boundary conditions	64
4.4	Variation of pressure with respect to time	67
4.5	Flow chart for simulation procedure of hybrid-AM by LSP	68
4.6	Stress profiles comparison of AM model with hybrid-AM models	70
4.7	Residual stress fields developed in each model	71
4.8	Stress profile evolution of hybrid-AM model with laser peening every 10 layers	73
4.9	Stress profile evolution of hybrid-AM model with laser peening every 5 layers	76
4.10	Stress profile evolution of hybrid-AM model with laser peening every 3 layers	77
4.11	Stress profile evolution of hybrid-AM model with laser peening every layer.....	78
4.12	Variation of residual stresses at element 44250 in laser peening every 10 layer model.....	79
4.13	Variation of residual stresses at element 44250 in laser peening every 5 layer model.....	80
4.14	Variation of residual stresses at element 44250 in laser peening every 3 layer model.....	81
4.15	Variation of residual stresses at element 44250 in laser peening every layer model.....	82
4.16	Experimentally measured residual stress (hole drilling technique) on austenitic SS 316L after hybrid-AM by laser shock peening using M2 PBF printer; (a) 40% and (b) 80% overlap ratios. Circles indicate depth at laser peened layers	83

PREFACE

There exist a **need** to print functional mechanical properties in a material. One solution to accomplish functionally gradient mechanical properties is hybrid additive manufacturing (hybrid-AM). By coupling additive manufacturing with a secondary process in a cyclic process chain, layer-by-layer cold working or thermal treatments are possible to functionalize local properties. The research area of hybrid-AM is in its infancy. Therefore, one primary focus of this work is to define the field of hybrid-AM and provide a literature review on efforts in this area. One of the most important questions related to hybrid processing is to know which layers need secondary processing. It is often too costly and impractical to secondarily process every layer. Therefore, the second focus of this work is to begin understanding which layers require processing in order to achieve the desired residual stress field.

The two main contributions of my work are the following: 1) defining hybrid-AM processing and a literature review on different hybrid-AM processes and 2) modeling residual stress development in hybrid processing by additive manufacturing and laser shock peening using the finite element method. The end result for these efforts is to develop a hybrid processing design platform that can be applied to any loading conditions, geometry, or material.

Organization of thesis

Chapter 1 focuses on defining hybrid additive manufacturing (hybrid-AM) processes and how it is different from the current established definition of hybrid manufacturing. In this chapter, a literature review was completed on currently available

hybrid-AM processes and other manufacturing processes that have the capacity to become hybridized with additive manufacturing. A secondary process of interest in this research is laser shock peening. **Chapter 2** describes how the additive manufacturing process known as directed energy deposition (DED) and the surface treatment process known as laser shock peening (LSP) were modeled in literature. Key process parameters from DED and LSP will be examined in order to identify key hybrid process parameters. **Chapter 3** examines the effect of layer thickness and peening pressure on residual stresses during hybrid processing by selective laser melting (SLM) and laser shock peening (LSP). Layer thickness and peening pressure were proposed as critical parameters in hybrid-AM for residual stress development in layers. **Chapter 4** focuses on the effect of layer peening frequency on residual stress development in hybrid-AM by DED and LSP. In this chapter, thermal and mechanical cancellation of residual stresses were defined and were quantified after layer peening frequencies of 1, 3, 5, 10, and 20 layers. Thermal and mechanical cancellation was highly dependent on layer peening frequency. Finally, **Chapter 5** provides a summary and the conclusions from this work. Future work is proposed that more directly validates the magnitudes of residual stresses from hybrid processing.

Publications Relating to Thesis

- [1] M.P. Sealy, G. Madireddy, R.E. Williams, P. Rao, M. Toursangsaraki, (2018) "Hybrid processes in additive manufacturing," *ASME Journal of Manufacturing Science and Engineering*, **140**, pp. 060801:1-13. doi:10.1115/1.4038644
- [2] M.P. Sealy, G. Madireddy, C. Li, Y.B. Guo, (2016) "Finite element modeling of hybrid additive manufacturing by laser shock peening," *Solid Freeform Fabrication Symposium*, Texas, Austin. pp. 306-316.

Publications in Preparation Relating to Thesis

- [1] G. Madireddy, M.P. Sealy, C. Li, (2018) “Modeling residual stress development in hybrid processing by directed energy deposition and laser shock peening,” To be determined.

CHAPTER 1

HYBRID PROCESSES IN ADDITIVE MANUFACTURING

1.1 Introduction

The term “hybrid” has been widely applied to many areas of manufacturing. Naturally, that term has found a home in additive manufacturing as well [1-4]. Hybrid additive manufacturing or hybrid-AM has been used to describe multi-material printing, combined machines (*e.g.*, deposition printing and milling machine center), and combined processes (*e.g.*, printing and interlayer laser re-melting). These capabilities afforded by hybrid-AM are rewriting the design rules for materials and adding a new dimension in the design for additive manufacturing paradigm. This thesis primarily focuses on defining hybrid-AM in relation to hybrid manufacturing and classifying hybrid-AM processes. Hybrid-AM processes are defined as the use of AM with one or more secondary processes or energy sources that are fully coupled and synergistically affect part quality, functionality, and/or process performance. By their nature, these hybrid-AM processes do not often meet the International Academy for Production Engineering’s (CIRP) definition of hybrid processes; *i.e.*, the simultaneous and controlled interaction of process mechanisms and/or energy sources/tools having a significant effect on process performance [5]. Hybrid-AM processes are typically a cyclical process chain rather than simultaneous processes and rarely influence the primary manufacturing process. In fact, hybrid-AM processes are more commonly designed to enhance *part* performance or functionality rather than the *primary build process* itself. The following sections describe how this definition was derived, and examples of hybrid-AM processes are provided.

1.2 Hybrid Manufacturing

In order to define hybrid additive manufacturing (hybrid-AM), it is important to have a clear understanding of hybrid manufacturing (HM). The concept of hybrid manufacturing has been in use for many years as a solution for improving part quality and productivity via the use of two or more methodologies [6, 7]. The terminology has been widely applied in literature to describe several hybrid techniques: (1) hybrid processes, (2) hybrid machines, and (3) hybrid materials, structures, or functions, see [Figure 1.1](#) [5, 8, 9].

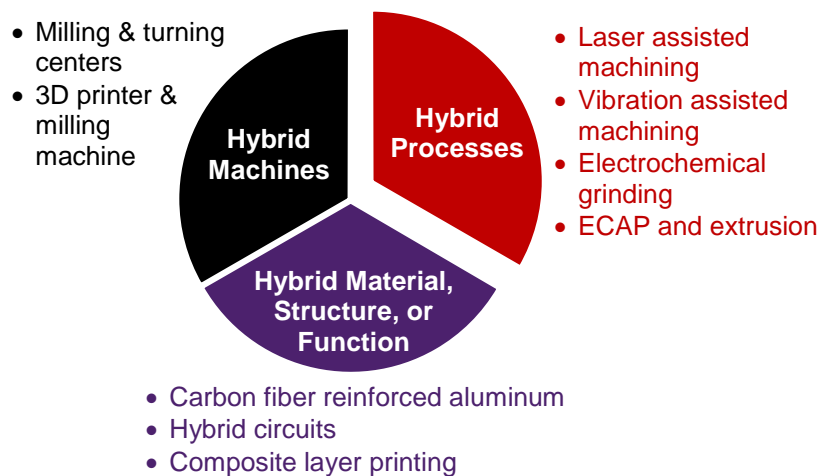


Fig. 1.1 Hybrid manufacturing methodologies. Modified from [5, 8].

Hybrid processes refers to the ever-increasing list of methods to coalesce two or more manufacturing processes. According to Kozak and Rajurkar, hybrid processes, namely machining, must make use of the combined or mutually enhanced advantages as well as avoid or reduce adverse effects the constituent processes produce when applied individually [10]. A similar interpretation is that the sum of the hybrid process is greater than the sum of the individual processes, *i.e.*, the “1+1=3” effect [8]. The International

Academy for Production Engineering (CIRP) further elaborates on the definition of hybrid processes to be the simultaneous and controlled interaction of process mechanisms and/or energy sources/tools having a significant effect on process performance [5]. One of the most commonly used examples is laser-assisted turning, whereby a laser simultaneously acts in conjunction with turning to improve the cutting process.

Hybrid processes are not to be confused with hybrid machines. Hybrid machines include multiple manufacturing processes in one machine platform. For example, a combined milling and turning machining center or a combined 3D printer and milling machine. The salient point is that hybrid machines refers to the machine platform rather than the constituent processes.

Hybrid materials, structures, or functions are concerned with combining one or more materials to have a hybrid composition, structure, or function [11, 12]. A hybrid material should result in either enhanced or completely new properties. Hybrid materials, structures, and functions have been widely investigated in literature across multiple fields of science and engineering for several decades. This work focuses namely on hybrid-AM processes, and therefore has limited discussion on hybrid materials, structures, or functions as related to additive manufacturing. Examples of hybrid materials include composite, sandwich, lattice, and segmented structures [11].

One of the primary objectives of this thesis are to define hybrid additive manufacturing (hybrid-AM) and summarize hybrid-AM processes reported in literature. In order to do so, *hybrid manufacturing* processes will be introduced and compared to *hybrid additive manufacturing* (hybrid-AM) processes. For completeness in defining the

field of hybrid additive manufacturing, hybridization of materials, structures, function, and machines as related to additive manufacturing will be defined and briefly discussed.

1.3 Hybrid Manufacturing Processes

According to CIRP's most recent classification efforts, there are two major types of hybrid manufacturing (HM) processes: (1) assisted processes and (2) mixed or combined processes, see [Figure 1.2](#). In assisted processes, a secondary process or energy source assists the primary process for the purpose of enhancing the total process performance. Three primary assisting processes frequently found in literature include: (1) vibration-assisted machining (implements vibration to assist with material removal or byproduct/waste removal or disposal) [13, 14]; laser-assisted machining (eases machining forces by softening the workpiece) [15-20]; and (3) media-assisted manufacturing (uses a coolant or lubricant to assist the primary process) [21-24].

In mixed processes, two or more processes are combined and occur somewhat simultaneously [5]. Examples include (1) combining electrochemical machining (ECM) or electrical discharge machining (EDM) with grinding [5, 10, 29-33] or (2) combining equal channel angular pressing (ECAP) with extrusion [34, 35].

Whether referring to assisted or mixed processes, hybrid manufacturing (HM) processes have traditionally targeted efficiency and productivity of the process as improvement criteria. The central theme to hybrid processing is that the *process* performance is improved by the hybrid approach. However, the emergence of additive manufacturing to print functional parts has expanded the possibilities for a hybrid

approach in this field, where improvement is focused primarily on part quality and subsequent functionality rather than solely on the process.

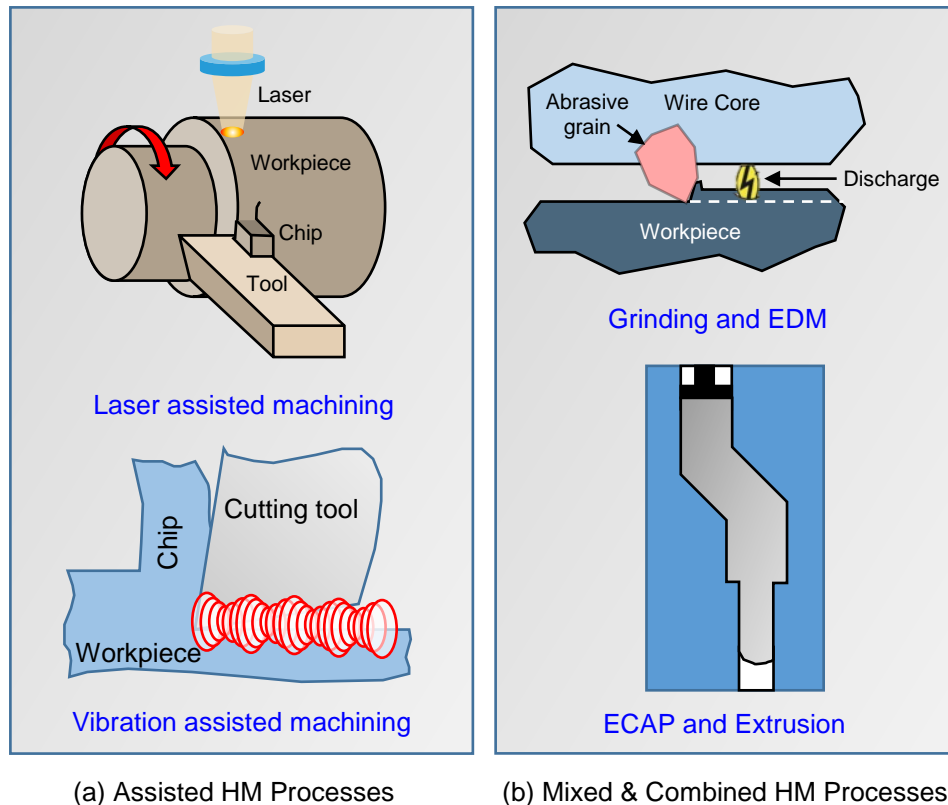


Fig. 1.2 Hybrid manufacturing (HM) processes: (a) assisted HM processes and (b) mixed or combined HM processes. Adapted from [25-28].

1.4 Hybrid Additive Manufacturing (Hybrid-AM) Processes

Analogous to hybrid manufacturing as identified by [5], hybrid-AM is concerned with several hybrid methodologies related to processes, materials, and machines. The following sections define hybrid-AM processes and explore multiple hybrid-AM processes in depth.

In this work, hybrid-AM processes are defined as the use of AM with one or more secondary processes or energy sources that are fully coupled and synergistically affect part quality, functionality, and/or process performance. Three key features to this definition include: (a) fully coupled processes, (b) synergy, and (c) part and/or process improvement.

1.4.1 Fully coupled processes

The first key feature of this definition relates to the fully coupled nature of the two (or more) processes. To be precise, the secondary process cannot be decoupled from the AM process during the build. Processes that occur pre- or post-printing are not considered coupled. The intent is to separate hybrid-AM processes from those considered to be pre-processing steps prior to layer assembly and post-processing steps once the build is complete.

An example of pre-processing that does not meet the fully coupled criterion is CIRTES Stratoconception[®] process [36]. In this case, individual layers called strata are pre-cut by milling or laser cutting prior to assembly. Two common examples of post-processing after 3D printing that typically would not comply with the fully coupled criterion are hot isostatic pressing (HIP) and abrasive flow machining (AFM). Both processes are often used on 3D printed parts to reduce porosity (*e.g.*, HIPing) or to reduce surface roughness and sealing of conformal heating and cooling passages (*e.g.*, AFM) [37, 38].

1.4.2 Synergy

The second key feature to this definition relates to the synergistic nature between the two or more processes. That is, the secondary process and the AM process work together either simultaneously or as a cyclical process chain to produce an enhanced

result that is unachievable by the individual processes. This is analogous to the “1+1=3” effect. An example of simultaneous process synergy would be laser-assisted plasma deposition. A laser provides a second energy source to enhance the deposition process. The majority of hybrid-AM processes are not typically simultaneous and therefore take place in a cyclic sequence of steps, *i.e.*, a cyclic process chain. An example of synergy using a process chain would be cyclically alternating laser shock peening (LSP) and 3D printing. The secondary LSP process imparts deep compressive residual stresses and is fully coupled since it occurs between printed layers. Coupling two processes results in a part with improved mechanical properties throughout the entire build volume.

1.4.3 Part and/or process improvement

Lastly, the third key feature of this definition relates to how the hybrid-AM process affects one or more of the following: part quality, part functionality, or process performance. Traditionally, hybrid manufacturing processes benefit process performance (*e.g.*, increase material removal rate or prolong tool life). Some hybrid processes benefit part quality and functionality as well. For example, combining ECAP and extrusion improves strength and ductility [28, 39].

In contrast to hybrid manufacturing processes, the majority of secondary processes in hybrid-AM do not assist the build process. Rather, the primary benefit is to the part or its functionality. Using the same example above, cyclically alternating laser shock peening (LSP) and additive manufacturing (AM) results in a part with improved mechanical properties. In this example, the primary objective is to enhance part quality and functionality rather than the build process. Even though LSP has no effect on the

build process, the two processes must be coupled in a cyclic process chain during the build in order to achieve the desired result.

There are some hybrid-AM processes where the objective is to benefit the build process rather than improving the part. An example of a secondary process improving the build process is laser-assisted plasma deposition (LAPD) [40] and is discussed further in Section 4.1.5. In LAPD, an assisting laser provides a secondary heat source in addition to the heat generated by the plasma arc in order to decrease melt pool diameter and improve plasma arc stability. In doing so, the primary build process was affected by the secondary manufacturing process.

1.5 Classification of Hybrid-AM processes

Each of these hybrid-AM processes can be classified several ways and are a unique subset of hybrid manufacturing processes where many do not meet the consensus definition from CIRP. The most common class of hybrid-AM processes is machining, where the primary goal is usually to improve surface finish and geometrical accuracy [1]. The second most common class of hybrid-AM processes are thermal in nature and include (1) laser-assisted melting [40] and (2) surface treatments such as laser re-melting or erosion [41-46]. These secondary processes employ thermal energy to improve the printing process or recondition the material properties of a previously deposited layer. Another class of secondary processes includes mechanical surface treatments such as peening [47-59] or rolling [60-71]. These processes re-form the printed layer and can result in improved surface finishes, refined microstructures, minimized distortion, increased hardness, improved part density, favorable compressive residual stresses, and stress relieving. A

lesser-explored class of hybrid-AM processing is solid state stirring. Combining additive manufacturing with friction stir processing can result in enhanced mechanical properties by refining the microstructure. The following sections survey the literature on hybrid additive manufacturing (hybrid-AM) processes beginning with machining. A process schematic is presented along with an analysis of each hybrid-AM process.

1.5.1 Hybrid-AM by machining

Hybrid additive manufacturing (hybrid-AM) by machining is most widely investigated hybrid-AM process. In this process machining is done between layer intervals for complex geometries or internal features. Machining simple geometries with easily accessible external surfaces would most likely occur post-printing and would not be considered as a hybrid-AM process. Hybrid-AM by machining requires an AM process coupled with material removal process (milling or turning). AM process provides near net shape parts while machining sequential layer intervals provides improved surface finish and better geometrical accuracy.

The first hybrid-AM machining processes were developed in the area of welding [50, 72, 73]. The additive processes that have been coupled to machining include selective laser welding, MIG welding, ultrasonic welding, laser melting, laser deposition, laser cladding, plasma deposition, and sheet lamination. All these AM processes can be categorized into three primary AM processes: directed energy deposition (DED), powder bed fusion (PBF), and sheet lamination. [Table 1.1](#) classifies hybrid-AM machining processes by AM energy sources and indicates process category based on ISO/ASTM 52900:2015 terminology [74]. In DED, material in the form powder or wire is melted by

a heat source and deposited on a substrate to form layers. In PBF, thin layers of powder are melted onto a substrate using a laser or electron beam. In case of sheet laminations, sheets of metal are stacked and bonded together by oscillatory shear stresses at ultrasonic frequencies. This is a solid state fusion process where coalescence is achieved by forming a strong metallurgical bonds between the surfaces. Once one or more layers have been printed, the next step is to mill the deposited layers to achieve precise dimensions.

Table 1.1 Classification of Hybrid-AM Machining Processes

	AM Process Category	Material Feedstock	Type of Material	Material Distribution	
<i>Laser</i>					
Laser welding + Milling	DED	Powder	Metal	Deposition nozzle	[72, 73, 75-78]
Laser cladding + Milling	DED	Powder	Metal	Deposition nozzle	[79, 80]
Laser deposition + Milling	DED	Powder	Metal	Deposition nozzle	[81]
Selective laser sintering + Milling	PBF	Powder	Metal	Powder bed	[82]
<i>Plasma / Arc</i>					
3D Welding + Milling	DED	Wire	Metal	Deposition nozzle	[72, 83-86]
Plasma deposition + Milling	DED	Powder	Metal	Deposition nozzle	[87, 88]
Microcasting + Milling + Shot Peening	DED	Powder	Metal	Deposition nozzle	[50, 89]
<i>Solid State Fusion</i>					
Ultrasonic welding + Milling	Sheet lamination	Sheet	Metal	Sheet stack	[73, 90, 91]
Layered compaction manufacturing + Milling + Sintering	PBF	Powder	Ceramic	High density green compact	[92]

ISO/ASTM 52900:2015(E)

DED: directed energy deposition

PBF: powder bed fusion

The most common machining reported in literature is milling. In most cases, the objective of milling is to improve the sidewall's surface finish on one or more layers

using end mill (Figure 1.3a). In other cases, the objective is to face mill the top surface of a printed layer to provide a smooth, fresh surface for subsequent printing (Figure 1.3b) [83, 84, 86, 87, 93]. The purpose of end milling is to improve surface finish of final part while the purpose of face milling the top of each layer is to maintain constant layer thickness improving Z-axis accuracy.

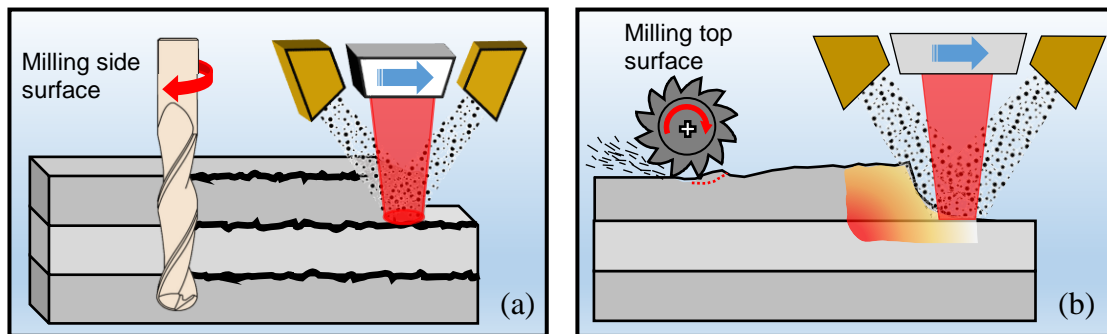


Fig. 1.3 Schematic of a hybrid-AM machining process on (a) side surface and (b) top surface.

Usually machining the surface does not affect build process; however, Karunakaran *et al.* reported that face milling removed oxidized layer that negatively impacted the build process (in this case, arc welding) and provided for a more stabilized arc and consistent weld bead [83, 86].

1.5.2 Hybrid-AM by ablation or erosion

This hybrid-AM process uses a laser electron beam as a secondary energy source to ablate or erode the top layer of deposited material (Figure 1.4). Ablation between printed layers is a fully coupled non-contact process that synergistically affects part quality and performance. Similar to hybrid-AM by machining, this subtractive process

can create smooth and precise surfaces by material removal. Furthermore, this approach can be applied towards micro-machining of interlayer features in additive manufacturing since the energy source erodes material.

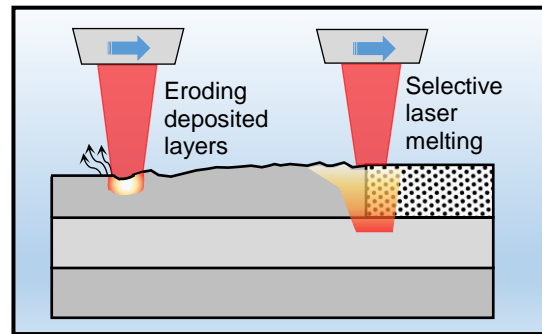


Fig. 1.4 Selective laser erosion of SLM printed part.

Yasa *et al.* investigated hybrid-AM by ablation on AISI 316L stainless steel with the use of selective laser melting (SLM) coupled to a pulsed Q-switched Nd:YAG laser ($\lambda = 1094 \text{ nm}$) for selective laser erosion [45, 94]. Using this hybrid approach, the accuracy in the build direction (z -direction) can be improved by reducing the layer thickness or removing irregularities. The authors report that a 50% reduction in roughness is achievable.

1.5.3 Hybrid-AM by re-melting

Hybrid-AM by re-melting uses an energy source (*e.g.*, laser or electron beam) to re-melt previously fused material (Figure 1.5). As the laser power is low, instead of vaporizing the material the laser re-melts the previously deposited layer. This re-melting fills the pores formed during 3D printing increasing part density greater than 99%. Re-melting can take place after each layer or a sequence of layers. For a given material, the

mechanical, physical, and chemical changes to the re-melted region depends on the laser scanning speed, scan pattern, and laser power.

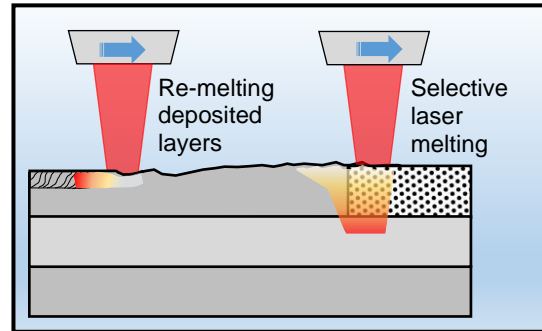


Fig. 1.5 Selective laser re-melting of SLM printed part.

The advantages of laser re-melting are (1) increased part density, (2) relief of residual stresses [95], and (3) modified material properties. The disadvantages to this process include increased processing time, since the energy beam should make at least twice the number of scans and added energy input required for processing.

Yasa *et al.* investigated the effect of laser re-melting SLM parts [43-45] on part density, microstructure, hardness, and external surface roughness (Figure 1.6). Although authors investigated improving external surface roughness, the same approach could be applied layer-by-layer (or multiples thereof) to provide a smooth layer, improved part density, and refined grain structure to improve properties of material. Roughness decreased 50% to 75% depending on process conditions. R_a was 2 μm to 8 μm after re-melting. The authors also showed that re-melting decreased the average porosity from 0.77% (SLM-only part) to 0.032% (re-melted part) using optimal laser parameters, *i.e.*, low laser power (85 W) and high scanning speed (100-200 mm/s). Interestingly, multiple

passes for laser re-melting (up to three) did not significantly decrease porosity. The microstructure changed to a lamellar pattern with a refined grain size that typically exhibited an increased microhardness if sufficient energy was applied [44].

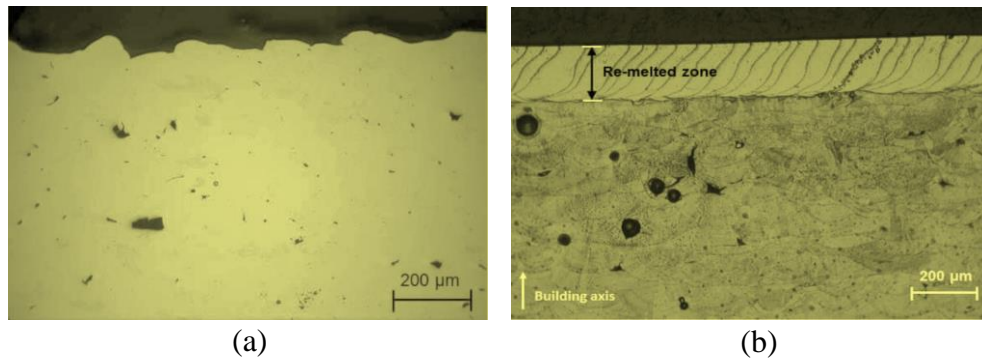


Fig. 1.6 Cross-sectional optical microscopy image of (a) only-SLM part (b) SLM with laser re-melting [43].

1.5.4 Hybrid-AM by laser assisted plasma deposition

Unlike the other processes mentioned above, this hybrid-AM process employs an assisting laser during plasma deposition (Figure 1.7). Plasma deposition deposits material and a laser adds a secondary energy source applied simultaneously at the same location to assist the build process and improve build quality.

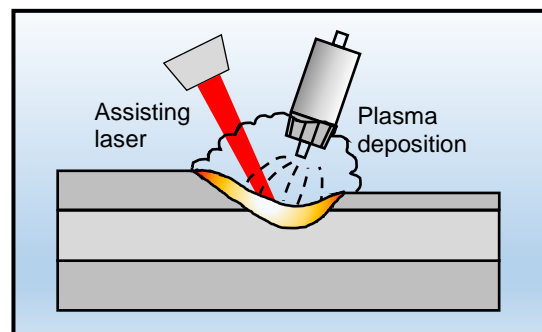


Fig. 1.7 Laser-assisted plasma deposition.

Qian *et al.* investigated effect of using a laser as an assisting heat source in plasma-arc deposition [40]. This example demonstrates the use of an assisting energy source in additive manufacturing to improve both process performance and part quality. The laser entered the plasma arc beam to provide more thermal energy. Shielding gas used in plasma arc deposition absorbed the energy and ionized gas molecules. The energy density of the plasma arc was improved, and the plasma arc diameter favorably decreased, which improved accuracy of the part. At the same time, arc igniting became easier because of plasma induced by laser. With more energy, the depth of melt pool increased and improved the microstructure and decreased porosity.

1.5.5 Hybrid-AM by peening

Hybrid additive manufacturing using surface treatments is a widely unexplored research area. There have been a few patents issued in USA, Europe, and Canada, for last 25 years [48, 53-58]. But, there exists a major knowledge gap in use of surface treatments in additive manufacturing. Using surface treatments, such as peening, to print functionally gradient material properties in additive manufacturing is poorly understood and of critical importance for military, aerospace, automotive, and biomedical applications. The following sections identify research activity related to different peening surface treatments.

(a) *Laser shock peening*

Hybrid-AM by laser shock peening (LSP) is the combination of any additive manufacturing process with laser shock peening, also known as laser shot peening or

laser peening. Similar to previously mentioned hybrid-AM processes, the secondary peening process occurs layer-by-layer or multiples thereof as a cyclic process chain. After a laser is peened, another layer or set of layers is printed and the cycle repeats until the completion of the build. This approach allows for functionally gradient properties throughout the build volume. [Figure 1.8](#) is a schematic of hybrid-AM by LSP.

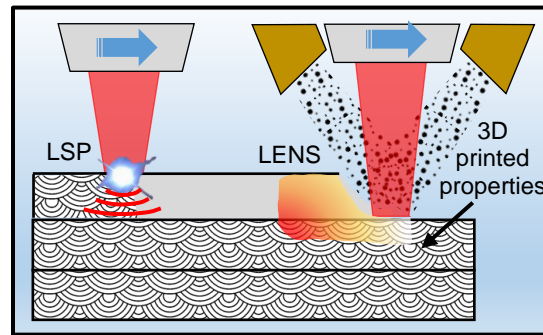


Fig. 1.8 Hybrid-AM by laser shock peening (LSP).

LSP is a surface treatment where shock waves from rapidly expanding plasma plastically deform a work piece. Plasma forms from the interaction of the work piece with a pulsed nanosecond range laser. An ablative layer is typically used as a protective coating to prevent thermal damage from laser on the surface of work piece, making the process mechanical. However, LSP becomes thermo-mechanical phenomenon without an ablative layer, leading to re-melted and re-cast material in addition to shock wave.

M. Sealy's group at University of Nebraska-Lincoln are currently investigating the use of LSP during powder bed fusion (PBF) and directed energy deposition (DED) processes to understand thermal cancellation of favorable stress fields [47]. The objective

is to print favorable mechanical properties such as compressive residual stress and increased microhardness to improve performance of AM parts.

R. Logé's group at the Laboratory of Thermomechanical Metallurgy at the Ecole Polytechnique Federale De Lausanne (EPFL) in Switzerland is investigating the use of LSP in selective laser melting to control residual stress [59]. Experimentally measured residual stress profiles using the hole drilling technique after hybrid-AM by laser shock peening is shown in [Figure 1.9](#) [59]. Austenitic SS 316L was printed on a Concept Laser, GmbH in Germany. Once a prescribed number of layers were built, the samples were re-introduced to the build chamber for subsequent printing. The results compared an as-built sample (without laser peening) to ones that were laser peened on external surface (1mm spot size with 40% and 80% overlap) and hybrid-AM samples (3D LSP samples; 1 mm spot size with 40% and 80% overlap) where laser peening occurred every 1, 3, or 10 layers. At 40% overlap ([Figure 1.9a](#)), the maximum compressive residual stress (CRS) and depth of the CRS increased 34% and 69% on average, respectively. At 80% overlap ([Figure 1.9b](#)), the magnitude of the CRS did not increase significantly compared to externally peened surface; however, the depth of the CRS increased for the hybrid-AM samples and may have indicated saturation point was reached due to the high amount of overlap. Interestingly, peening every 10 layers was shown to have deeper residual stresses than peening every one or three layers at 80% overlap. These results showed that hybrid-AM by LSP can improve the properties of material by inducing favorable CRS into the layers. Also, thermal cancellation from subsequent printing did not relax away all of the favorable CRS. Since this was a powder bed fusion (PBF) process, the heat affected zone was minimal compared to a directed energy deposition (DED) process.

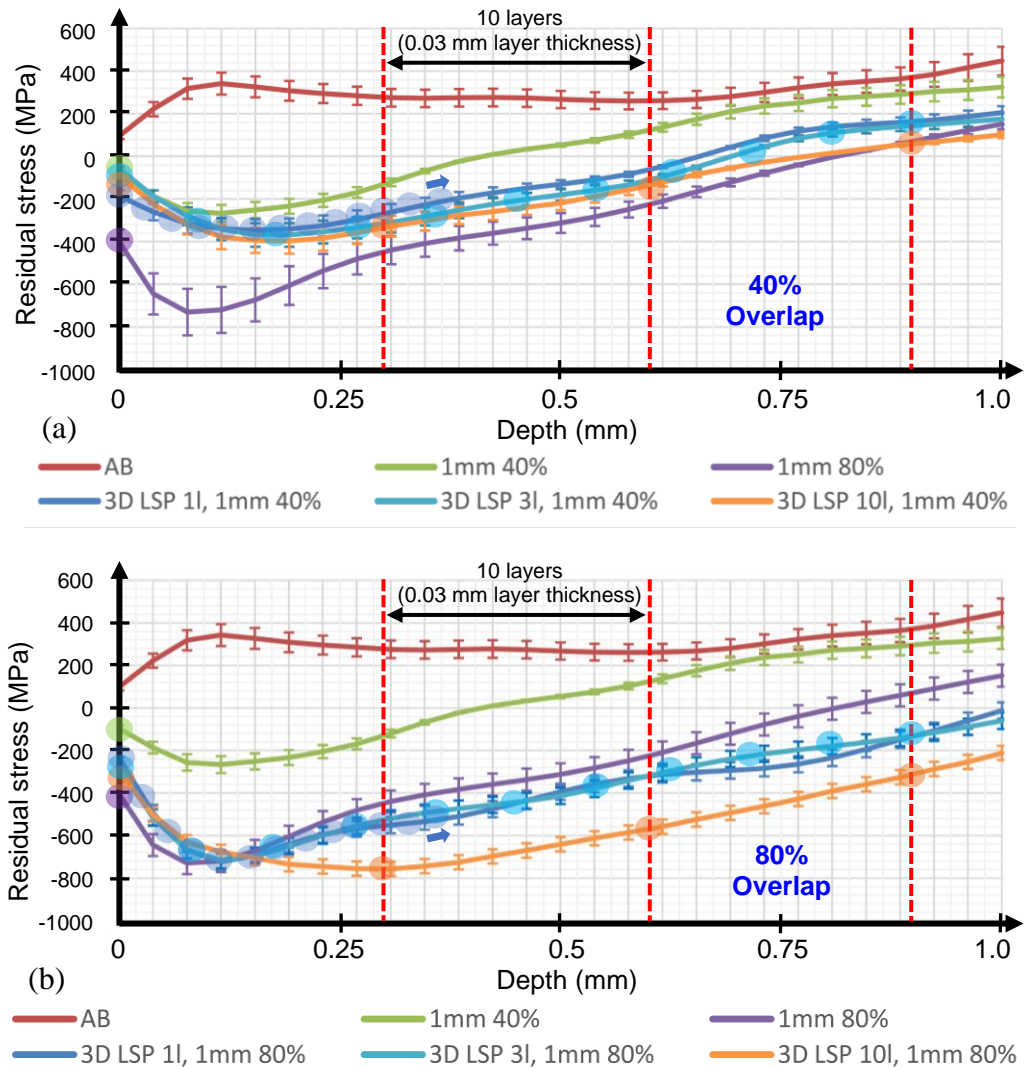


Fig. 1.9 Experimentally measured residual stress (hole drilling technique) on austenitic SS 316L after hybrid-AM by laser shock peening using M2 PBF printer; (a) 40% and (b) 80% overlap ratios. Circles indicate depth at laser peened layers. Modified from [59].

(b) Ultrasonic peening

Hybrid-AM by ultrasonic peening (UP) applies ultrasonic energy to a work piece using an electro-mechanical transducer layer-by-layer or multiples thereof, see [Figure 1.10](#). This mechanical/acoustic surface treatment is also known as ultrasonic impact treatment (UTT) and is capable of imparting compressive residual stress, stress

relief, and microstructural grain refinement. UP can improve the fatigue, corrosion, and tribological performance of AM components.

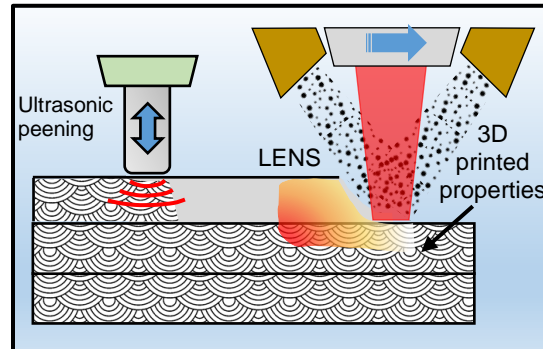


Fig. 1.10 Hybrid-AM using ultrasonic peening (UP).

The use of UP in hybrid-AM is a low cost, quick, and simple solution to improve properties in practically any AM process. A. Achutan's group from Clarkson University investigated ultrasonic peening (UP) layer-by-layer to strengthen selective laser melted (SLM) parts [96]. The results showed that hybrid-AM by UP was able to increase the yield strength and refine the microstructure of Inconel and stainless steel.

(c) Shot peening

Shot peening is a surface treatment that improves the mechanical properties of a near surface layer by directing a stochastic stream of beads at high velocities under controlled coverage conditions. The impact of bead on the surface induces plastic deformation that results in strain hardening and compressive residual stress. Depending on material of interest, beads can be composed of glass, metal, or ceramic.

Shot peening external surfaces of additive parts has been investigated in academia [50, 89, 97-100] and widely applied in industry to improve surface integrity. Intra-layer shot peening as a hybrid-AM process has not been widely explored. M. Sangid's group at Purdue University investigated the use of fine particle shot peening (FPSP) on AlSi10Mg during powder bed fusion (PBF) process [101]. Incorporating shot peening during the build cycle as shown in [Figure 1.11](#) has several benefits and also introduces new processing challenges. For example, shot peening is a relatively low cost and quick (in terms of processing time) solution to improve surface integrity; however, bead size is often one to three orders of magnitude larger than powders used in AM processes and requires additional sifting from recycled powder and cutting chips in hybrid-AM machines. Traditional shot peening is ideally suited for directed energy deposition, sheet lamination, or material extrusion processes since particle size can be much larger and will not directly interfere with subsequent printing. In PBF, shot peening can become more problematic if a secondary material is introduced as the peening media because of part contamination issues. An alternative is to use the AM powder itself as the peening media. Current literature has indicated a minimal or negligible effect from AM powder bed peening [101]. Referred to as fine particle shot peening (FPSP), the process limits the penetration depth for micro-hardness and compressive residual stress such that any favorable mechanical properties may become thermally cancelled by subsequent printing [101]. Furthermore, peening soft materials with soft powders, for example aluminum alloys with an aluminum alloy powder, may not generate enough contact pressure because the limited strength and hardness of the peening media.

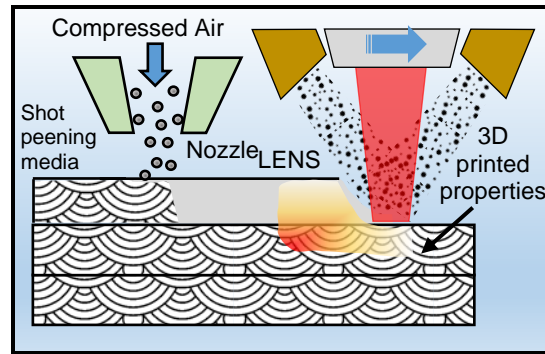


Fig. 1.11 Hybrid-AM using shot peening (SP).

(d) Pulsed laser deposition

The use of pulsed lasers as opposed to continuous lasers is continuing to grow in additive manufacturing [102]. High powered pulsed lasers have been used for many years as a method to print thin layers of material on a substrate [103, 104]. This process is known as pulsed laser deposition (PLD). When a pulsed laser impinges the powder, rapid heating and vaporization occurs and is accompanied by the formation of plasma plume (see Figure 1.12). The plasma plume creates a shock wave that plastically deforms the surface during printing [105]. In fact, the principle mechanism of PLD is similar to LSP. The key distinction is that PLD combines printing and peening processes into a single laser source. Favorable compressive residual stresses are possible by PLD [106].

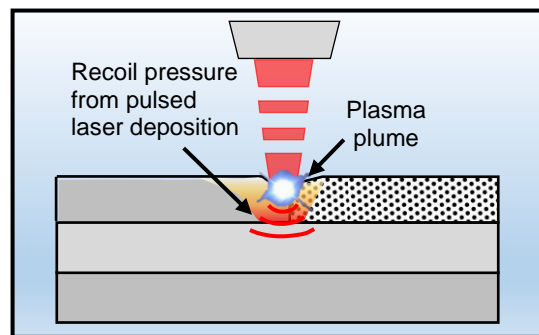


Fig. 1.12 Hybrid-AM using pulsed laser deposition (PLD) that combines printing and peening using a single laser source.

1.5.6 Hybrid-AM by rolling & burnishing

Another class of hybrid-AM processes that form (i.e., shape) and improve properties of work piece are rolling and burnishing, see [Figure 1.13](#). Hybrid-AM by rolling solves two of the major problems of additive manufacturing. Firstly, inaccuracies due to beads or layers overlap. This can be eliminated by machining but, with rolling these inaccuracies can be reduced without removing the material. Secondly, undesired residual stresses from building process. Although the previous peening surface treatments relieve internal stresses, rolling achieves both stress relaxation and forming for dimensional accuracy without removing material.

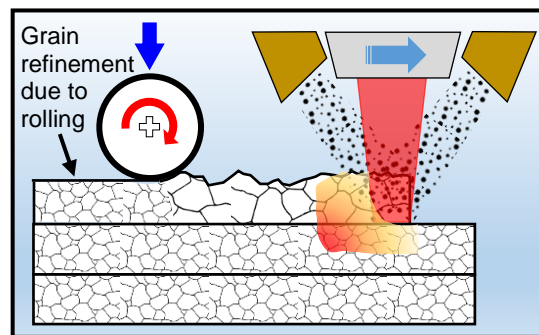


Fig. 1.13 Microstructural grain refinement during hybrid-AM by rolling.

There are two primary research groups active in hybrid-AM by rolling:

P.Colegrove's group from Cranfield University in U.K. [63-66] and H. Zhang's group from Huazhong University of Science and Technology in China [67-71]. Colegrove's group used wire-arc AM and applied profiled and slotted rolling tools after deposition of each layer. Results showed decreased distortion, grain refinement, and improved mechanical properties (see [Figures 1.14 & 1.15](#)). Maximum strength, hardness, and

elongation of hybrid-AM rolled samples were higher than as-cast material. In addition, rolling reduced tensile stresses in the samples.

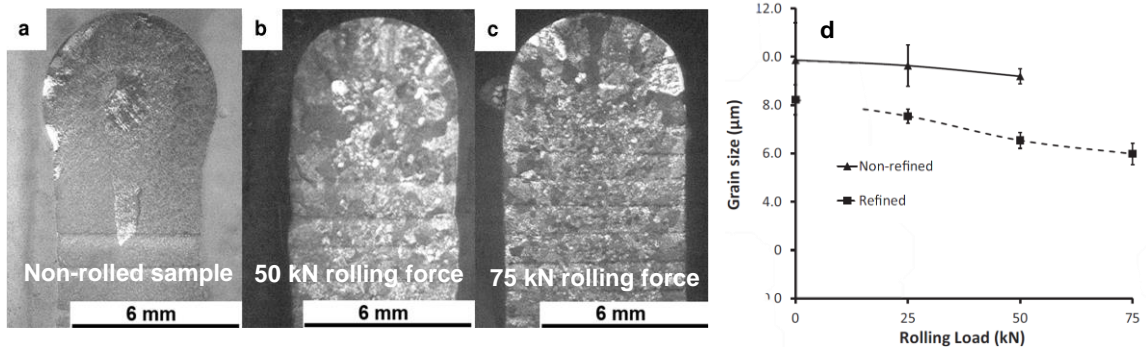


Fig. 1.14 Comparison of microstructure for (a) non-rolled sample, (b) rolled sample with a 50 kN rolling force, and (c) rolled sample with a 75 kN rolling force [63]; (d) grain size as a function of rolling force [64].

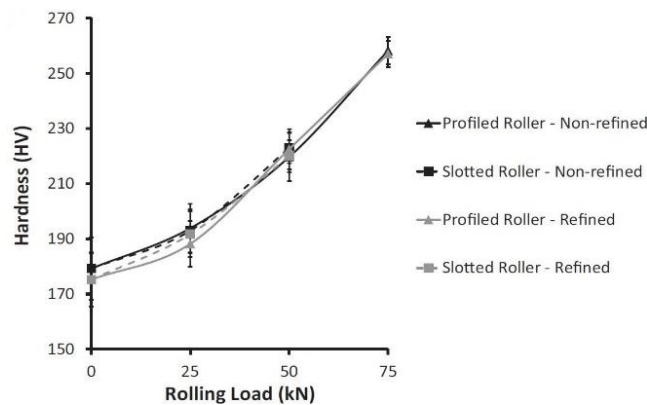


Fig. 1.15 Micro-hardness as a function of rolling force using profiled and slotted rollers [64].

Zhang's group used a metamorphic hot-rolling tool that was adaptable to rolling one, two, or three sides of a component. A metamorphic rolling tool has three rollers: one horizontal and two vertical rollers. The horizontal roller acts on the top planar surface while the vertical rollers act on the vertical faces of workpiece. Results showed that hot

rolling (rolling temperature above recrystallization temperature) resulted in a refined grain structure, instead tensile strength (approximately 33% over conventional sample), and improved dimensional accuracy.

Similar to rolling, burnishing is a surface treatment process to improve surface integrity (surface roughness, residual stresses, microstructure, and hardness) of a part. Burnishing consists of a rolling/sliding tool (*e.g.*, ball or cylinder). The tool moves on the surface of material causing plastic deformation in a thin surface layer. This plastic deformation causes material to flow such that peaks and valleys in the surface diminish. If burnishing occurs between printed layers, there is a possibility of producing functionally graded properties (similar to hybrid-AM by peening) with dimensionally accurate parts.

Book and Sangid used a variation of burnishing, referred to as sliding severe plastic deformation (SPD), on AlSi10Mg to test the feasibility of intra-layer processing [101]. SPD employs a highly negative rake angle tool that severely deforms the workpiece without generating a cutting chip. The surface is compressed in a similar manner to a ball-burnishing tool. The end result is strain-hardened surface up to a depth of 1 to 2 mm that is highly plasticized and significantly rougher. If thermal cancellation can be avoided from subsequent printing of layers, SPD is a suitable process to generate intra-layer rough surfaces with enhanced mechanical and metallurgical properties.

Surface treatments such as rolling or burnishing do not affect the AM process; however, without the use of a cyclical process chain that included rolling/burnishing, beneficial effects for fatigue, corrosion, or wear cannot be fully realized. Therefore, these

processes must be fully coupled in hybrid-AM in order to synergistically affect part performance.

1.5.7 Hybrid-AM by friction stir processing (FSP)

Friction stir additive manufacturing (FSAM) is an additive process where the primary principle is based on friction stir welding (FSW) to permanently join two surfaces. In FSAM, a rotating non-consumable tool consisting of a pin and shoulder made from refractory materials plunges into a work piece [107]. The tool crosses the surface of the part creating heat and considerable plastic deformation that joins two layers by mixing the highly plasticized material. Similar to FSW, the workpiece does not melt to achieve coalescence. The result in metals is typically significant grain refinement and recrystallization. These improvements to metallurgical properties have translated into better mechanical and fatigue performance. In addition to metals, FSW has been successfully demonstrated on polymers and composites. The same approach could be extended to FSAM. Although FSAM is not a hybrid-AM process, friction stirring can be easily applied layer-by-layer to parts built using other additive processes (Figure 1.16), such as directed energy deposition (DED) or material extrusion, to improve mechanical, metallurgical, and chemical properties.

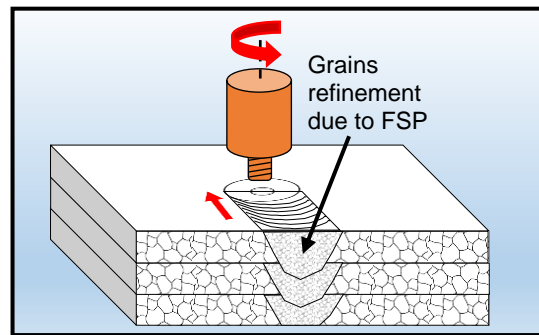


Fig. 1.16 Intra-layer friction stir additive manufacturing (iFSAM).

Francis *et al.* investigated the effect of friction stir processing (FSP) on Ti-6Al-4V parts produced by directed energy deposition [108]. The grains were refined and the hardness increased. The authors also mentioned that fatigue life would be improved based on figure studies of similar microstructures. Hybrid-AM by FSP is another example where the secondary process has no direct influence on the primary build process; however, a cyclic process chain is required in order to achieve the desired mechanical, chemical, and physical properties.

CHAPTER 2

LITERATURE REVIEW

The following literature review consists of two parts: (I) laser shock peening and (II) directed energy deposition. Each part describes the process mechanism and examines how each process has been modeled in literature.

PART I: LASER SHOCK PEENING

2.1 Introduction to Laser Shock Peening

Laser shock peening (LSP) is a surface treatment technique to improve mechanical properties of metal components. LSP improves the fatigue strength and life of metallic components by inducing compressive residual stresses below the surface of a material. Improvements in hardness and yield strength of metal parts is attributed to high density array of dislocations generated by a shock wave.

The ability of a shock wave to plastically deform metal parts to improve properties was first investigated in 1963 and was later developed over the years for commercial applications [109]. Although traditional shot peening existed in industry, the ability of LSP to reach complex shaped parts and induce higher compressive stresses than shot peening made this process a desirable substitute for shot peening. LSP is used in the aviation industry to decrease foreign object damage and the tooling industry to improve the life of tools. Recently, applications of LSP have expanded to biomedical field for controlling corrosion rate of medical implants [110, 111].

2.2 Process Mechanism of Laser Shock Peening

A schematic representation of the laser shock peening (LSP) process is shown in [Figure 2.1](#). When a laser pulse with sufficient intensity irradiates a metal surface with an energy absorbent coating through a confining layer for short period of time (≈ 30 ns), the coating is vaporized and reaches temperatures above $10,000$ °C. At these temperatures, the vapor is transformed into high-energy plasma by ionization. This plasma continues to absorb the laser energy until the end of deposition time. The plasma energy is confined on to the metal surface by the confining layer and is transmitted into the metal surface in the form of shock waves. When pressure from shock waves exceed the dynamic yield strength of a material, plastic deformation occurs, which consequently modifies subsurface microstructure and properties.

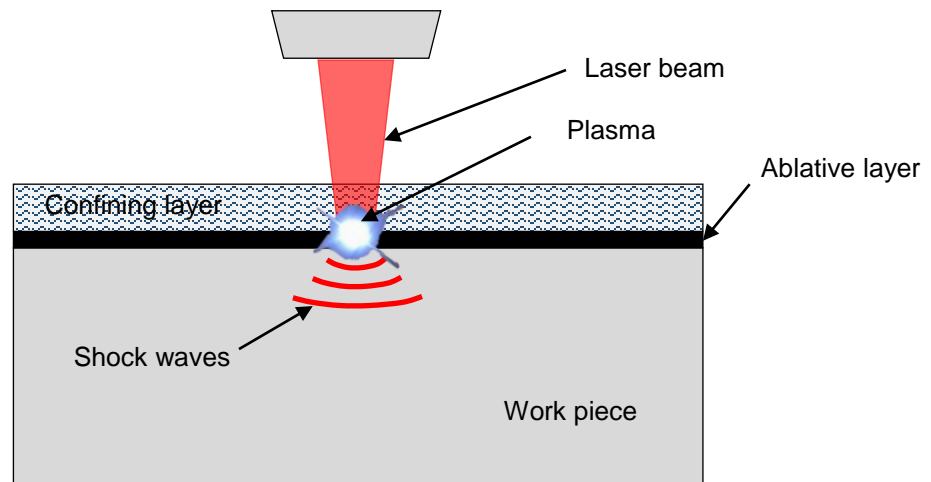


Fig. 2.1 Schematic representation of laser shock peening.

Usually LSP is applied with a confining layer on surface, such as water, glass, or any other transparent material. The interaction of plasma in the presence of a confined

layer is called “confined ablation.” Without the confined layer, the interaction of plasma with the surface is “direct ablation.” In confined ablation, the layer traps the expanding plasma over the surface causing very high plasma pressures ranging from 1 GPa-10 GPa depending on the laser parameters and the material. In direct ablation, only some tenths of a gigapascal pressure is achieved [112].

On the surface of metal parts, a thermal protective layer or an absorbent layer is used. The function of this absorbent layer is to increase shockwave intensity in addition to protecting the metal surface from laser ablation and melting. Metallic foils, organic paints, or a flat black paint can be used as a sacrificial coating.

2.3 Literature Review on Laser Shock Peening

Since the development of laser shock peening (LSP), several researchers have investigated the effect of different process parameters on a wide array of metals and their alloys. Process parameters of interests includes: laser power and spot size; multiple laser peening (*i.e.*, coverage); overlap, and ablative and confining layers. This review gives an outlook on effect of LSP on surface integrity and performance of metal parts and to provide insight as how it might affect a material when coupled with additive manufacturing layer-by-layer. Later in this section it was given how LSP was modeled in literature.

2.3.1 Effect of LSP on surface integrity

Surface integrity is the study and control of the surface and subsurface layer and the changes in it that occur during processing which may influence the performance of a

finished part or product [113]. Surface integrity of a material includes, but is not limited to, topography, microhardness, microstructure, and residual stress. The plastic deformation of metal due to a pressure shock wave from LSP affects surface roughness, hardness, residual stresses, etc. The following sections explore the effects of LSP on surface integrity of different metals.

(a) Topography

When a laser shock peening was applied on the surface of a metal, the plasma formed applies pressure in the form of shock waves. These shock waves push the surface layers of material by plastic deformation. This deformation on the surface creates a rougher surface. The study of topography of a laser peened material is important as the surface roughness of material increases the willingness to corrode a material in a particular environment increases, thereby decreasing the life of part. To understand how surface roughness varies with LSP, Peyre *et al.* applied multiple LSP on aluminum alloys. The average and peak surface roughness was higher than as-milled samples [114]. When compared to the roughness created by other surface treatment process like shot peening, the roughness values are relatively low. Similarly, Salimianrizi *et al.* investigated effect of peening overlap on surface roughness [115]. He observed that with an increase in peening overlap ratio from 20% to 50%, the surface roughness decreased. Interestingly, further increasing the overlap ratio beyond 50% caused the surface roughness to increase due to the formation of dimples from local plastic deformation, forming a texture like surface (Figure 2.2).

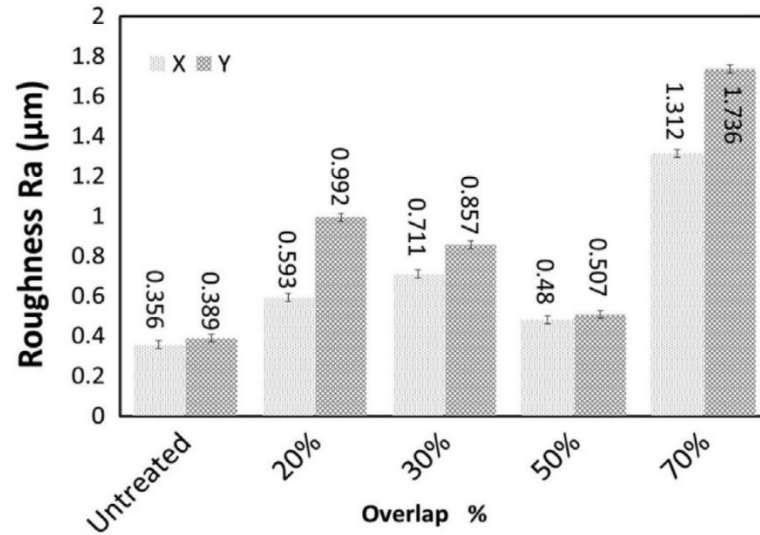


Fig. 2.2 Change in roughness of laser peened Al6061-T6 alloy at 1.2 J laser pulse with increase in overlap ratio [115].

(b) Microhardness

Hardness reduces fatigue crack propagation in a material. LSP improves the material properties by hardening the surface below the laser irradiated area. The magnitude of hardness depends on laser parameters, type of metals, alloys, and their microstructure. LSP has shown to increase hardness by at least 10% for some materials and more than double for others [114, 116, 117]. The percentage increase in hardness depends on type of metal and its microstructure, multiple LSP, and overlap ratio. Zhang *et al.* showed that double peening the same spot on Ti-6Al-4V material resulted in a 24% increase in hardness [118] (Figure 2.3).

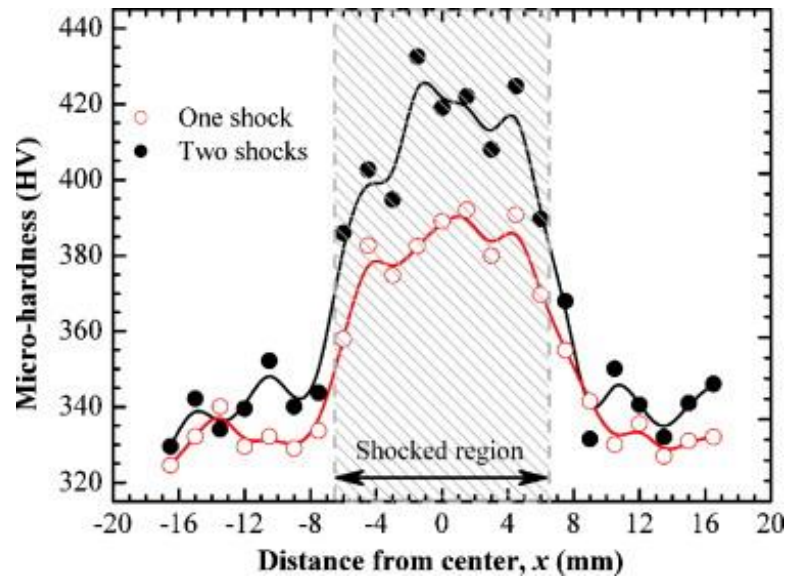


Fig. 2.3 Vickers micro-hardness along the surface from laser shock peening Ti-6Al-4V with single and double pulses [118].

Similarly, increasing the pulse overlap also increases the microhardness in the subsurface of materials. Hu *et al.* investigated effect of pulse overlap on AISI 1040 steel and found that the hardness increased from 12% to 20% with increase in pulse overlap from 50% to 90% [119].

(c) **Residual stresses**

Stresses that remain in a material after the original cause of stress is removed is referred to as residual stress. When a surface treatment like LSP is applied on a metal surface, the material undergoes plastic deformation. This plastic deformation in material induces compressive residual stresses in the material. These compressive residual stresses increase fatigue life by decreasing the rate of crack propagation. This improves the life of a metal part. Similar to hardness, residual stresses also depend on laser parameters, laser overlap, and material.

Zhang *et al.* investigated the effect of one and two peenings on Ti-6Al-4V and the resulting residual stress profile is shown in Figure 2.4 [118]. He found that as the number on peens on the same spot increases the residual stresses in material increases. The magnitude of compressive residual stresses in a material also depends on other laser peening conditions such as laser power, spot size *etc.*

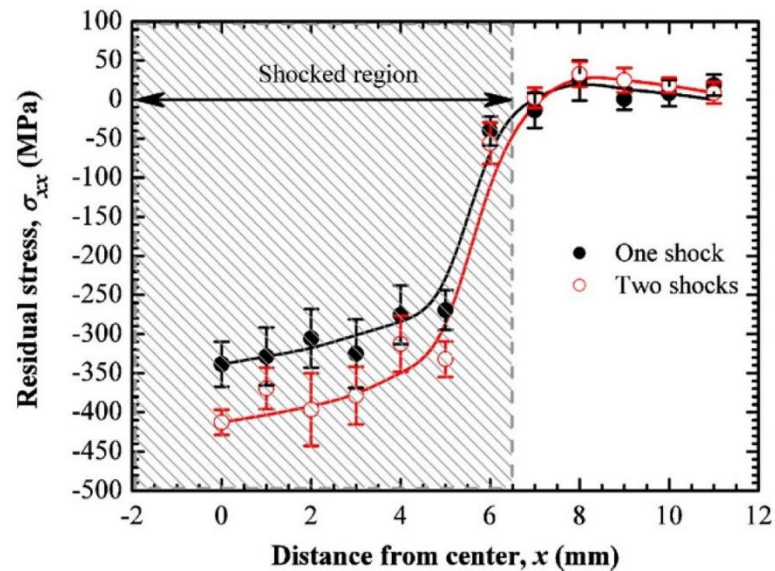


Fig 2.4 Residual stresses in Ti-6Al-4V alloy due to LSP with different number of shocks.

2.3.2 Effect of LSP on performance

(a) Fatigue

In 1996, Peyre *et al.* investigated the effect of laser shock peening on fatigue behavior of aluminum alloys [114]. For these experiments, Peyre used a notched sample to localize the crack initiation, and laser shock peening was applied with 50% overlap at the notch. Under high cycle fatigue test of samples using three point bending test, he found that for a fatigue life of 10 million cycles, the fatigue limit was increased 36% for

A356-T6, 22% for Al12Si-T6, and 23% for Al7075 and the corresponding plots are shown below in [Figure 2.5](#).

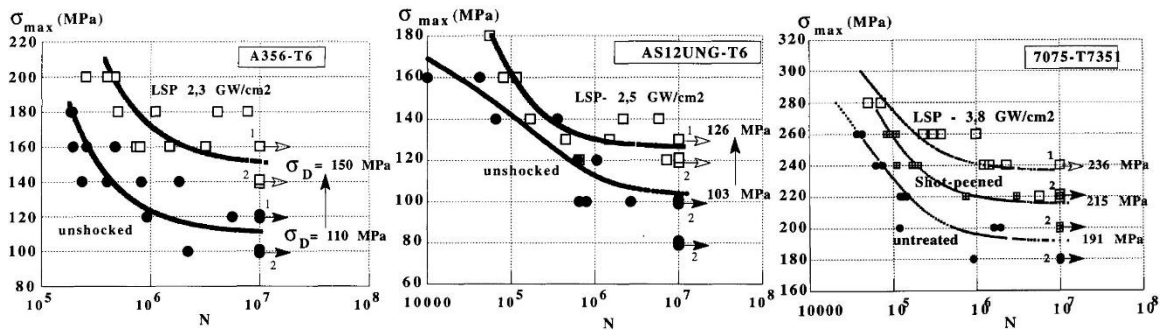


Fig. 2.5 σ_{max} - N curves for unshocked and shock peened aluminum alloys [114].

(b) Corrosion

Laser shock peening can also be used for improving the corrosion resistance of metallic materials. Several researchers have worked on the effect of laser shock peening on corrosion behavior of biodegradable magnesium alloys [111, 120] and stress corrosion cracking in steel alloys [121]. Sealy *et al.* has performed corrosion tests on laser shock peened MgCa alloy using potentiodynamic test in Hank's solution [111]. The correlation between laser shock peening, surface integrity, and corrosion was established in this paper. From the [Figure 2.6a](#), the corrosion rate of MgCa decreased with the application laser shock peening at 3W and 25% overlap and decreased further with increase in overlap ratio. But, the corrosion at 8W was higher than 3W due to the increase in surface roughness at higher laser power. Similarly, the corrosion potential also decreased with the application of laser shock peening and the trend can be seen in [Figure 2.6b](#).

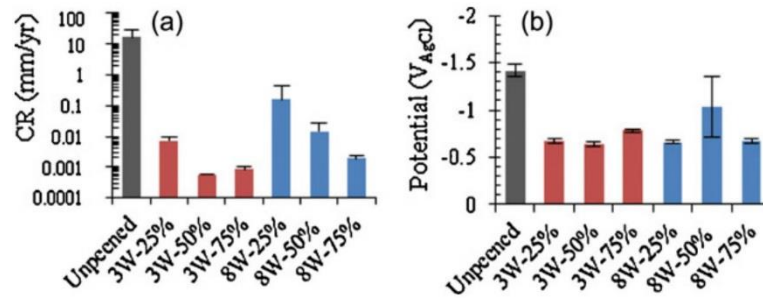


Fig. 2.6 Corrosion rate and corrosion potentials of MgCa samples [111].

2.3.3 Modeling LSP

In order to create a finite element model of LSP it is better to understand how the load is applied on a surface and dynamic response of the material under the high strain rates and the residual stresses formation due to the applied load. The following subsections explain each of these and how these were used in literature to model LSP.

(a) Solver

Commercial finite element code Abaqus can be used to determine both short duration shock wave response and resulting residual stresses. Abaqus/explicit is a non-linear elastic-plastic time integration finite element code specifically designed for short duration transient analysis. Whereas, Abaqus/Standard is a non-linear elastic-plastic implicit time integration code used for static calculations. Abaqus/Explicit can be used for both dynamic response of the material and determining the residual stresses in material but, the plastic deformation in material during LSP takes much longer than pulse duration and the convergence towards the residuals stress state is extremely slow. Abaqus/Standard can also be used for simulating the dynamic response of material and

determining the residual stresses in material but, the computational expense of determining the residual stresses is very-high. So, in order to simulate LSP both Explicit and Standard codes are used. Explicit is used to determine the dynamic response of material and the data is transferred to Standard for residual stress calculation. The flow chart of the simulation procedure is shown in [Figure 2.7](#).

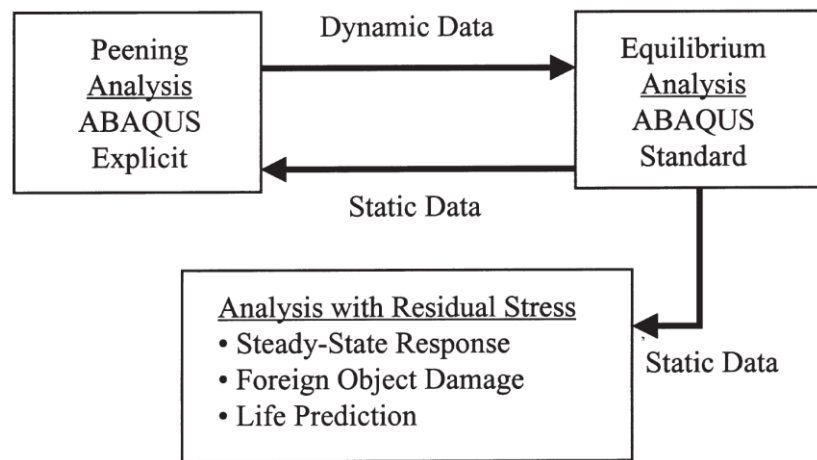


Fig. 2.7 LSP analysis procedure using Abaqus [122].

Similarly, finite element simulation of LSP including dynamic analysis can also be done using LS-DYNA for dynamic response of material and static stress analysis can be done using ANSYS, the simulation flow chart is shown in [Figure 2.8](#) below.

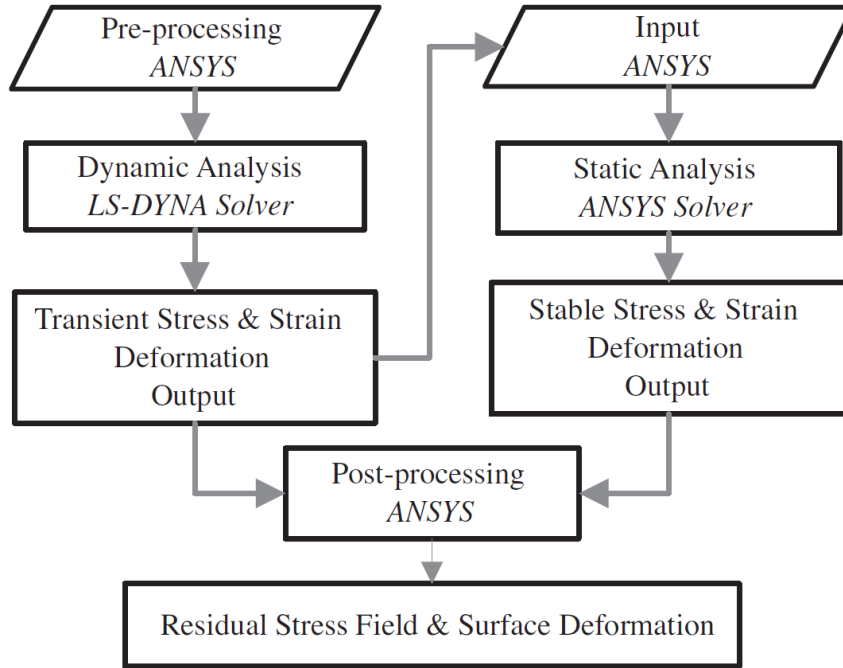


Fig. 2.8 LSP analysis procedure using LS-DYNA and ANSYS [123].

(b) Material model

For modeling high strain rate behavior of the materials due to LSP, the most common material model was Johnson-Cook (JC). The expression for equivalent strength for a given temperature T is given by

$$\sigma_{eq} = (A + B\varepsilon_{eq}^n) \left[1 + C \ln \left(\frac{\dot{\varepsilon}}{\dot{\varepsilon}_0} \right) \right] \left[1 - \left(\frac{T - T_0}{T_{melt} - T_0} \right)^m \right] \quad (2.1)$$

where T_0 is the reference temperature, T_{melt} is the melting temperature of material, ε_{eq}^n is the equivalent plastic strain, $\dot{\varepsilon}$ is the plastic strain rate, $\dot{\varepsilon}_0$ plastic strain rate in quasi-static state of the material and A, B, C, n, m are the material constants in Johnson-Cook model.

This model is considered as simplified representation of material's stress-strain

characteristic. In this model the equivalent strength depends on strain hardening, strain rate, and temperature but, the model did not include interdependency of the terms.

Bammann has developed an internal state variable (ISV) plasticity model for high strain rate, temperature, and hardening dependent constitutive model [124-126]. This constitutive model can predict deformation and failure in a material. LSP requires a material model that accounts for dynamic yield stress. A material user subroutine UMAT/VUMAT was coded to incorporate it into Abaqus. Below are the corresponding constitutive equations.

$$\dot{\underline{\sigma}} = \lambda \text{tr}(\underline{D}^e) \underline{I} + 2\mu \underline{D}^e \quad (2.2)$$

$$\underline{D}^e = \underline{D} - \underline{D}^p \quad (2.3)$$

$$\underline{D}^p = f(T) \sinh \left[\frac{\|\underline{\sigma} - \underline{\alpha}\| - \{R + Y(T)\}}{V[T]} \right] \frac{\underline{\sigma} - \underline{\alpha}}{\|\underline{\sigma} - \underline{\alpha}\|} \quad (2.4)$$

$$\dot{\underline{\alpha}} = h(T) \underline{D}^p - \left[\sqrt{\frac{2}{3}} r_d(T) \|\underline{D}^p\| + r_s(T) \right] \frac{\underline{\alpha}}{\|\underline{\alpha}\|} \quad (2.5)$$

$$\dot{R} = H(T) \underline{D}^p - \left[\sqrt{\frac{2}{3}} R_d(T) \|\underline{D}^p\| + R_s(T) \right] R^2 \quad (2.6)$$

where $\dot{\underline{\sigma}}$ is the flow stress which is a function of elastic strain \underline{D}^e . The evolution equations for the internal state variables $\underline{\alpha}$ and R are motivated from dislocation mechanics and are in a hardening-minus-recovery format. The kinematic hardening internal state variable $\underline{\alpha}$, representing directional hardening, is related to the dislocations in cell interior. The variable captures the softening effect due to unloading, also termed as Bauschinger's effect. The isotropic hardening internal state variable R is related to the

dislocation in walls and it captures the continued hardening at large strains. The use of internal state variable and evolution equations enable the prediction of strain rate history and temperature history effects.

The model uses nine temperature dependent functions to describe the inelastic response. They can be classified into three basic type: those associated with the initial yield, the hardening functions, and the recovery functions. The rate-independent yield stress $Y(T)$, the function $f(T)$ which determines when the rate-dependence affects after initial yielding, and the magnitude of rate-dependence of yielding $V(T)$ are assumed to be of the form:

$$V(T) = C_1 \exp(-C_2/T) \quad (2.7)$$

$$Y(T) = C_3 \exp(C_4/T) \quad (2.8)$$

$$f(T) = C_5 \exp(-C_6/T) \quad (2.9)$$

The kinematic hardening internal state variable, $\underline{\alpha}$ reflects the effect of anisotropic dislocation density, and the isotropic hardening internal state variable R , reflects the effect of the global dislocation density. As such, the hardenings are cast in a hardening-recovery format that includes dynamic and static recovery. The functions $r_s(T)$ and $R_s(T)$ are scalar in nature and describe the diffusion-controlled static or thermal recovery, while $r_d(T)$ and $R_d(T)$ are scalar functions describing dynamic recovery. Hence, the two main types of recovery that are exhibited by populations of dislocations within crystallographic materials are captured in the ISVs. The anisotropic hardening modulus $h(T)$, and the isotropic hardening modulus is $H(T)$. The description of individual constants C_1 - C_{20} are given in [Appendix](#).

$$h(T) = C_9 - C_{10}T \quad (2.10)$$

$$H(T) = C_{15} - C_{16}T \quad (2.11)$$

$$r_d(T) = C_7 \exp(-C_8/T) \quad (2.12)$$

$$R_d(T) = C_{13} \exp(-C_{14}/T) \quad (2.13)$$

$$r_s(T) = C_{11} \exp(-C_{12}/T) \quad (2.14)$$

$$R_s(T) = C_{17} \exp(-C_{18}/T) \quad (2.15)$$

(c) LSP Loading

In modeling laser peening (LSP), instead of simulating laser material interaction, the pressure wave that was generated during this process was simulated. During LSP, as the laser hits the metal surface, the plasma formed on the surface continues to absorb laser energy and releases that energy into metal surface as a pressure wave. This pressure wave was modeled as a function of both radial distance and peening time and is defined as follows [127, 128].

$$P(r, t) = P(t) \exp\left(-\frac{r^2}{2R^2}\right) \quad (2.16)$$

where $P(t)$ is the magnitude of pressure at any time t , r is the radial distance from the center of the spot, and R is the spot size. Each of these parameters significantly affect the compressive residual stresses induced in the material. For example, Peyre *et al.* observed that with increase in the laser spot size, the depth of compressive residual stresses increases significantly even though there was not a significant change in magnitude [129]. The pressure time history is defined using Gaussian temporal profile with short

rise time [114, 130-133]. Although the temporal profile was described as Gaussian, Braisted and Brockman used a triangular pulse because of very narrow pulse duration [122] (Figure 2.9). These spatial and temporal pressure distributions during LSP is neither uniform nor linear, so a subroutine DLOAD/VDLOAD can be used to apply these non-uniform shock pressure [128, 134]. This subroutine allows the pressure to vary with respect to both the radius of laser spot and time.

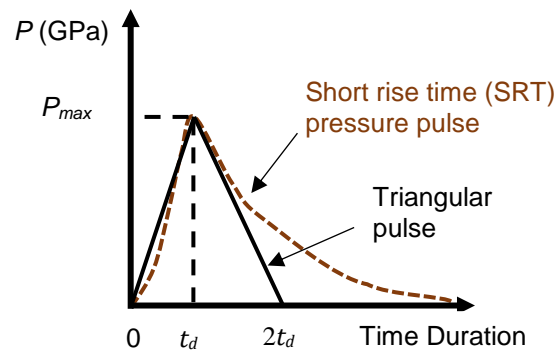


Fig. 2.9 Pressure-time profile of single LSP.

The depth and magnitude of compressive residual stresses in material depends on pulse pressure, spot size, pulse overlap, and pulse duration. These parameters affect the residual stresses generated in the material. However, the most important parameter is the pulse pressure which depends on the laser power and intensity. Increasing the laser intensity increases both depth and magnitude of compressive residual stresses but, the stresses in material reach saturation point after a particular laser intensity [114].

Warren *et al.* has simulated laser shock peening on AISI 52100 with laser spot size as $9\ \mu\text{m}$ and has observed that the residual stresses (Figure 2.10) in material increases as the

laser intensity increases but they saturate after 4 GW/cm² as the peak compressive residual stresses did not change significantly.

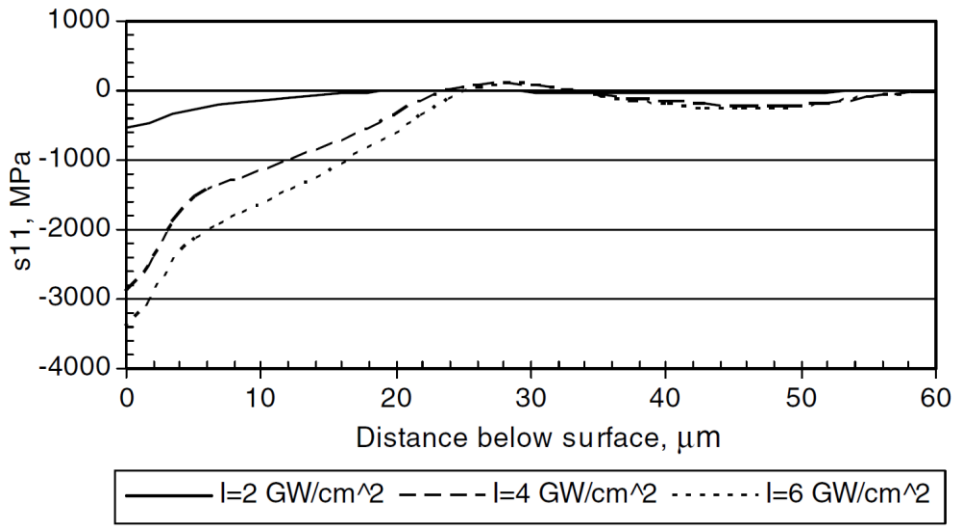


Fig 2.10 Effect of laser intensity on residual stresses in AISI 52100 shock peened for 40 ns with 9 μm spot size.

PART II: DIRECTED ENERGY DEPOSITION

2.4 Introduction to Directed Energy Deposition

According to ISO/ASTM 52900, directed energy deposition (DED) is defined as an AM process in which focused thermal energy fuses materials by melting as layers are being deposited [74]. In DED, raw materials can be in the form of metal powder or filament and the focused thermal energy to melt and deposit layers can be laser beam, electron beam, or plasma arc. Metal additive manufacturing is classified mainly into three categories: (1) directed energy deposition (DED), (2) powder bed fusion (PBF), and (3) sheet lamination. In DED, focused thermal energy is used to fuse materials by melting as they are being deposited. In contrast, PBF directs a thermal energy source onto a stationary bed of metal powder and thereby selectively fusing powder to form a layer. Sheet lamination ultrasonically bonds sheets of metal to form a final part. One of the main advantages of DED compared to PBF is that the build rate is typically 10 times faster. Also, the material composition can be changed on the fly. The disadvantage of DED is that surface finish is poor and requires additional post-processing. Also, internal features, such as conformal cooling channels, are difficult to print with DED.

2.5 Process Mechanism of Directed Energy Deposition

Laser Engineered Net Shaping (LENSTM) is one type of a DED process that was developed by Sandia National Laboratories in the 1990's. Optomec in Albuquerque, New Mexico, USA later commercialized the LENSTM process. A LENSTM system consists of a high-powered laser, a powder delivery system, a controlled atmosphere (optional), and a

computer-controlled positioning system. A schematic representation is shown in [Figure 2.11](#) below.

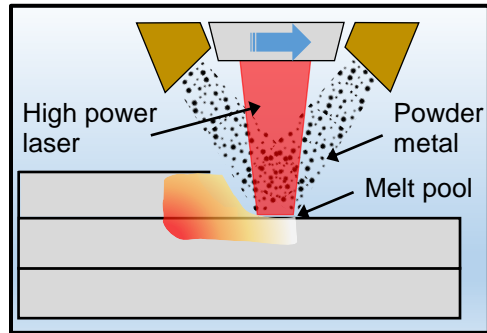


Fig. 2.11 Schematic representation of LENS™ process [135].

A solid substrate is used as a base plate for building the part, and the laser beam is applied on the substrate creating a melt pool. The powder particles are simultaneously injected into the melt pool through a powder delivery system. Next, the substrate is moved beneath the laser beam leaving behind a narrow deposit of material of prescribed thickness and height. Substrate height is adjusted to maintain constant focusing position. The same procedure is repeated until all the layers are printed creating the part. Powder is supplied to the deposition region via a carrier gas, and powder volume is regulated by powder delivery unit [136].

During the addition of layers in DED, residual stresses can develop in a part, which subsequently affect mechanical properties. Residual stresses developed in a material can be predicted by modeling the DED process. Modelling DED requires the following: (1) a moving thermal source (laser or electron beam), (2) a technique for addition of new layers, (3) a model for boundary conditions, and (4) a material model to

define material properties at elevated temperatures. Researchers have simulated different types of DED processes, including laser engineered net shaping (LENSTM) [137-145], direct laser metal deposition (DLMD) [146, 147], shape metal deposition (SMD) [148, 149], and laser cladding [150-152].

2.6 Literature Review on Modeling DED

2.6.1 Heat flux

A heat flux is typically used to model the heat source from additive manufacturing. The input heat flux applied on layers in DED is modeled based on the input energy source (*e.g.*, laser, electron beam, plasma arc). Heat flux models found in literature are provided in [Table 2.1](#). These heat flux models are used in different processes like laser engineered net shaping (LENSTM), laser cladding, and laser metal deposition and welding processes.

The most common heat flux model in a DED process is a Gaussian distribution function. This model was first proposed by Pavelic for modeling welding processes. It has the capability to model various melt pool parameters by changing few variables in the Gaussian function. The heat flux equation is given in [Table 2.1](#). The constant c in the equation represents the effects of reflectivity, beam distribution parameter, and the absorptivity of the workpiece material. The parameter r^2 in the model changes to $r^2 = x^2 + y^2$ for 3D models.

The other common heat flux model is a double ellipsoidal model proposed by Goldak *et al.* [153]. The main feature of this model is that it can be easily changed to represent both shallow penetration of an arc in welding and deeper penetration from a

laser and electron beam processes. The constants a , b , and c define the melt pool dimensions and these values are different for front and rear ellipsoids. The values of these constants depends on the specific heat source and material being modeled.

Table 2.1 Heat Flux (Q) Models

Heat flux equations		Ref.
$Q = \frac{cP}{\pi r_0^2} e^{-\left(\frac{2r^2}{r_0^2}\right)}$	Gaussian heat flux distribution function	[137, 138, 140, 145, 146, 151, 152, 154, 155]
<p>where, c = absorption coefficient P = laser power r_0 = initial radius r = current radius</p>		
$Q = \frac{6\sqrt{3} P\eta f}{abc \pi\sqrt{\pi}} e^{-\left[\frac{3x^2}{a^2} + \frac{3y^2}{b^2} + \frac{3(z+v_w t)^2}{c^2}\right]}$	Double ellipsoid model as laser heat source	[139, 148, 149, 156, 157]
<p>where, P = Laser power η = absorption efficiency f = process scaling factor a = transverse dimension of ellipsoid b = depth of melt pool c = longitudinal dimension of ellipsoid t = time v_w = heat source travel speed</p>		

2.6.2 Material deposition

In order to model deposition of layers during directed energy deposition (DED), most researchers use two types of techniques: quiet element method and inactive element method [137, 139, 143, 145, 147, 151, 154, 156-158]. In the quiet element method, unprinted elements are present in the model, but they are assigned reduced material properties. These properties are obtained by multiplying with a scaling factor. Elements with reduced properties will not affect the analysis. As the analysis progresses and these

quiet elements are ready to be “printed”, actual material properties are assigned to the quiet elements to establish their presence in the model.

Inactive elements is another approach that is similar to the quiet element method. However, the difference is that all the elements in layers that are to be deposited during DED process are deactivated at beginning of the analysis. Elements in each layer are activated in each step individually as the heat source acts upon that layer. Layers are reactivated one by one as the material is being deposited.

2.6.3 Boundary conditions

In DED, it is important to have boundary conditions to accurately calculate temperatures developed in layers during material deposition. These boundary conditions depend on the surrounding environment of the build platform. Most thermal models in literature have both convective and radiation heat transfer conditions on all surfaces [138, 139, 145-147, 149-151, 154, 157-159]. This allows for heat to escape the part into the surrounding medium (typically air, nitrogen, or argon). In a vacuum, Denlinger *et al.* did not use convective heat transfer boundary conditions in modeling electron beam direct manufacturing [156]. Only radiation heat transfer was considered. Other researchers included initial conditions for the model and maintained a base plate at constant temperature along with convective and radiation heat transfer boundary conditions [140, 145, 155].

2.6.4 Material properties

Due to thermal characteristics of the DED process, temperature-dependent properties of a material should be incorporated into the simulation. These temperature-

dependent properties account for phase transformation, melting, and re-solidification of the material. The transformation of material from liquid phase to solid phase can be defined by latent heat and specific heat. Most researchers used temperature dependent thermal conductivity, specific heat, and density [143, 145, 146, 160]. Other mechanical properties, such as a temperature dependent elastic modulus or thermal expansion, can be used to determine stresses and deformations developed in a model due to material deposition.

CHAPTER 3

EFFECT OF LAYER THICKNESS AND PEENING PRESSURE ON RESIDUAL STRESSES IN HYBRID PROCESSING BY LASER SHOCK PEENING

3.1 Introduction

I have developed this finite element model as a preliminary study to understand the effect of laser shock peening (LSP) in hybrid-AM process using selective laser melting. Many researchers have investigated the effect of LSP on different materials and confirmed that LSP can improve the properties by inducing compressive residual stresses [112, 122, 127, 161]. Additive manufacturing is a process of joining materials to make parts from a 3D model, usually layer upon layer, as opposed to subtractive manufacturing and formative manufacturing methodologies. Additive manufacturing processes, such as selective laser melting (SLM), selective laser sintering (SLS), and electron beam melting (EBM), can produce products with tensile residual stresses [95, 162]. It is hypothesized that these tensile stresses can be altered by employing laser shock peening between printed layers. With the change in residual stresses and increased hardness, the performance of a part can be improved or manipulated. This hybrid additive manufacturing approach enables one to design and print preferential mechanical properties for specific applications. In this study, hybrid additive manufacturing via powder bed fusion and laser shock peening was modeled in Abaqus. The effects of layer thickness and peening pressure on the residual stresses were studied.

3.2 Finite Element Modeling

3.2.1 Model geometry

A series of two-dimensional finite element models were developed in Abaqus Standard to simulate consecutive layers of selective laser melting (SLM) followed by laser shock peening (LSP) on Ti64. The simulation was based on the work from Sealy and Guo [110, 128] and Chao and Guo [163]. The objective was to model a hybrid additive manufacturing process, *i.e.* SLM and LSP, to determine the effect of successive printed layers on the enhanced mechanical properties from LSP. The simulation procedure applied a moving heat flux in a thermal model and imported the resulting temperatures into a stress model. Importing temperatures accounted for thermal strains caused by the heat flux. After allowing the temperatures to cool for 5 seconds, laser shock peening was applied to each printed layer via a shock pressure load. This process was repeated for each printed layer.

The work piece was divided into four parts: substrate, layer 1, layer 2, and layer 3, see [Figure 3.1](#). The substrate was 4 mm (length) by 1 mm (thickness). Each layer was 2 mm long. Three different layer thicknesses were investigated: 100 μm , 300 μm , and 600 μm . In each model, three layers were printed and subsequently peened. Layer build-up was accomplished by first deactivating the entire mesh and then activating each layer in each active heat flux step. The thermal model used 4-node linear diffusive heat transfer elements (DC2D4), and the stress model used 4-node bilinear plain stress elements with reduced integration (CPS4R). Plain stress elements were chosen as one single printed line was assumed to be a thin body.

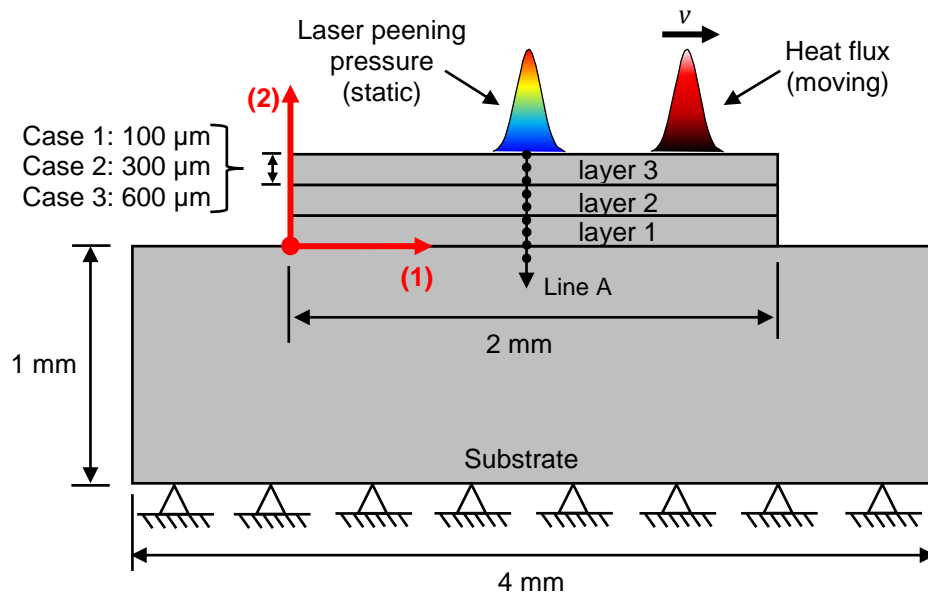


Fig. 3.1 Two-dimensional model of hybrid additive manufacturing by SLM and LSP.

3.2.2 Material model

The material used for this model was Ti64. The physical and thermal properties as well as the temperature dependent thermal and mechanical properties used in the analysis are shown in the [Appendix](#) [164-167]. At room temperature, the elastic modulus was 110 GPa and the yield strength was 910 MPa. At 1655 °C, the elastic modulus and yield strength decreased to 10% of that at room temperature. Since laser peening involves high strain rates (on the order of 10^6) that significantly affects the flow stress, future studies will incorporate more complex material models such as Johnson-Cook or an Internal State Variable (ISV) plasticity model to capture such rate dependent effects.

3.2.3 Thermal and mechanical loading

Thermal Model: The heat flux in the thermal model was applied using a DFLUX user subroutine in Abaqus/Standard. The output of the heat flux (Q) as a function of position (x) and time (t) was given by the following:

$$Q = \frac{CP}{\pi r^2} e^{-\frac{2(x-vt)^2}{r^2}} \quad (3.1)$$

where C is the absorption factor, P is laser power in watts, r is the laser beam radius in meters, and v was the scanning speed of the heat flux [168]. The process parameters for the applied heat flux during selective laser melting are given in [Table 3.1](#).

Table 3.1 Heat Flux Process Parameters during Selective Laser Melting

Laser power (W)	Scan speed (mm/s)	Layer thickness (μm)	Laser spot radius (μm)	Scan length (mm)
20	50	100, 300, 600	36	2

Stress Model: Laser peening was applied in the stress analysis after selective laser melting. To model laser shock peening, a simplified pressure load was applied to capture the highly transient, dynamic nature of a shock wave produced by plasma expansion. The laser spot size from peening was $500 \mu\text{m}$. The pressure pulse was assumed to be 2 to 3 times longer than a typical 5 to 7 ns laser pulse [130, 169]. The pressure pulse width was 20 ns, and the peak pressure was 1 GPa or 2 GPa. The peening pressure $P(r, t)$ as a function of both radial position and time is given by

$$P(r, t) = P(t) e^{-\frac{x^2}{2r^2}} \quad (3.2)$$

where $P(t)$ represents pressure at any time t , and r is the radius of the laser spot [170]. Typically, the pressure pulse as a function of time has a Gaussian profile with a short rise time [130-133]. In this study, a simplified triangular pulse of the pressure as a function of time was used (Figure 3.2). The pressure was applied in the center of the mesh.

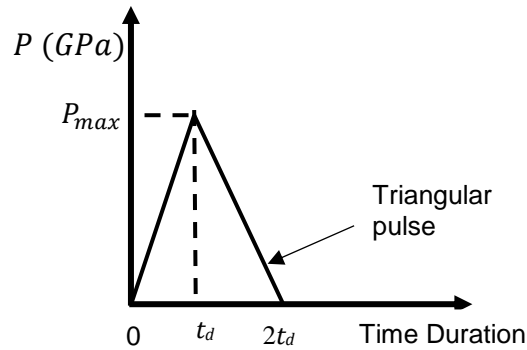


Fig. 3.2 Pressure-time history of a single pressure pulse from LSP.

3.2.4 Initial and boundary conditions

The initial temperature of the model was 20 °C. During the stress analysis, the nodal temperatures were imported from the thermal model as a prescribed condition during the active heat flux step. Heat was allowed to conduct through the material. No heat transfer boundary conditions were prescribed. The displacement and rotation degrees of freedom along the bottom of the substrate were constrained in the analysis.

3.3 Results and Discussion

The temperature and stress fields are plotted along the depth direction at the center of the mesh, *i.e.* along Line A in Figure 3.1. The temperature profiles are shown

when the heat flux was directly over Line A. For the stress profiles, the heat flux passed over the layer and the stress S11 was plotted 0.1 ms after the pressure pulse.

3.3.1 Displacement

The magnitude of displacement (U) for a 100 μm , 300 μm , and 600 μm layer thickness exposed to a 1 GPa and 2 GPa peening pressure is shown in Figure 3.3. It was observed that 1 GPa peening pressure did not cause severe plastic deformation. The maximum transient deformation was approximately 10 μm during peening. The maximum deformation after relaxation was approximately 2-3 μm . At 2 GPa, the deformation was considerably higher. The deformation following relaxation was greater than 200 μm . Also, it was observed that deformation in 300 μm layer model was higher than in the 600 μm layer model. This may be attributed to the expansion during the thermal load varies depending on layer thickness and affects the deformation.

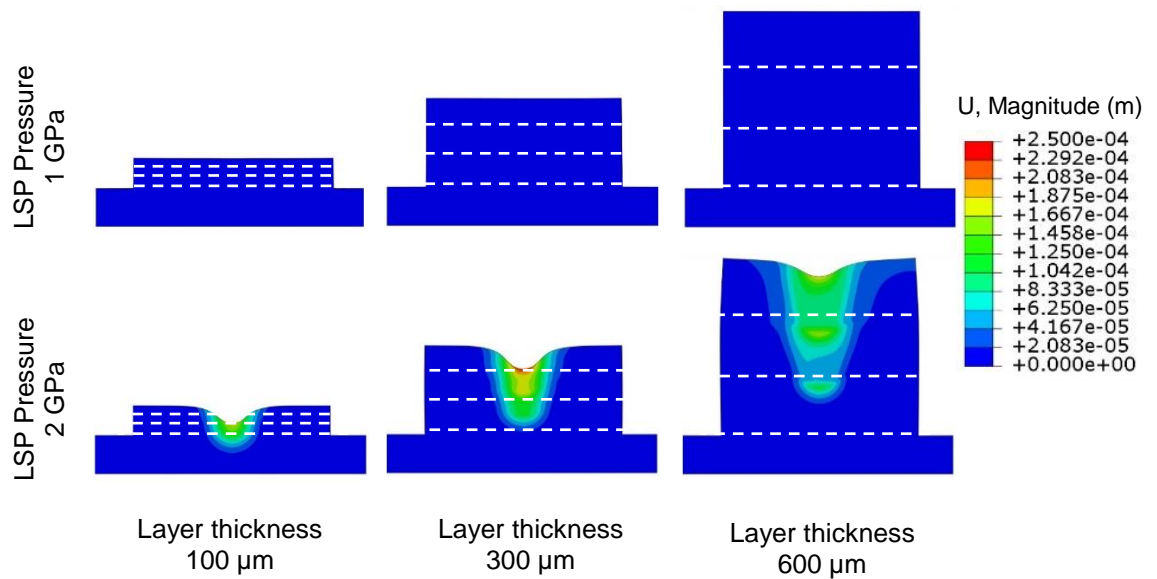


Fig. 3.3 Magnitude of deformation in a 100 μm , 300 μm , and 600 μm layer thickness model exposed to a 1 GPa and 2 GPa peening pressure.

3.3.2 Nodal temperatures

Nodal temperatures from the applied heat flux for a 100 μm , 300 μm , and 600 μm layer thickness are shown in Figure 3.4. The blue triangles represent the temperatures while printing layer 1, the red squares represent the temperature while printing layer 2, and the black circles represent the temperature while printing layer 3. In selective laser melting, the top surface is constantly changing by adding subsequent layers. Therefore, note that a zero depth corresponds to the top of layer 3. If the layer thickness is 100 μm (Figure 3.4a), the top of layer 1 corresponds to a depth of 200 μm . For a 600 μm layer thickness (Figure 3.4c), the top of layer 1 corresponds to a depth of 1200 μm .

The nodal temperatures exceeded 3000 $^{\circ}\text{C}$ on the top surface. For the given heat flux conditions, the results indicated that when the layer thickness was 100 μm (Figure 3.4a), the temperature in layer 1 while printing layer 2 was between 800 $^{\circ}\text{C}$ and 1800 $^{\circ}\text{C}$. The temperature was relatively high considering that the solidus temperature of Ti64 was 1605 $^{\circ}\text{C}$. This indicates that part of layer 1 was re-melted during the printing of layer 2. When printing layer 3, the temperature in layer 1 ranged from 200 $^{\circ}\text{C}$ to 600 $^{\circ}\text{C}$.

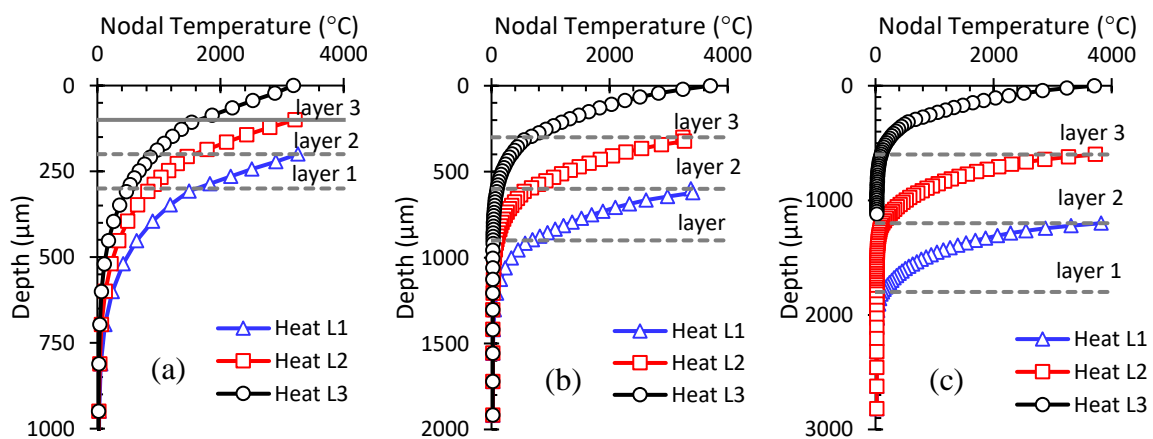


Fig. 3.4 Nodal temperatures (NT11) along the depth direction below applied heat flux for a (a) 100 μm , (b) 300 μm , and (c) 600 μm layer thickness.

When the layer thickness was 300 μm , the maximum temperature in layer 1 while printing layer 2 was approximately 450 $^{\circ}\text{C}$. The maximum temperature in layer 1 while printing layer 3 was 75 $^{\circ}\text{C}$. As the layer thickness increased to 600 μm , the temperatures in layer 1 while printing layer 2 was nearly room temperature. The results indicated that for the given heat flux in this study, the layer thickness needs to be greater than 300 μm to avoid significantly raising the temperature of previously laser peened layers. Models such as this can help determine the critical layer thickness for hybrid additive manufacturing processes so that thermal loads from SLM do not negate enhanced mechanical or physical properties in prior layers.

3.3.3 Residual stress after LSP

The residual stress (S11) along the depth direction after laser shock peening with a pressure of 1 GPa (Figure 3.5) and 2 GPa (Figure 3.6) with a layer thickness of 100 μm , 300 μm , and 600 μm is shown below. For a layer thickness of 100 μm , 1 GPa was not significant enough to cause compressive residual stress in the printed layer, see Figure 3.5a. The stress in each layer was a tensile and between 400 MPa and 800 MPa. When the pressure increased to 2 GPa (Figure 3.6a), significant compressive residual stresses were imparted in layers 1, 2, and 3. When printing subsequent layers, *e.g.* layer 3, the heat flux caused the compressive stress from peening in layers 1 and 2 to turn tensile. The layer thickness was relatively small such that the thermal load from the subsequent layer's heat flux may be expanding the work piece such that the compressive residual stresses are reversed. Furthermore, the higher pressure (2 GPa) coupled with such a thin layer resulted in layer 1 shifting to compression when layer 3 was peened.

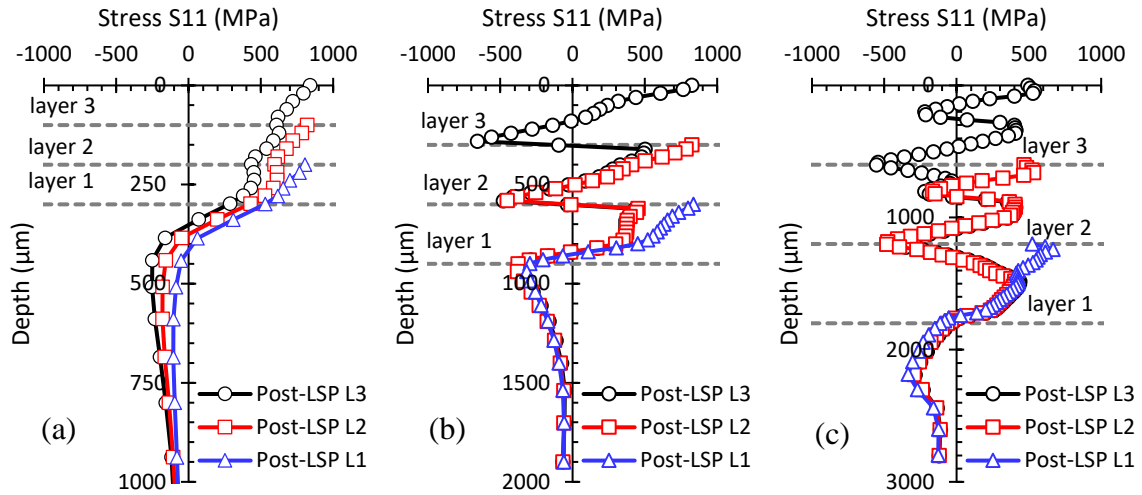


Fig. 3.5 S11 along the depth direction after laser peening with a pressure of 1 GPa for (a) 100 μm, (b) 300 μm, and (c) 600 μm layer thickness.

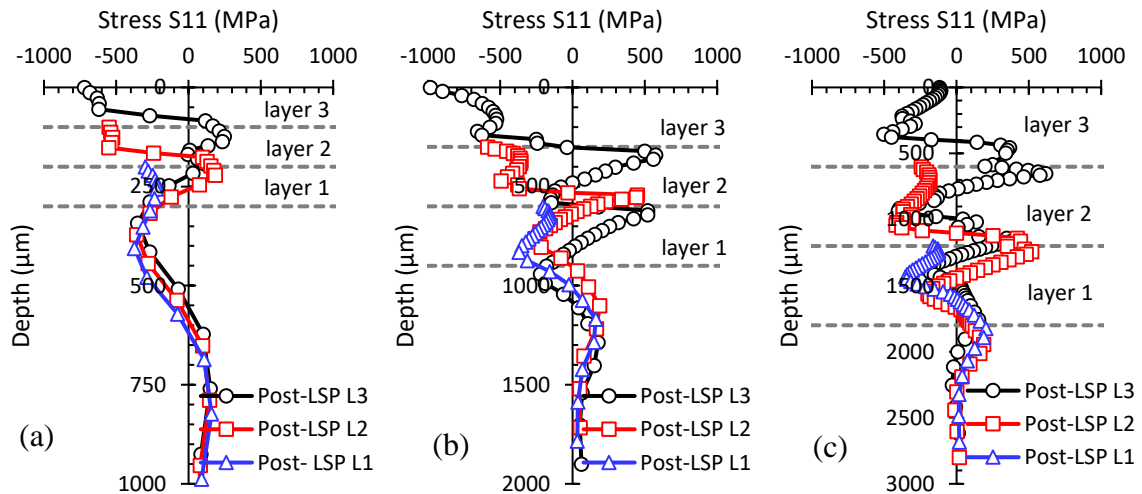


Fig. 3.6 S11 along the depth direction after laser peening with a pressure of 2 GPa for (a) 100 μm, (b) 300 μm, and (c) 600 μm layer thickness.

In the 300 μm layer thick model, a similar trend was observed. The high tensile stresses in between the layers were due to the fact that the heat flux from a subsequent layer caused significant thermal expansion and resulted in high tensile stresses. With 2 GPa peening pressures, the maximum compressive stress was more than 900 MPa. The

tensile stresses in layer 1 developed during thermal loading of layer 2 remained tensile even after the peening layer 2.

Similarly, in the 600 μm layer thick model, the tensile stresses joining two layers were due to the thermal loads and the compressive stresses within the layers were due to peening. The compressive stresses were not as high as those in the 300 μm layer thick model because all of the heat energy accumulated in one thick layer. Significant thermal expansion ensued and led to tensile stresses on the order of 500 MPa. Subsequent peening did not have a significant effect because the layers were much thicker.

The maximum tensile stresses occurred at the boundary between layers. This was due to an excessive amount of thermal expansion during thermal loading and the fact that layers were added as plates on one another. In reality, the starting material in SLM is powder which would be deposited and melted to the substrate. In that case, there should be less thermal expansion than what was observed in a plate.

3.4 Summary and Conclusions

This work presents a finite element model of a hybrid additive manufacturing process that couples selective laser melting (SLM) and laser shock peening (LSP). The model adds a new layer that is subsequently laser peened. The process is repeated for three layers. The objective was to quantify the effects of single shot LSP after printing multiple layers. In other words, how does the thermal load from subsequent printed layers influence the residual stress imparted by LSP in prior layers? The effects of laser peening pressure and layer thickness on the residual stress fields were analyzed. This model established the fact that layer thickness plays a critical role on the resulting residual stress

fields. If a layer is thicker than a critical value, the thermal loads from printing more layers will not significantly alter the residual stress field in previous layers. For thinner layers, more substantial pressures are needed to cause deeper compressive residual stresses. The results suggest that peening conditions can eventually be optimized to have the desired residual stress contour for a given application. Further studies are needed to incorporate microstructural evolution from hybrid printing multiple layers in a model.

CHAPTER 4

EFFECT OF LAYER PEENING FREQUENCY ON RESIDUAL STRESSES DEVELOPMENT IN HYBRID PROCESSING BY LASER SHOCK PEENING

4.1 Introduction

The overarching objective of this chapter is to investigate the role laser peening (LSP) has on layer-by-layer processing of 3D printed metals. This chapter primarily focuses modeling hybrid-AM by coupling directed energy deposition (DED) and LSP to understand the role of hybrid process parameters on temporal and spatial residual stress development. A finite element model was developed to help understand thermal and mechanical cancellation of residual stress when cyclically coupling printing and peening. Results indicate layer peening frequency is a critical process parameter and highly interdependent on the heat generated by the printing laser source. Optimum hybrid process conditions were found to exist that favorably enhance mechanical properties. With this demonstration, hybrid-AM has ushered in the next evolutionary step in additive manufacturing and has the potential to profoundly change the way high value metal goods are manufactured.

Recall that hybrid additive manufacturing (hybrid-AM) processes are defined as the use of additive manufacturing (AM) with one or more secondary processes or energy sources that are fully coupled and synergistically affect part quality and/or process performance. The explanation of this definition was presented in [Chapter 1](#). In this chapter, laser engineered net shaping (LENSTM) process was coupled with laser peening (LSP) as the secondary process. The schematic of this hybrid-AM is shown in [Figure 4.1](#).

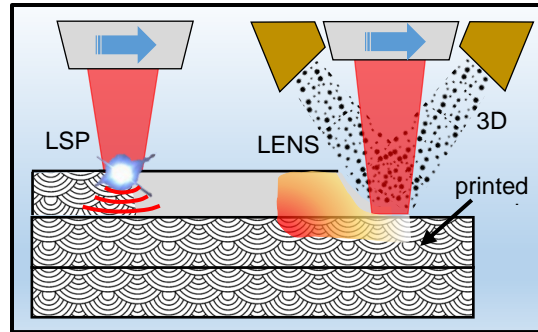


Fig. 4.1 Schematic representation of hybrid-AM by laser peening.

Although this hybrid-AM process has the capability to improve mechanical properties, there are new manufacturing challenges associated with coupling peening and 3D printing. Thermal and mechanical cancellation must be better understood for this approach to meaningfully impact the manufacturing industry. Thermal cancellation refers to the *loss* of favorable residual stress from heat. Mechanical cancellation refers to the *loss* of favorable residual stresses from unfavorable stress redistribution.

In hybrid-AM, thermal cancellation occurs when a new layer is added on a peened surface (Figure 4.2a); the heat generated during material deposition has the potential to cancel any beneficial mechanical properties induced by LSP. This will eliminate bulk property generation in layers. This phenomenon of eliminating/reducing the magnitude of favorable compressive residual stresses from the additive manufacturing heat source is referred to as “thermal cancellation.”

Mechanical cancellation in hybrid-AM is the reduction of compressive residual stresses present below the surface due to application of LSP on subsequent layers. Since peening induces both compressive and tensile residual stresses below the surface of parts, peening new layers on top of previously peened layers redistributes residual stresses

fields. The tensile component of peening one layer may diminish the magnitude of compressive residual stress of a previous layer. Consider the case in Figure 4.2b, when a new LSP is applied on the top surface the stress profile developed by new LSP redistributes/cancels the magnitude of compressive residual stress from previous LSP.

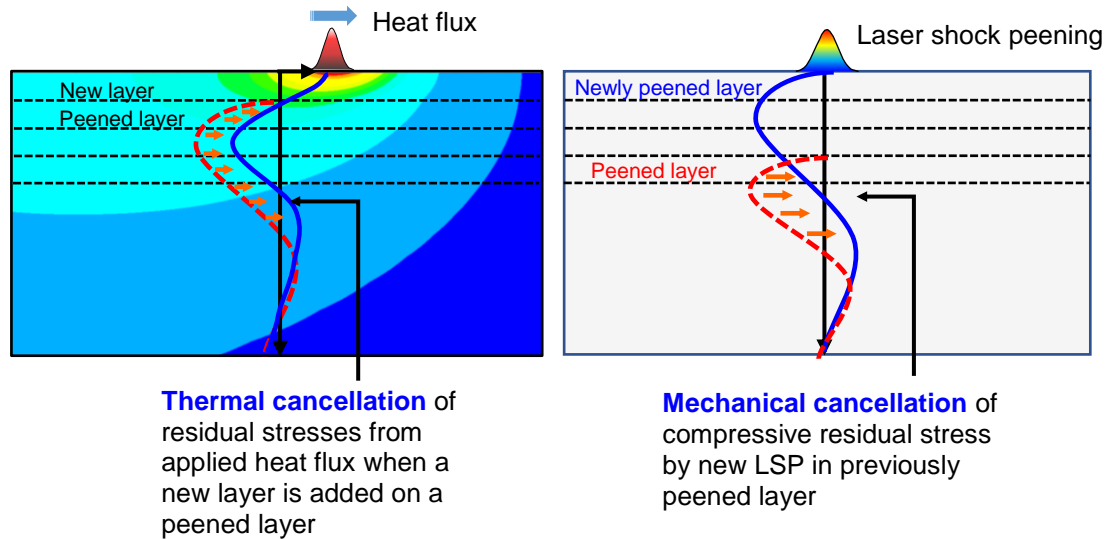


Fig. 4.2 Schematic representation of (a) thermal cancellation and (b) mechanical cancellation.

AISI 52100 steel was used as material to model thermal and mechanical cancellation in hybrid-AM by DED and laser peening. This type of steel is mainly used in tool and die industry. The main problem with current tools is the easy crack propagation in tool reduces fatigue life of tool steels. It is well known that with laser peening compressive residual stresses are induced in subsurface of material reducing crack propagation by improving fatigue life. Hybrid-AM by laser peening improves bulk mechanical properties of tool by inducing preferential compressive residual stresses. Compressive residual stresses in materials do not allow cracks to propagate, improving the fatigue life of tool.

The objective of this chapter is to introduce thermal and mechanical cancellation of residual stresses in hybrid-AM by laser peening and to begin understanding the phenomenon through finite element (FE) analysis. A two-dimensional finite element model of hybrid-AM by laser peening was developed in Abaqus to examine thermal and mechanical cancellation with varying the layer peening frequency. The evolution of residual stresses from different peening frequencies and its effect on thermal and mechanical cancellation were studied.

4.2 Finite Element Modeling

4.2.1 Model geometry

In this study I have developed a two-dimensional model as shown in the [Figure 4.3](#). Total number of layers deposited on the substrate were 20; each layer was 30 mm wide and 0.3 mm thick. Only 20 layers were added to model residual stress development in hybrid-AM process to study thermal and mechanical cancellation without increasing computational cost. The substrate below the layers had dimensions of 30 mm by 8 mm. The elements in the thermal model used to evaluate temperatures developed during the application of moving heat source were DC2D4 type, which stands for 4-node diffusive conductive heat transfer. The elements in the stress models were CPE4 which is 4-node bilinear plane strain element to capture the stresses due to the heat source and due to application of laser peening. Plane strain elements were used assuming there was no strain in the Z-direction (perpendicular to the plane formed by axis 1 and 2). The element size in the layers was $20 \times 20 \mu\text{m}$, and a gradient mesh rule was given to the elements along axis-2 in the substrate to accurately capture all the temperatures and stresses in

layers while not increasing the computational time. The addition of material during AM was simulated by means of successive discrete activation of new set of elements in the model at the beginning of each step.

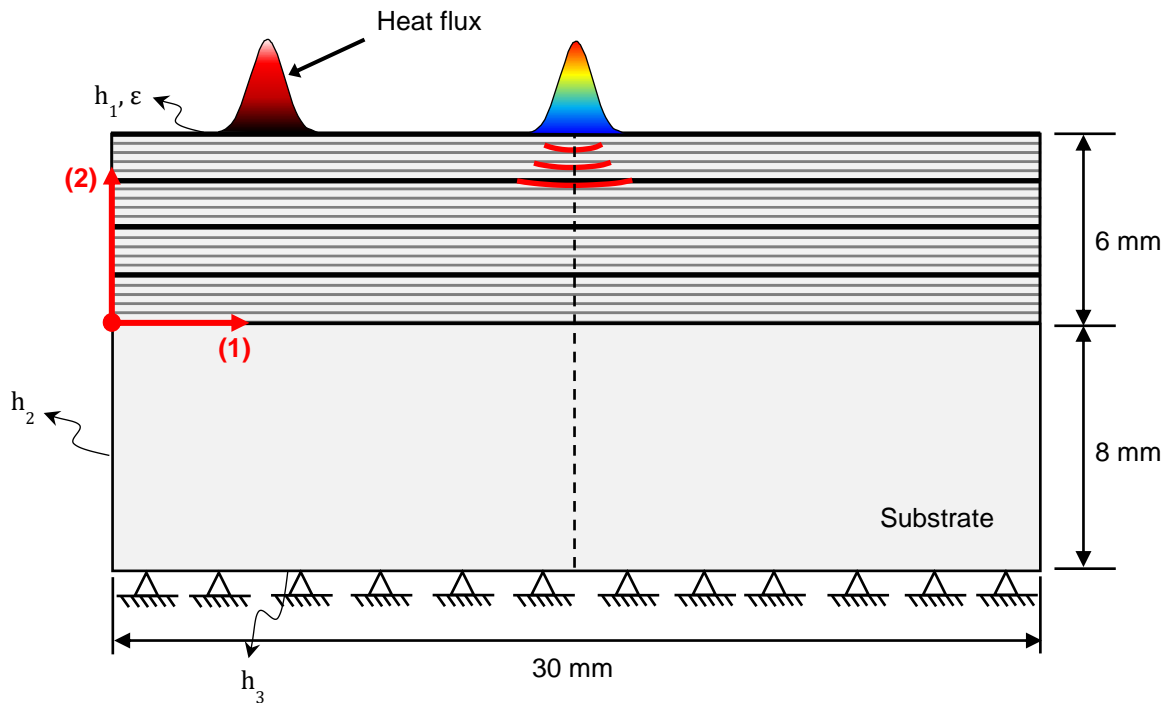


Fig. 4.3 Schematic of hybrid-AM model with thermal and mechanical boundary conditions.

This model also proves that the dynamic response of the material from LSP and formation of residual stresses in material can be modeled using Abaqus/Standard. Unlike it was mentioned in literature review where most of the researchers used Abaqus/Explicit to model LSP. Because, in this thesis hybrid-AM model was developed where modeling AM process includes deactivation and activation of elements for the addition of layers. Abaqus/Explicit does not allow to deactivate and activate elements during a simulation as explicit solves the equations based on previous steps. If the elements were absent in the

next step the explicit solver will not be able to solve the equation. While the standard solver uses all the equations present in the model to solve the equations and when a new set of elements were added standard calculates the equations based on the new equations. So, in this thesis standard solver was used to both AM and simulate laser shock peening.

4.2.2 Material model

Hardened steel AISI 52100 was considered for this simulation because of its wide range of applications in tool and die industry. In heat transfer analysis, thermo-physical properties were used to evaluate temperatures and can be found in the [Appendix](#). In stress analysis without LSP, temperature dependent elastic and plastic properties (young's modulus, Poisson's ratio, yield strength) were give along with temperature-dependent thermal expansion of the material. For the stress analysis with LSP, internal state variable plasticity model (ISV model) was used (see [Appendix](#)).

4.2.3 Loading and boundary conditions

Heat transfer analysis: The schematic ([Figure 4.3](#)) above shows different loading and boundary conditions in the analysis. On top of each layer, a moving heat flux was applied to simulate the temperatures developed in the DED process. The heat flux was modeled as a non-uniform distributed flux as a function of position and time. The heat flux given by the equation below follows Gaussian distribution and was modeled using the Abaqus user subroutine DFLUX.

$$Q = \frac{CP}{\pi r^2} e^{\frac{-2(x-vt)^2}{r^2}} \quad (4.1)$$

where C is absorption coefficient, P is laser power in watts, r is the radius of laser beam in meters, v is scanning speed of heat flux in m/s. Table 4.1 identifies LENSTM process parameters that were used to simulate AM in this chapter.

Table 4.1 Heat Flux Process Parameters

Laser power (W)	Laser spot size (mm)	Scan speed (mm/s)	Scan length (mm)
400	1.36	10	30

Thermal boundary conditions were applied on model in terms of conduction, convection, and radiation. Heat transfer in between the layers was given in terms of a conduction coefficient (k). The heat conducted into the substrate was given in terms of convection at the bottom of the substrate ($h_3 = 1000 \text{ W/m}^2 \text{ K}$). A forced convection and radiation heat transfer boundary conditions were given on the top surface of each layer while depositing ($h_1 = 100 \text{ W/m}^2 \text{ K}$, $\varepsilon = 0.62$) to account for heat transferred through inert gas blown into the melt pool and through radiation to the surrounding environment. Free convection to the surrounding environment was given as a boundary condition on the edges of layers and substrate ($h_2 = 25 \text{ W/m}^2 \text{ K}$).

Stress analysis: The pressure wave from LSP was modeled as a function of radial distance and peening time as mentioned in literature review. The pressure varying with peening time follows a short rise time pulse as shown in figure below. It was assumed that the pressure duration was three time longer than pulse duration and glass was used as confining layer. Under these assumptions a peak pressure of 5.17 GPa was applied during laser shock peening to induce compressive residual stresses into the material. The load was

applied on material for 30 ns in loading step and was allowed to relax for 10^{-4} s for the material to relax and form residual stresses in material.

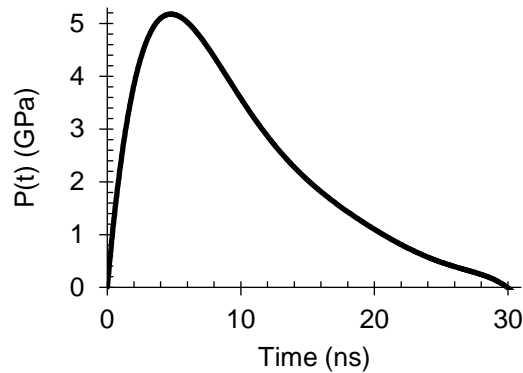


Fig. 4.4 Variation of pressure with respect to time.

Table 4.2 LSP Process Parameters

Pressure duration (ns)	Spot size (mm)	Peak pressure (GPa)	Pulse duration (ns)	Laser intensity (GW/cm^2)	Laser power (J)
30	2.25	5.177	10	3.59	1.42

4.2.4 Simulation procedure

A commercial finite element software Abaqus/Standard was used to simulate hybrid processing by directed energy deposition (DED) and laser peening. The simulation procedure is shown in the flow chart (Figure 4.5) below. To simulate this process, two models of identical geometry were developed: one model for heat transfer analysis with DC2D4 elements and the other for stress analysis with CPE4 elements. In the heat transfer analysis, temperatures developed during DED were computed and imported to a stress analysis. The stresses from the temperatures and LSP were determined using static/general stress analysis.

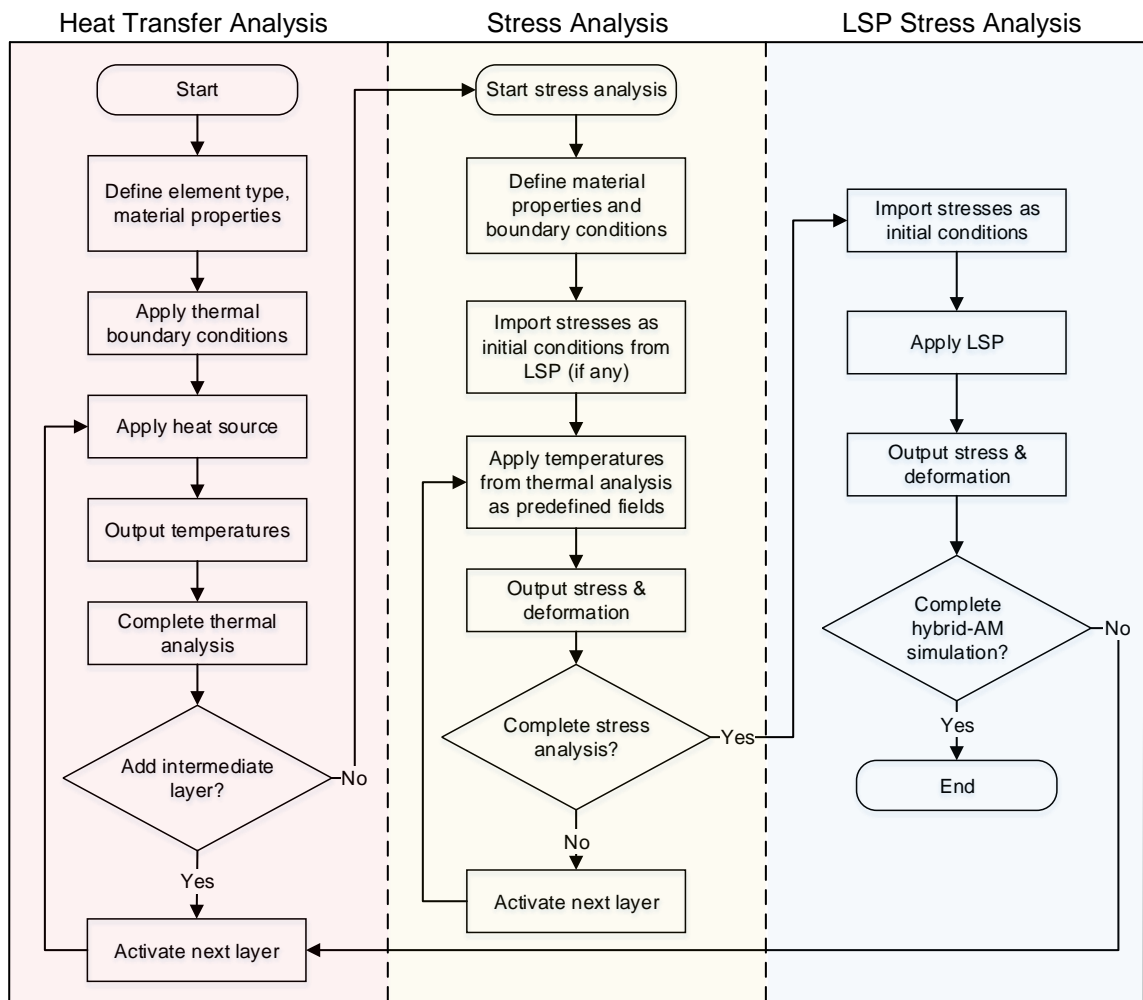


Fig. 4.5 Flow chart for simulation procedure of hybrid-AM by LSP.

In hybrid-AM by laser peening, first a heat transfer analysis was developed. The temperatures developed in heat transfer were imported to stress analysis to calculate stresses from temperatures. Now in the laser peening analysis, the stresses from adding layers were imported as initial conditions, and laser peening was applied completing the first peening cycle. In the next cycle, another set of layers were added in heat transfer analysis and stresses from those temperatures were calculated with stresses from previous

laser peening as initial conditions followed by a laser peening analysis. The same cycle was repeated until all layers were printed.

Case study ($C_i = 5$, $n_t = 20$): To explain the simulation procedure, a case study was done with laser peening on every fifth layer (number of printing layers in each cycle $C_i = 5$) until twenty layers were deposited ($n_t = 20$). In this simulation, there were four cycles/iterations. Each cycle contained a heat transfer analysis, a stress analysis, and a laser peening analysis. In the first heat transfer analysis, layers 1-5 were added one-by-one and heat flux was applied on each layer to incorporate temperatures generated in an AM process along with the thermal boundary conditions. These temperatures were imported to a stress analysis of five printed layers to compute stresses. Now, the stresses generated by adding 1-5 layers in AM process were imported to a laser peening analysis as initial conditions. In laser peening analysis, a single laser peening was applied on the fifth layer and stresses developed were computed. This completes one of the four cycles of hybrid-AM process. In second heat transfer analysis, layers 6-10 were added one-by-one with heat flux applied on each layer. Next, similar to previous stress analysis, the temperatures were imported to evaluate stresses developed, but here along with temperatures, stresses were also imported from previous laser peening analysis as initial conditions. This was to determine the effect of addition of new layers on a laser peened surface in terms of residual stresses. The stresses from stress analysis of 1-10 printed layers were imported as initial conditions and laser peening was applied on tenth layer inducing compressive stresses. This completes the second cycle. Like the second cycle, in third cycle, layers 11-15 were added, and stresses were calculated by importing temperatures as predefined fields and stresses from second laser peening as initial

conditions and laser peening is applied on the fifteenth layer. Similarly, the final set of layers were added, and stresses were computed.

4.3 Results

4.3.1 Final residual stresses from different layer peening frequencies

The final residual stresses developed in each model are plotted below (Figure 4.6). In the plot, the curve 20L SA represents stresses in a AM model with no LSP and the curves 20L LSP, 10L LSP, 5L LSP, 3L LSP, 1L LSP represents laser peening after every 20 layers (equivalent to an external surface treatment in this model), 10 layers, 5 layers, 3 layers, and 1 layer, respectively. The stresses developed in direction-1 for all the models developed, and were plotted along a vertical line at the center of the model. A full residual stress field map is shown in Figure 4.7 for each condition.

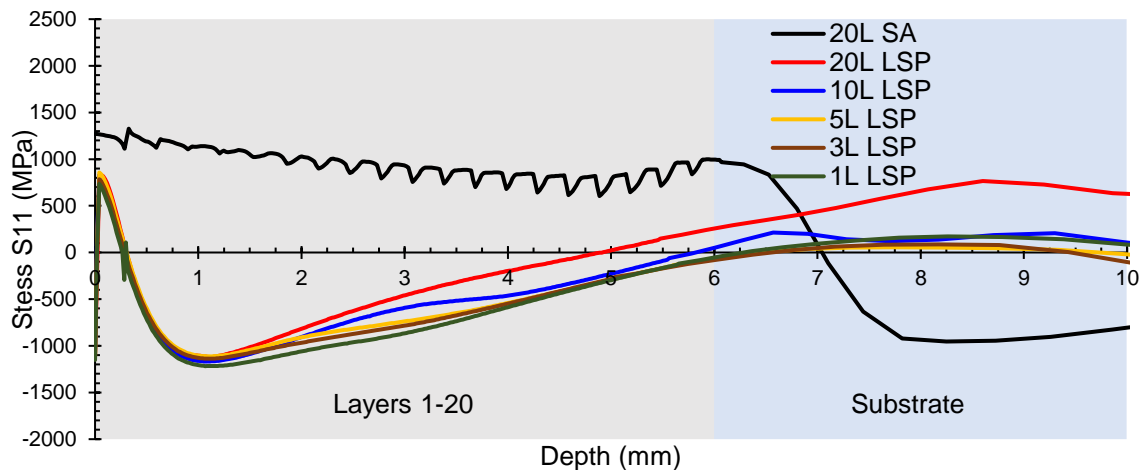


Fig. 4.6 Stress profiles comparison of AM model with hybrid-AM models.

In the Figure 4.6, 20L SA represents the stress model of DED process without any LSP. From the plot, it was observed that the stresses in layers were tensile because of the

continuous application of heat flux on layers. This flux expands the material and forms tensile residual stresses in layers. The magnitude of stresses in layers varied from 600 MPa to 1325 MPa.

The next curve in the plot (Figure 4.6) was 20L LSP *i.e.*, a single laser shock peening was applied on the surface after twenty layers were added in DED process. The tensile stresses from adding layers were turned compressive and a peak compressive residual stress of -1120 MPa was developed. The residual stress field from 20L LSP is shown in Figure 4.7. The compressive residual stresses from a single laser shock peening on a DED part reached a depth of 4.9 mm before turning tensile. This case is not a hybrid-AM process as laser peening was done only on the top surface. Therefore, the peening was not fully coupled; rather they were sequentially coupled as would be the case in a traditional surface treatment.

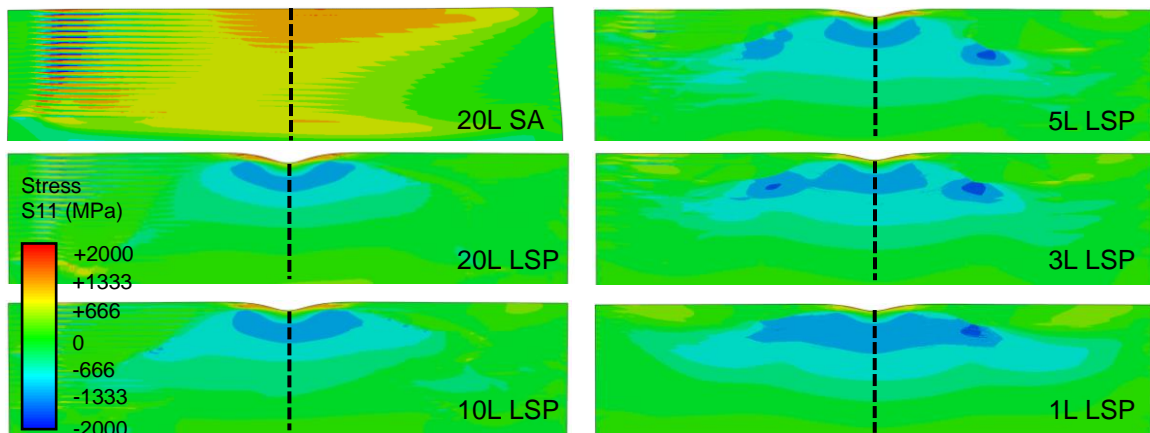


Fig. 4.7 Residual stress fields developed in each model.

The next plots were four hybrid-AM by LSP processes with different layer peening frequencies. From the plot, it was observed the depth of compressive residual stresses

increases as the peening frequency increases from peening every 20 layers (4.9 mm) to peening every 5 layers (6.5 mm). Further decreasing peening frequency to every 3 layers slightly increased the reversal depth to 6.58 mm. This may be due to saturation of residual stresses. For peening every layer, the depth decreased to 6.3 mm. The magnitude of compressive stress for all the cases were in the range of -1120 MPa to -1220 MPa.

The [Table 4.1](#) below shows the width and depth of compressive residual stresses with a magnitude of -650 MPa or higher. [Figure 4.7](#) shows a 2D the residual stress field distribution. The blue regions correspond to stress fields greater than -650 MPa. From the table and figure below, it was observed that as the peening frequency decreases, the width and depth of residual stress regions were increasing. This was because as the frequency decreased the layers were peened more number of times increasing the compressive residual stress regions. That is, more frequent peening resulted in a more sustained residual stress band.

Table. 4.1 Width and Depth of Compressive Residual Stress Region Greater than -650 MPa

Model	Width (mm)	Depth (mm)
20L SA	n/a	n/a
20L LSP	12.22	2.54
10L LSP	15.29	2.59
5L LSP	16.53	3.18
3L LSP	18.54	3.54
1L LSP	22.09	3.66

4.3.2 Residual stress evolution

(a) *LSP every 10 layers*

In this case of hybrid-AM by LSP, the curves ([Figure 4.8](#)) were plotted along the dotted line shows the stress profile development in direction-1 along the depth below the

surface as the layers were being added. The stress profile when a new layer added was represented as solid line and laser peened layer was represented with dotted line (this applies to all the stress vs depth plots in this paper).

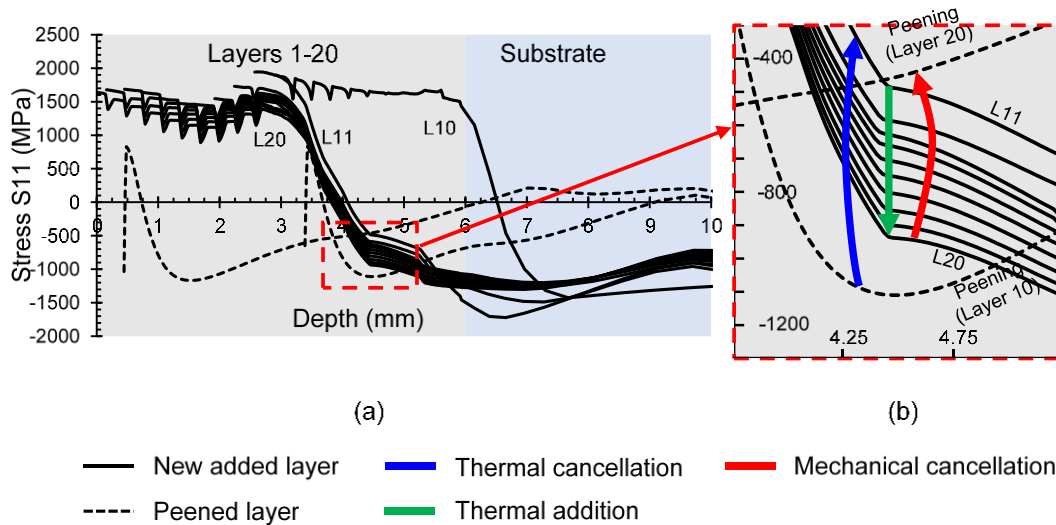


Fig. 4.8 Stress profile evolution of hybrid-AM model with laser peening every 10 layers.

In the [Figure 4.8a](#), the line L10 represents stresses in layers after printing ten layers. This was similar to the DED only model curve (*i.e.*, 20L SA in [Figure 4.6](#)), and maximum tensile stresses developed in layers was 1900 MPa. The peening layer 10 in [Figure 4.8b](#) represents the stresses after the laser peening was done on tenth layer. From this curve, it was observed that all the tensile stresses present in ten layers were converted to compressive after tenth layer was laser peened, and the peak compressive stress induced was -1110 MPa. Now, a new layer (11th layer) was added on the laser peened layer (*i.e.*, 10th layer). Here some interesting process phenomenon were observed. In the newly added layer, tensile stresses were developed as expected from an AM process, but

in the laser peened layer below it, the peak compressive stress reduced from -1100 MPa to -490 MPa. This reduction in peak compressive stress when a new layer was added on laser peened layer was called “thermal cancellation” (see [Figure 4.8b](#)). This was due to the heat conduction from layer 11 to layer 10 causing an expansion of material in layer 10 and reducing the amount of compressive stress. In the next step, the 12th layer was added. Similar to the previous layer, tensile stresses were developed in layer 12, but in the laser peened layer (10th layer) the compressive stresses increased from -490 MPa to -590 MPa. This increase in compressive stress in the peened layer due to the addition of new layers was called “thermal addition.” At the end of adding the 20th layer, there was a peak tensile stress of 1660 MPa in layers 11-20 and compressive stress was approximately -938 MPa in the 10th layer, implying there was an increase of -448 MPa in the 10th layer due to thermal addition. Next, another laser peening was applied on layer 20. This laser peening induced a peak compressive stress of -1170 MPa. Another interesting phenomenon observed here was the compressive stress in the 10th layer before applying laser peening on the 20th layer was -938 MPa, but after the 20th layer was laser peened this compressive stress in the 10th layer reduced to -456 MPa. This reduction in compressive stress in layer 10 after the 20th layer was laser peened is called “mechanical cancellation.” This may be due to the hook shape development of stress profile after laser peening. This makes the stresses tensile after a certain depth. As there exist compressive stresses before applying LSP on the 20th layer, this made the new stress profile more compressive than previous model (20 LSP). This may be the reason why the depth of compressive stresses in peening every 10 layers model was 6.25 mm while it was 4.9 mm in LSP on 20th layer only case.

(b) LSP every 5 layers

In this case, laser peening was applied every fifth layer. Next, another five layers were added, and laser peening was applied on the tenth layer. The process was repeated until all 20 layers were added. Figure 4.9 shows stress profile evolution in the 1-direction along the depth as new layers were added on a peened surface.

The curve L5 in Figure 4.9a represents the stress profile after adding five layers. When LSP was applied on the fifth layer, the tensile stresses present in layers 1-5 turned compressive. In the next step, the 6th layer was added, and stresses in the 6th layer were tensile toward the surface as expected; however, stresses further below the surface where laser peening was applied were more compressive (Figure 4.9a). Instead of thermal cancellation as observed in the previous case (LSP on every 10 layers), thermal addition made the stresses more compressive at this depth. This thermal addition was continued until the 10th layer was added. On the 10th layer, LSP was applied, and mechanical cancellation was observed. A similar trend of thermal addition and mechanical cancellation were observed for the next cycle: layers 11-15. In the next step, the 16th layer was added. Thermal cancellation was first observed followed by thermal addition as the layers were being added until layer 20. Laser shock peening was applied on the 20th layer. Instead of mechanical cancellation, mechanical addition was observed in laser peened layer (layer 15). When laser peening was applied on the 20th layer, instead of mechanical cancellation as we have seen in all the plots above, “mechanical addition” was observed (Figure 4.9b). Mechanical addition is defined as addition of compressive stresses in previously peened layers when a newly added layer in AM process was peened.

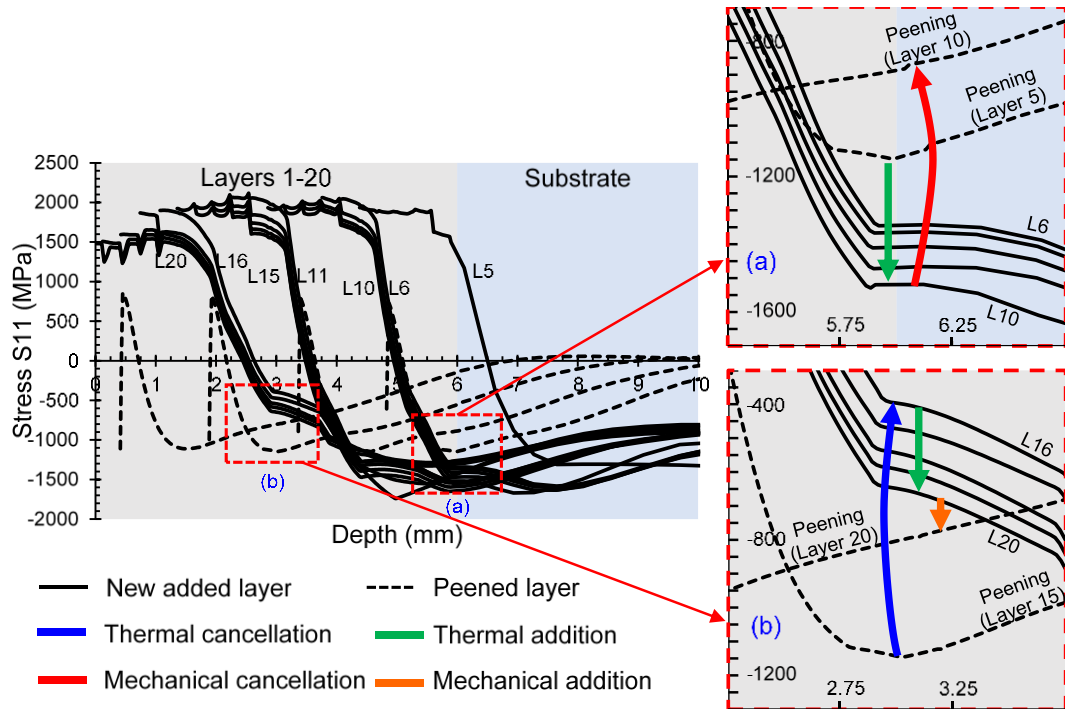


Fig. 4.9 Stress profile evolution of hybrid-AM model with laser peening every 5 layers.

(c) *LSP every 3 layers*

In this case, laser peening was applied every 3 layers. After the addition of 3 layers, laser peening was applied on it, and compressive stresses were developed. Next, a fourth layer was added inducing tensile stresses in it and reducing compressive stresses in laser peened layer by thermal cancellation. Two more layers were added which increased the compressive stresses in the peened layer (*i.e.*, thermal addition), and then laser peening was applied on layer 6. This induced compressive stress in layer 6 and increased the magnitude of compressive stresses in layer 3, which is referred to as mechanical addition (Figure 4.10b). Mechanical addition was observed because of increased peening frequency. In this case, every third layer was peened. The thickness of three layers was 0.9 mm, whereas the depth of peak compressive stress induced by LSP was greater than 1

mm. Therefore, mechanical addition was observed. In the next step, three more layers were added and peened and the same phenomenon (*i.e.*, thermal cancellation, thermal addition, and mechanical addition) were observed in the same order for all the cycles until 18 layers were added.

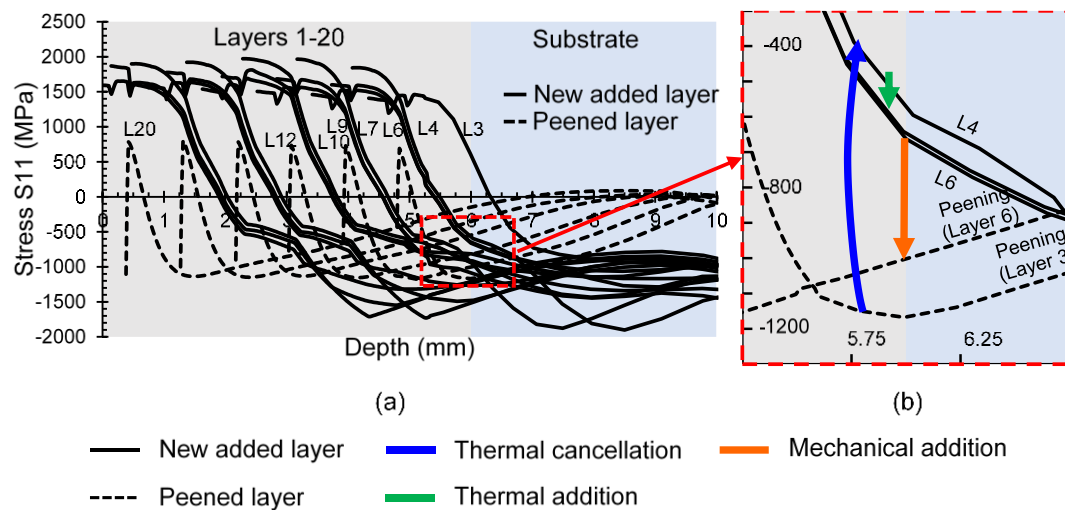


Fig. 4.10 Stress profile evolution of hybrid-AM model with laser peening every 3 layers.

(d) LSP every layer

In this case, laser peening was applied on every layer. When a new layer was added on a peened layer, the compressive stresses in the peened layer decreased (*i.e.*, thermal cancellation). After LSP, compressive stresses increase in a peened layer (*i.e.*, mechanical addition). The same cycle of thermal cancellation and mechanical addition was observed for all 20 layers. This stress evolution is plotted below (Figure 4.11).

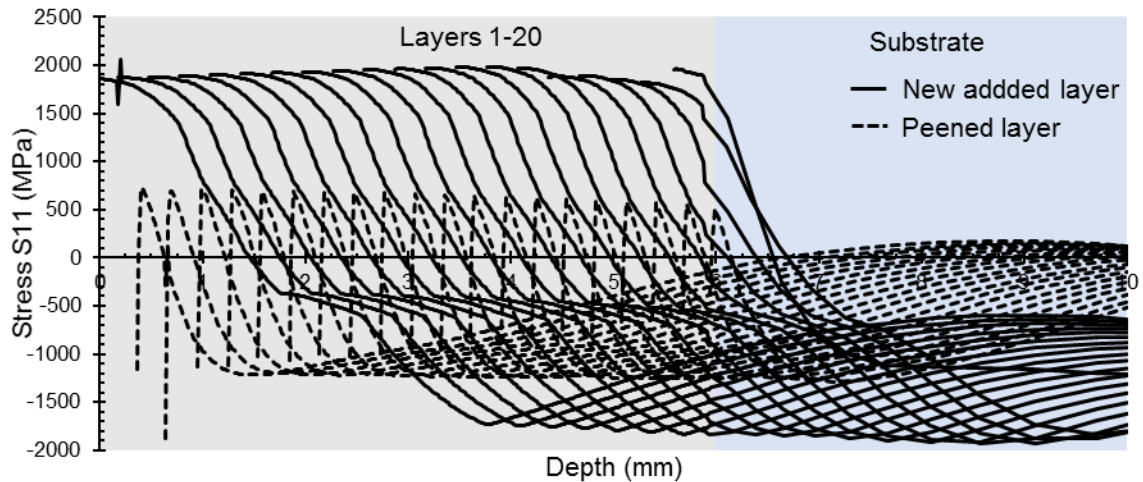


Fig. 4.11 Stress profile evolution of hybrid-AM model with laser peening every layer.

4.3.3 Step history evolution of stresses

All the plots until this point are local time histories of individual models, but the step histories of these models conveys more information. The following sections represent the residual stress variation at element 44250, which is at the center of the top center of the substrate. This element was chosen in order to have a comparable location across all models. These plots show the changes in stress values as the number of layers are being added. Each step corresponds to the addition of a new layer or laser peening of a layer.

(a) *LSP every 10 layers*

Figure 4.12 shows the step history after laser peening every 10 layers. In the plot, the first 10 steps indicate the variation of stresses at element 44250 as the layers 1 through 10 were added. The 11th step indicates the application of LSP on layer 10 and is represented by blue circles in the plot. The stress in the element was a tensile 1500 MPa

until the addition of layer 10. When LSP was applied on layer 10, the stress decreased to -670 MPa. The change in stress was approximately 2.17 GPa. Further addition of layers from 11 to 20 maintained the stresses as compressive. When LSP was applied on the 20th layer, the compressive stress decreased from -1250 MPa to -75 MPa. With the application of LSP every 10 layers, the stresses changed from tensile to compressive and then back tensile. Each time the change in stresses were on the order of gigapascals, which is significant for stress overloading.

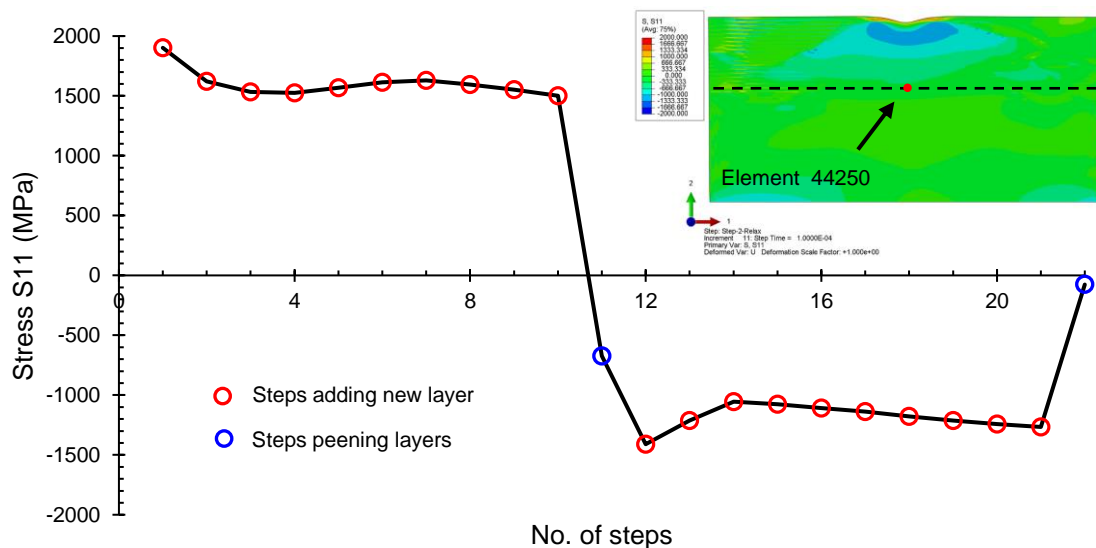


Fig. 4.12 Variation of residual stresses at element 44250 in laser peening every 10 layer model.

(b) LSP every 5 layers

In this model, the stress at element 44250 changed from tensile to compressive after layer 5 was peened. With LSP, a tensile stress of 1500 MPa turned compressive and a stress of -1120 MPa was observed implying a change in stress of 2.6 GPa (Figure 4.13). As the layers were being added, the stresses in the element remained compressive until a

peening was applied on 10th layer (step 12), which decreased the magnitude of compressive stresses by 650 MPa. This change in magnitude further increased to 1100 MPa when the 15th layer was peened (step 18). When LSP was applied on the 20th layer (step 24), the reversal in stress between printing and peening further increased to 1500 MPa. This is significant because the dramatic reversals in stresses between printing and peening can affect performance based on the step history of the stresses.

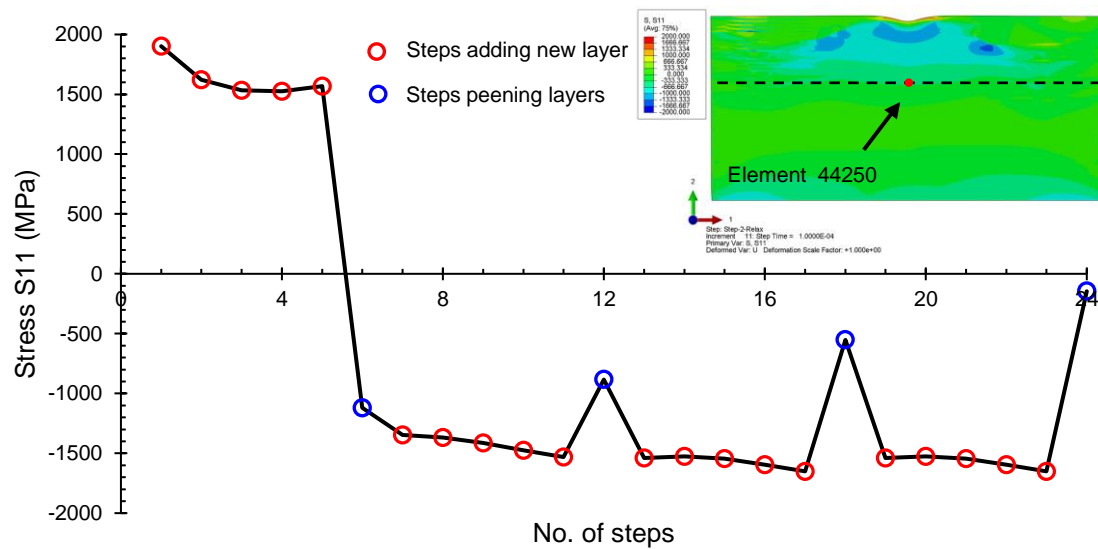


Fig. 4.13 Variation of residual stresses at element 44250 in laser peening every 5 layer model.

(c) *LSP every 3 layers*

Figure 4.14 represents the step history evolution of stresses in hybrid-AM by laser peening every 3 layers. From the plot, it can be observed that the stresses were tensile with a magnitude of 1435 MPa after the first three layers were added. With the application of LSP, these tensile stresses turned compressive to -1090 MPa. After the addition of 4th layer on the peened surface (step 5), the stresses became tensile (325 MPa)

unlike the models above which stayed compressive. This may be because of the heat from addition of 4th layer conducting into the layers below allowing the material to expand thereby inducing tensile stresses. After LSP was applied on the 6th layer (step 8), and the stresses remained compressive with the addition of new layers. After printing the 9th layer (step 11), the stresses at the element became more compressive as new layers were added and less compressive as the layers were being peened. By the end of the simulation, the stresses were tending to tensile.

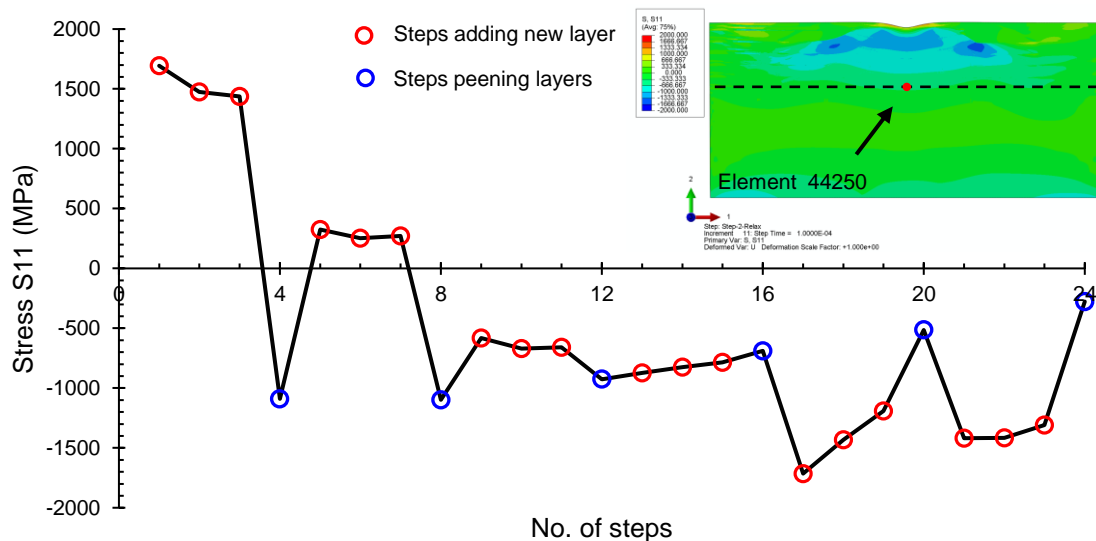


Fig. 4.14 Variation of residual stresses at element 44250 in laser peening every 3 layer model.

(d) *LSP every layer*

In Figure 4.15, the odd number steps indicate the stress values after the addition of new layers, and the even step numbers indicate the stress values after the particular layers were peened. In this case of hybrid-AM by peening every layer model, large changes in stress were observed. For example, after the addition of a layer, the stress was

approximately 1900 MPa. After LSP was applied on layer 1, the stress dropped to -200 MPa, *i.e.*, with the application of LSP there was a change in stress of 2.1 GPa. Similarly, the change in stress varied from 2.1 GPa to a few hundreds of megapascals as the layers were being added. Until this point, the new added layers induced tensile stresses while the LSP induced compressive stresses. After the addition of the 11th layer, this trend was reversed. That is, after adding 11 layer, the stresses became compressive instead of tensile while the stress due to LSP became tensile instead of compressive. This trend continued until all the remaining layers were added.

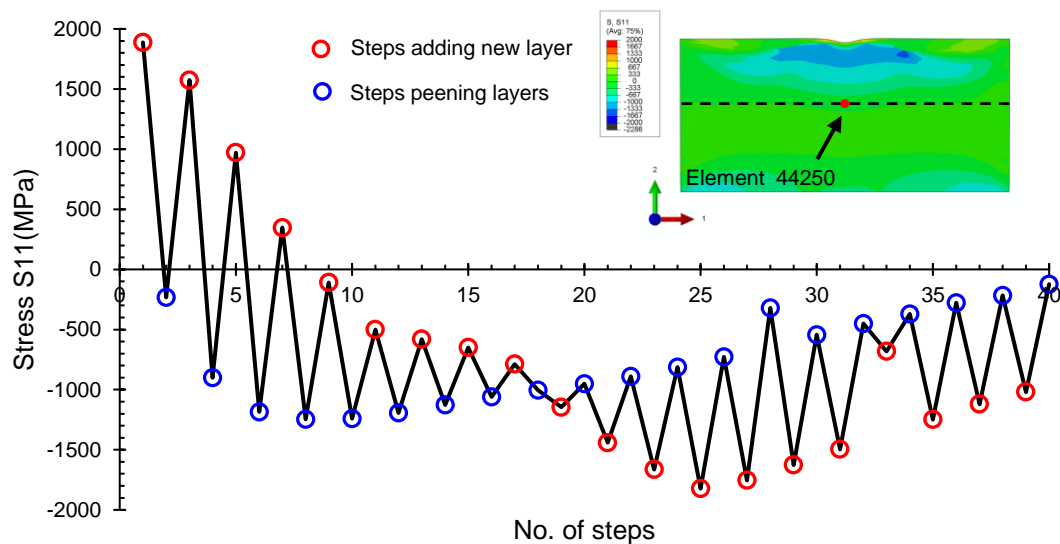


Fig. 4.15 Variation of residual stresses at element 44250 in laser peening every one layer model.

Experimental work done by R. Logé's group at the Laboratory of Thermomechanical Metallurgy at the Ecole Polytechnique Federale De Lausanne (EPFL) in Switzerland was used to validate trends observed in the model [59]. R. Logé's group investigated the use of LSP in selective laser melting to control residual stress.

Experimentally measured residual stress profiles using the hole drilling technique after hybrid-AM by laser shock peening is shown in Figure 4.16 [59]. Austenitic SS 316L was printed on a Concept Laser, GmbH in Germany. Once a prescribed number of layers were built, the samples were re-introduced to the build chamber for subsequent printing.

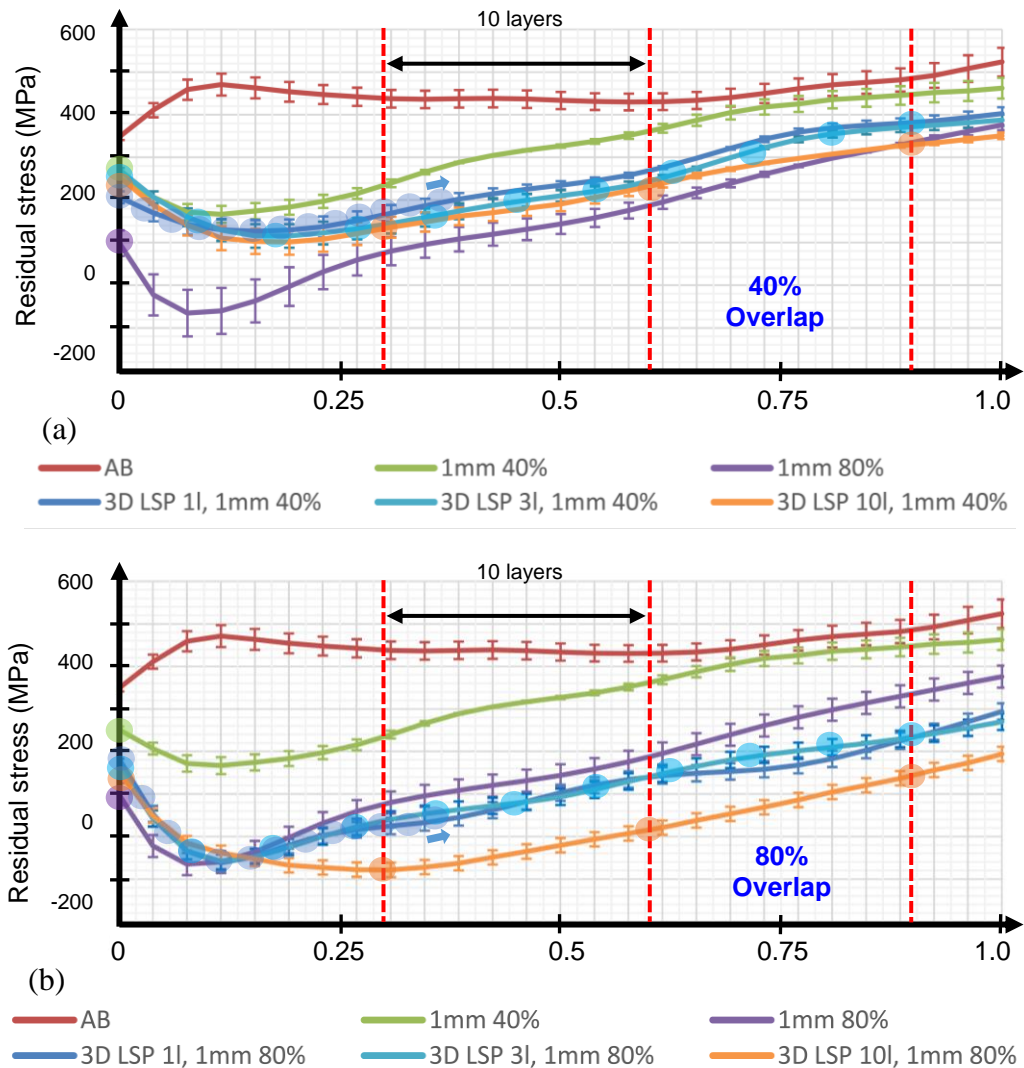


Fig. 4.16 Experimentally measured residual stress (hole drilling technique) on austenitic SS 316L after hybrid-AM by laser shock peening using M2 PBF printer; (a) 40% and (b) 80% overlap ratios. Circles indicate depth at laser peened layers. Modified from [59].

The results compared an as-built sample (without laser peening) to ones that were laser peened on the external surface (1 mm spot size with 40% and 80% overlap) and hybrid-AM samples (3D LSP samples; 1 mm spot size with 40% and 80% overlap) where laser peening occurred every 1, 3, or 10 layers. At 40% overlap (Figure 4.16a), the maximum compressive residual stress (CRS) and depth of the CRS increased 34% and 69% on average, respectively. At 80% overlap (Figure 4.16b), the magnitude of the CRS did not increase significantly compared to externally peened surface; however, the depth of the CRS increased for the hybrid-AM samples and may have indicated saturation point was reached due to the high amount of overlap. Interestingly, peening every 10 layers was shown to have deeper residual stresses than peening every one or three layers at 80% overlap. These results showed that hybrid-AM by LSP can improve the properties of material by inducing favorable CRS into the layers.

Certain similarities and differences were observed when the experimental results were compared to simulation results from this chapter. The similarities include the secondary process which is LSP, formation of tensile stresses in layers without the application of LSP, and the formation of residual stresses in the material from hybrid-AM process.

There were some dissimilarities between experimental results and simulations. First and foremost was that the primary AM process, which was powder bed fusion (PBF) in the experiments and directed energy deposition (DED) in the simulation. The main difference was the heat affected zone between PBF and DED. The heat affected zone in PBF was minimal compared to a directed energy deposition (DED) process.

The next difference was the type of material. Even though both materials are steels, the AISI 52100 used in simulations has very high yield strength of 2 GPa, thereby increasing the magnitude of compressive residual stresses either during the addition of layer or during the hybrid-AM process.

It should also be mentioned that the model used a single peening while the experimental data used overlapping peening. Single peening ignores the effects from neighboring peens that will influence the final residual stress profile. Future finite element models will include overlapping laser peening to more accurately capture the final stress field.

By comparing the experimental and simulation model, it can be summarized that even though the processes or the processing conditions are different in both hybrid-AM cases, favorable compressive residual stresses were observed. In the simulated results, peening at a higher layer frequency with DED increased the depth of the compressive residual stress until a saturation point was reached. In the experimental data, the opposite trend was observed. The experiment using PBF showed that less frequent layer intervals produced deeper compressive residual stresses. The reason for the difference is likely attributed to the heat affected zone created by each AM process. Both the simulation and the model show that there are not significant changes in the magnitude of the residual stress from layer-by-layer peening.

CHAPTER 5

SUMMARY, CONCLUSIONS, AND FUTURE WORK

This work aims to accomplish the following: (1) define hybrid additive manufacturing (hybrid-AM) in relation to the well-established definition of hybrid manufacturing from the International Academy of Production Engineering (CIRP); (2) survey the literature on hybrid-AM processes; (3) develop a finite element model of hybrid-AM by laser shock peening (LSP); and (4) understand thermal and mechanical cancellation of residual stresses during hybrid-AM processing. Understanding thermal and mechanical cancellation is new manufacturing knowledge that could benefit several industries, including medical, aerospace, automotive, and tooling and die.

From the 2D finite element model of hybrid-AM by DED and LSP, it was shown that layer-by-layer peening during additive manufacturing (AM) induced compressive residual stresses in the workpiece that were not completely cancelled from heat or mechanical redistribution. Critical hybrid process parameters were identified, such as layer peening frequency, peening intensity (includes laser power and spot size), and layer thickness. It was shown that decreasing layer peening frequency (*i.e.*, peening more frequently) from 20 to 5 increases the depth of compressive residual stresses (CRS). The depth of CRS saturated below a peening frequency of every 5 layers. That is, peening more frequently than every 5 layers did not improve the depth of CRS. In single peening mode, the peak CRS below the surface was similar (± 100 MPa) for all layer peening frequencies. Interestingly, the width and thickness of the CRS, referred to as the CRS band, increased with more frequent layer peening. Peening every layer had the widest and thickest CRS band. Based on these results, it is hypothesized that peening fewer layers

with multiple peenings would be equivalent to peening every layer with a single peening. Multiple peenings should increase the width and thickness of the CRS band.

The stress profile evolution in the model with a layer peening frequency of 10 exhibited thermal cancellation, thermal addition, and mechanical cancellation. When peening every 5 layers, in layers 5 and 10, thermal addition and mechanical cancellation were observed. In layer 15, thermal cancellation and mechanical addition were observed. When peening every 3 layers and 1 layer, no mechanical cancellation was observed. This may be due to high peening frequency. The depth of the peak CRS from peening a layers reached the previously peened layers below and resulted in an increased CRS. This indicates complex residual stress histories exist that are dependent on the location in the workpiece. Understanding these histories may be important in designing for performance. In tool steels, the reversals in stress from thermal and mechanical cancellation were observed to be ranging from 100's of megapascals to a few gigapascals. Hybrid processing of a tool steel may result in short cycle fatigue failure when coupling printing and peening because of the dramatic reversals in CRS.

The future work includes the validation of results from these simulations by conducting experiments based on the simulation parameters. The simulations concluded that thermal and mechanical cancellation of the residual stresses exist during the hybrid-AM process and these phenomena have to be verified experimentally by measuring the stresses in build after the addition of layers on a peened surface. Another future work includes determining the effect of cyclic thermal and mechanical loading on the microstructure of steel. In this thesis, a single laser peening was applied on layers, further studies include multiple laser shock peenings on each layers with LSP overlap and find

the effect of change in overlap ratio of these multiple peenings to have maximum compressive residual stresses. Another future study includes to find maximum distance between the peens on a layer to have minimum favorable stresses in layers. That is, how far can the peens be placed to have favorable stresses?

APPENDIX

Material properties of AISI 52100**Table A.1** Physical Properties of AISI 52100

Latent heat of fusion	(KJ/kg)	276
Latent heat of vaporization	(KJ/kg)	6290
Melting point	(K)	1640
Boiling point	(K)	2750
Density	(kg/m ³)	7827

Table A.2 Temperature Dependent Thermal Expansion [171]

Thermal expansion (μK^{-1})	Temperature (K)
11.5	298
12.6	477
13.6	671
14.9	977
15.3	1077

Table A.3 Temperature dependent elastic properties [172]

Young's Modulus (GPa)	Poisson's ratio	Temperature (K)
201.33	0.277	295
178.58	0.269	473
162.72	0.255	673
103.42	0.342	873
86.87	0.396	1073
66.88	0.490	1273

Table A.4 Temperature dependent plastic properties [172]

Yield Stress (MPa)	Plastic strain	Temperature (K)
1600	0	293
1900	0.002	293
2000	0	493
2300	0.025	493
1180	0	693
1220	0.045	693
20	0	5000
23	0.02	5000

Table A.5 ISV Constants for AISI 52100 [173]

Material Constants		
Shear Modulus (G)	(MPa)	78500
a		1.23
Bulk Modulus (K)	(MPa)	152000
b		-1.85E10
Melting Point	(K)	1640
C ₁	(MPa)	1
C ₂	(K)	1
C ₃	(MPa)	1070
C ₄	(K)	58.5
C ₅	(1/s)	1
C ₆	(K)	-12000
C ₇	(1/MPa)	0.04
C ₈	(K)	0
C ₉	(MPa)	5600
C ₁₀	(MPa/K)	9
C ₁₁	(1/MPa)	0.002385
C ₁₂	(K)	400
C ₁₃	(1/MPa)	0.05
C ₁₄	(K)	0
C ₁₅	(MPa)	150
C ₁₆	(MPa/K)	-14
C ₁₇	(MPa/s)	0.0027
C ₁₈	(K)	0
C ₁₉	(1/K)	0.004148
C ₂₀	(K)	665
Initial Temperature	(K)	293
Heat coefficient	m ³ K/J	2.43E-07
Initial damage		0.01
Damage exponent		3

Description of constants in ISV model

- C₁ Constant term in V(T) Arrhenius-type equation which determines the magnitude of rate dependence on yielding
- C₂ Temperature dependent activation term in V(T) Arrhenius-type equation
- C₃ Constant term in Y(T) Arrhenius-type equation which is the rate independent yield stress
- C₄ Temperature dependent activation term in Y(T) Arrhenius-type equation
- C₅ Constant term in f(T) Arrhenius-type equation which determined the transition strain rate from rate independent to dependent yield
- C₆ Temperature dependent activation term in f(T) Arrhenius-type equation
- C₇ Constant term in r_{d1} equation which described kinematic dynamic recovery
- C₈ Temperature dependent activation term in r_{d1} equation
- C₉ Constant term in h_1 equation which describes the kinematic anisotropic hardening modulus
- C₁₀ v term in $h(T)$ equation
- C₁₁ Constant term in $r_s(T)$ equation which describes the kinematic static recovery
- C₁₂ Temperature dependent activation term in $r_s(T)$ equation
- C₁₃ Constant term in $R_d(T)$ equation which describes the isotropic dynamic recovery
- C₁₄ Temperature dependent activation term in $R_d(T)$ equation
- C₁₅ Constant term in $H(T)$ equation which describes the isotropic hardening modulus
- C₁₆ Temperature dependent activation term in $H(T)$ equation
- C₁₇ Constant term in $R_s(T)$ which describes the isotropic static recovery
- C₁₈ Temperature dependent activation term in $R_s(T)$ equation
- C₁₉ Multiplication term in equation $1+\tanh(C_{19}(C_{20}-T))$, which is an adjustment to the yield strength over a large temperature range
- C₂₀ Used in yield strength adjustment equation

Table A.6 Temperature dependent specific heat [171]

Specific heat (J/kg.K)	Temperature (K)
458	300
640	473
745	699
798	810

Table A.7 Temperature dependent conductivity [174]

Conductivity (W/mK)	Temperature (K)
37	273
41	373
40	473
38	573
36	673
34	773
33	823
32	883
30	923
29	973
25	1023
25.5	1173

Material properties of Ti-6Al-4V

Table A.7 Physical and Thermal Properties of Ti64

Density	(kg/m ³)	4428
Latent heat	(J/kg)	365200
Solidus Temp	(°C)	1605
Liquidus Temp	(°C)	1655

Table A.8 Temperature Dependent Thermal Properties of Ti64

Temp. (°C)	Specific Heat (J/kg-K)	Temp. (°C)	Thermal Conductivity (W/m-K)	Temp. (°C)	Thermal Expansion (°C ⁻¹)
20	580	27	7.2	20	1.28×10 ⁻⁵
205	610	100	8.2	538	1.40×10 ⁻⁵
425	670	200	9.4	927	1.62×10 ⁻⁵
650	760	500	13.3		
870	930	876	18.2		
1000	936	1000	19.8		
1200	1016	1500	26.3		
1400	1095	1655	28.3		
1655	1126	2126	37		
		2427	42		

Table A.9 Temperature Dependent Elastic and Plastic Properties of Ti64

Temp. (°C)	<i>Elastic</i>		<i>Plastic</i>	
	Young's Modulus (GPa)	Poisson's Ratio	Yield Strength (MPa)	Plastic Strain
21	110	0.41	910	0.00
			1035	0.023
1655	11	0.45	91	0.00
			103.5	0.023

REFERENCES

- [1] Flynn, J.M., Shokrani, A., Newman, S.T., Dhokia, V., 2016. Hybrid additive and subtractive machine tools – Research and industrial developments, *International Journal of Machine Tools and Manufacture* 101, pp. 79-101.
- [2] Merklein, M., Junker, D., Schaub, A., Neubauer, F., 2016. Hybrid Additive Manufacturing Technologies – An Analysis Regarding Potentials and Applications, *Physics Procedia* 83, pp. 549-559.
- [3] Strong, D., Sirichakwal, I., Manogharan, G.P., Wakefield, T., 2017. Current state and potential of additive – hybrid manufacturing for metal parts, *Rapid Prototyping Journal* 23, pp. 577-588.
- [4] Lorenz, K.A., Jones, J.B., Wimpenny, D.I., Jackson, M.R., 2015. A Review of Hybrid Manufacturing, *Solid Freeform Fabrication Symposium*, Austin, Texas, pp. 96-108.
- [5] Lauwers, B., Klocke, F., Klink, A., Tekkaya, A.E., Neugebauer, R., Mcintosh, D., 2014. Hybrid processes in manufacturing, *CIRP Annals - Manufacturing Technology* 63, pp. 561-583.
- [6] Klocke, F., Roderburg, A., Zeppenfeld, C., 2011. Design methodology for hybrid production processes, *Procedia Engineering* 9, pp. 417-430.
- [7] Nau, B., Roderburg, A., Klocke, F., 2011. Ramp-up of hybrid manufacturing technologies, *CIRP Journal of Manufacturing Science and Technology* 4, pp. 313-316.
- [8] Schuh, G., Kreysa, J., Orilski, S., 2009. Roadmap "Hybride Produktion": Wie 1+1=3-Effekte in der Produktion maximiert werden können, *Zeitschrift für Wirtschaftlichen Fabrikbetrieb* 5, pp. 385-391.
- [9] Chu, W., Kim, C., Lee, H., Choi, J., Park, J., Song, J., Jang, K., Ahn, S., 2014. Hybrid manufacturing in micro/nano scale: A Review, *International Journal of Precision Engineering and Manufacturing-Green Technology* 1, pp. 75-92.
- [10] Kozak, J., Rajurkar, K.P., 2000. Hybrid Machining Process Evaluation and Development, Keynote Paper, *Proced. 2nd International Conference on Machining and Measurements of Sculptured Surfaces*, Kraków, Poland, pp. 501-536.
- [11] Ashby, M.F., 2005. Designing hybrid materials, in *Materials selection in mechanical design* M.F. Ashby, Editor. Butterworth-Heinemann, Amsterdam, pp. 339-377.

- [12] Kickelbick, G., 2006. Introduction to Hybrid Material, in *Hybrid Materials: Synthesis, Characterization, and Applications* G. Kickelbick, Editor. Wiley-VCH Verlag GmbH & Co. KGaA, Weinheim, Germany, pp. 1-48.
- [13] Brehl, D.E., Dow, T.A., 2008. Review of vibration-assisted machining, *Precision Engineering* 32, pp. 153-172.
- [14] Lauwers, B., Bleicher, F., Ten Haaf, P., Vanparys, M., Bernreiter, J., Jacobs, T., Loenders, J., 2010. Investigation of the process-material interaction in ultrasonic assisted grinding of ZrO₂ based ceramic materials, *Proceedings of the 4th CIRP International Conference on High Performance Cutting*, pp. 1-6.
- [15] Schmidt, M., Zaeh, M., Graf, T., Ostendorf, A., Brecher, C., Emonts, M., Rosen, C., Hermani, J., 2011. Lasers in Manufacturing 2011 - Proceedings of the Sixth International WLT Conference on Lasers in Manufacturing Laser-assisted Milling of Advanced Materials, *Physics Procedia* 12, pp. 599-606.
- [16] Brecher, C., Rosen, C., Emonts, M., 2010. Laser-assisted milling of advanced materials, *Physics Procedia - Laser Assisted Net Shape Engineering* 6, *Proceedings of the LANE 2010, Part 2* 5, pp. 259-272.
- [17] Ding, H., Shin, Y.C., 2010. Laser-assisted machining of hardened steel parts with surface integrity analysis, *International Journal of Machine Tools and Manufacture* 50, pp. 106-114.
- [18] Jeon, Y., Lee, C.M., 2012. Current research trend on laser assisted machining, *International Journal of Precision Engineering and Manufacturing* 13, pp. 311-317.
- [19] Sun, S., Brandt, M., Dargusch, M.S., 2010. Thermally enhanced machining of hard-to-machine materials—A review, *International Journal of Machine Tools and Manufacture* 50, pp. 663-680.
- [20] Kumar, M., Melkote, S., Lahoti, G., 2011. Laser-assisted microgrinding of ceramics, *CIRP Annals* 60, pp. 367-370.
- [21] Wang, Z.Y., Rajurkar, K.P., 2000. Cryogenic machining of hard-to-cut materials, *Wear* 239, pp. 168-175.
- [22] Ezugwu, E.O., Bonney, J., 2004. Effect of high-pressure coolant supply when machining nickel-base, Inconel 718, alloy with coated carbide tools, *Journal of Materials Processing Technology* 153-154, pp. 1045-1050.
- [23] Wertheim, R., Rotberg, J., Ber, A., 1992. Influence of High-pressure Flushing through the Rake Face of the Cutting Tool, *CIRP Annals* 41, pp. 101-106.

- [24] López, d.L., Pérez-Bilbatua, J., Sánchez, A.J., Llorente, I.J., Gutiérrez, A., Albóniga, J., 2000. Using High Pressure Coolant in the Drilling and Turning of Low Machinability Alloys, *The International Journal of Advanced Manufacturing Technology* 16, pp. 85-91.
- [25] Shin, Y.C., 2011. Laser Assisted Machining, www.industrial-lasers.com/ articles 26(1).
- [26] Xu, W., Zhang, L., 2015. Ultrasonic vibration-assisted machining: principle, design and application, *Advances in Manufacturing* 3, pp. 173-192.
- [27] Menzies, I., Koshy, P., 2008. Assessment of abrasion-assisted material removal in wire EDM, *CIRP Annals - Manufacturing Technology* 57, pp. 195-198.
- [28] Valiev, R., Zehetbauer, M., Estrin, Y., Höppel, H., Ivanisenko, Y., Hahn, H., Wilde, G., Roven, H., Sauvage, X., Langdon, T., 2007. The Innovation Potential of Bulk Nanostructured Materials, *Advanced Engineering Materials* 9, pp. 527-533.
- [29] Rajurkar, K.P., Zhu, D., McGeough, J.A., Kozak, J., De Silva, A., 1999. New Developments in Electro-Chemical Machining, *CIRP Annals - Manufacturing Technology* 48, pp. 567-579.
- [30] Kunieda, M., Okada, A., Furutani, K., Yamazaki, T., 2016. 18th CIRP Conference on Electro Physical and Chemical Machining (ISEM XVIII) Development of A Hybrid Multi-tasking Machine Tool: Integration of Additive Manufacturing Technology with CNC Machining, *Procedia CIRP* 42, pp. 81-86.
- [31] Zhu, D., Zeng, Y.B., Xu, Z.Y., Zhang, X.Y., 2011. Precision machining of small holes by the hybrid process of electrochemical removal and grinding, *CIRP Annals* 60, pp. 247-250.
- [32] Golabczak, A., Swiecik, R., 2010. Electro-discharge Grinding: Energy Consumption and internal stresses in the surface layer, *Proceedings of the 16th International Symposium on Electromachining*, pp. 517-522.
- [33] Koshy, P., Jain, V.K., Lal, G.K., 1997. Grinding of cemented carbide with electrical spark assistance, *Journal of Materials Processing Technology* 72, pp. 61-68.
- [34] Matsubara, K., Miyahara, Y., Horita, Z., Langdon, T.G., 2003. Developing superplasticity in a magnesium alloy through a combination of extrusion and ECAP, *Acta Materialia* 51, pp. 3073-3084.
- [35] Miyahara, Y., Horita, Z., Langdon, T.G., 2006. Exceptional superplasticity in an AZ61 magnesium alloy processed by extrusion and ECAP, *Materials Science and Engineering: A* 420, pp. 240-244.

- [36] CIRTES Stratoconception, 2017. Stratoconception Process, <http://www.stratoconception.com/procede>.
- [37] Williams, R.E., Melton, V.L., 1998. Abrasive flow finishing of stereolithography prototypes, *Rapid Prototyping Journal* 4, pp. 56-67.
- [38] Williams, R.E., Walczyk, D.F., Dang, H.T., 2007. Using abrasive flow machining to seal and finish conformal channels in laminated tooling, *Rapid Prototyping Journal* 13, pp. 64-75.
- [39] Azushima, A., Kopp, R., Korhonen, A., Yang, D.Y., Micari, F., Lahoti, G.D., Groche, P., Yanagimoto, J., Tsuji, N., Rosochowski, A., Yanagida, A., 2008. Severe plastic deformation (SPD) processes for metals, *CIRP Annals* 57, pp. 716-735.
- [40] Qian, Y., Huang, J., Zhang, H., Wang, G., 2008. Direct rapid high-temperature alloy prototyping by hybrid plasma-laser technology, *Journal of Materials Processing Technology* 208, pp. 99-104.
- [41] Lamikiz, A., Sánchez, J.A., López de Lacalle, L.N., Arana, J.L., 2007. Laser polishing of parts built up by selective laser sintering, *International Journal of Machine Tools and Manufacture* 47, pp. 2040-2050.
- [42] Ramos-Grez, J., Bourell, D.L., 2004. Reducing surface roughness of metallic freeform-fabricated parts using non-tactile finishing methods, *International Journal of Materials and Product Technology* 21, pp. 297-316.
- [43] Yasa, E., Kruth, J., 2011. Application of Laser Re-melting on Selective Laser Melting Parts, *Advances in Production Engineering and Management* 6, pp. 259-270.
- [44] Yasa, E., Deckers, J., Kruth, J.P., 2011. The investigation of the influence of laser re-melting on density, surface quality and microstructure of selective laser melting parts, *Rapid Prototyping Journal* 17, pp. 312-327.
- [45] Yasa, E., Kruth, J., Deckers, J., 2011. Manufacturing by combining Selective Laser Melting and Selective Laser Erosion/laser re-melting, *CIRP Annals - Manufacturing Technology* 60, pp. 263-266.
- [46] Campanelli, S.L., Casalino, G., Contuzzi, N., Ludovico, A.D., 2013. Taguchi Optimization of the Surface Finish Obtained by Laser Ablation on Selective Laser Molten Steel Parts, *Procedia CIRP* 12, pp. 462-467.
- [47] Sealy, M.P., Madireddy, G., Li, C., Guo, Y.B., 2016. Finite element modeling of hybrid additive manufacturing by laser shock peening, *Solid Freeform Fabrication symposium*, Austin, Texas, pp. 306-316.

- [48] Prinz, F.B., Weiss, L.E., 1993. Method and apparatus for fabrication of three-dimensional metal articles by weld deposition, US Patent 5207371 A.
- [49] Hartmann, K., Krishnan, R., Merz, R., Neplotnik, G., Prinz, F., Schultz, L., 1994. Robot-Assisted Shape Deposition Manufacturing, Proceedings of the 1994 IEEE International Conference on Robotics and Automation, San Diego, CA, p. 1-9.
- [50] Merz,R., Prinz,F.B., Ramaswami, K., Terk, M., Weiss, L.E., 1994. Shape deposition manufacturing, Solid Freeform Fabrication Symposium, Austin, Texas, pp. 1-8.
- [51] Prinz, F.B., Weiss, L., Amon, C., Beuth, J., 1995. Processing, Thermal and Mechanical Issues in Shape Deposition Manufacturing, Carnegie Mellon University Engineering Design Research Center, pp. 1-18.
- [52] Gale, J., Achuthan, A., Don, A.U., 2016. Material Property Enhancement in Additive Manufactured Materials Using an Ultrasonic Peening Technique, Solid Freeform Fabrication Symposium, Austin, Texas.
- [53] Bamberg, J., Hess, T., Hessert, R., Satzger, W., 2012. Verfahren zum herstellen, reparieren oder austauschen eines bauteils mit verfestigen mittels druckbeaufschlagung, Patent Application: WO 2012152259 A1.
- [54] El-Wardany, T.I., Lynch, M.E., Viens, D.V., Grelotti, R.A., 2014. Turbine disk fabrication with in situ material property variation, U.S. Patent Application No. 14/202,195.
- [55] Kramer, K.J., Bayramian, A., El-dasher, B.S., Farmer, J.C., 2014. System And Method For Enhanced Additive Manufacturing, U.S. Patent Application No. 14/303,642.
- [56] Sidhu, J., Wescott, A.D., 2016. Additive manufacturing and integrated impact post-treatment, Patent Application No: WO2016092253 A1.
- [57] Wu, Z., Li, Y., Abbott, D.H., Chen, X., Broderick, T.F., Marte, J.S., Woodfield, A.P.I., Ott, E.A., 2015. Method for Manufacturing Objects using Powder Products, U.S. Patent Application 20150283614 A1.
- [58] Kalentics, N., Logé, R., Boillat, E., 2017. Method and Device for Implementing Laser Shock Peening or Warm Laser Shock Peening During Selective Laser Melting, US Patent Application US2017/0087670 A1, pp. 1-12.
- [59] Kalentics, N., Boillat, E., Peyre, P., Gorny, C., Kenel, C., Leinenbach, C., Jhabvala, J., Logé, R., 2017. 3D Laser Shock Peening – A new method for the 3D control of residual stresses in selective laser melting, Materials & Design 130, pp. 350-356.

- [60] Colegrove, P.A., Donoghue, J., Martina, F., Gu, J., Prangnell, P., Hönnige, J., 2017. Application of bulk deformation methods for microstructural and material property improvement and residual stress and distortion control in additively manufactured components, *Scripta Materialia* 135, pp. 111-118.
- [61] Martina, F., Roy, M.J., Szost, B.A., Terzi, S., Colegrove, P.A., Williams, S.W., Withers, P.J., Meyer, J., Hofmann, M., 2016. Residual stress of as-deposited and rolled wire+arc additive manufacturing Ti-6Al-4V components, *Materials Science and Technology* 32, pp. 1439-1448.
- [62] Donoghue, J., Antonysamy, A.A., Martina, F., Colegrove, P.A., Williams, S.W., Prangnell, P.B., 2016. The effectiveness of combining rolling deformation with Wire-Arc Additive Manufacture on β -grain refinement and texture modification in Ti-6Al-4V, *Materials Characterization* 114, pp. 103-114.
- [63] Colegrove, P.A., Martina, F., Roy, M.J., Szost, B.A., Terzi, S., Williams, S.W., Withers, P.J., Jarvis, D., 2014. High Pressure Interpass Rolling of Wire + Arc Additively Manufactured Titanium Components, *Advanced Materials Research* 996, pp. 694-700.
- [64] Colegrove, P.A., Coules, H.E., Fairman, J., Martina, F., Kashoob, T., Mamash, H., Cozzolino, L.D., 2013. Microstructure and residual stress improvement in wire and arc additively manufactured parts through high-pressure rolling, *Journal of Materials Processing Technology* 213, pp. 1782-1791.
- [65] Martina, F., Williams, S.W., Colegrove, P., 2013. Improved microstructure and increased mechanical properties of additive manufacture produced Ti-6Al-4V by interpass cold rolling. *Solid Freeform Fabrication Symposium*, Austin, Texas, pp. 490-496.
- [66] Martina, F., Colegrove, P.A., Williams, S.W., Meyer, J., 2015. Microstructure of Interpass Rolled Wire + Arc Additive Manufacturing Ti-6Al-4V Components, *Metallurgical and Materials Transactions A* 46, pp. 6103-6118.
- [67] Zhang, H., Rui, D., Xie, Y., Wang, G., 2013. Study on Metamorphic Rolling Mechanism for Metal Hybrid Additive Manufacturing, *Solid Freeform Fabrication Symposium*, Austin, Texas, pp. 188-199.
- [68] Zhang, H., Xie, Y., Rui, D., Wang, G., 2013. Hybrid deposition and micro rolling manufacturing method of metallic parts, *Solid Freeform Fabrication Symposium*, Austin, Texas, pp. 267-281.
- [69] Xie, Y., Zhang, H., Wang, G., Zhou, F., 2014. A novel metamorphic mechanism for efficient additive manufacturing of components with variable wall thickness, *Solid Freeform Fabrication Symposium*, Austin, Texas, pp. 210-223.

- [70] Xie, Y., Zhang, H., Zhou, F., 2016. Improvement in Geometrical Accuracy and Mechanical Property for Arc-Based Additive Manufacturing Using Metamorphic Rolling Mechanism, *Journal of Manufacturing Science and Engineering* 138, pp. 111002-111002.
- [71] Zhou, X., Zhang, H., Wang, G., Bai, X., Fu, Y., Zhao, J., 2016. Simulation of microstructure evolution during hybrid deposition and micro-rolling process, *Journal of Materials Science* 51, pp. 6735-6749.
- [72] Song, Y., Park, S., Jee, H., Choi, D., Shin, B., 1999. 3D Welding and Milling - A direct Approach for Fabrication of Injection Molds, *Solid Freeform Fabrication Symposium*, Austin, Texas, pp. 793-800.
- [73] Pridham, M.S., Thomson, G., 1993. Part fabrication using Laser Machining and Welding, *Solid Freeform Fabrication Symposium*, Austin, Texas, pp. 74-80.
- [74] ISO/ASTM International, 2016. ISO/ASTM 52900:2015 (E) Standard Terminology for Additive Manufacturing - General Principles - Terminology, Committee F42 on Additive Manufacturing Technologies, pp. 1-9.
- [75] Choi, D., Lee, S.H., Shin, B.S., Whang, K.H., Song, Y.A., Park, S.H., Jee, H.S., 2001. Development of a direct metal freeform fabrication technique using CO2 laser welding and milling technology, *Journal of Materials Processing Technology* 113, pp. 273-279.
- [76] Klocke, F., Wirtz, D.-., 1996. Direct Manufacturing of Metal Prototypes and Prototype Tools, *Solid Freeform Fabrication Symposium*, Austin, Texas, pp. 141-148.
- [77] Yamazaki, T., 2016. Development of A Hybrid Multi-tasking Machine Tool: Integration of Additive Manufacturing Technology with CNC Machining, *Procedia CIRP* 42, pp. 81-86.
- [78] Song, Y., Park, S., Choi, D., Jee, H., 2005. 3D welding and milling: Part I—a direct approach for freeform fabrication of metallic prototypes, *International Journal of Machine Tools and Manufacture* 45, pp. 1057-1062.
- [79] Jeng, J., Lin, M., 2001. Mold fabrication and modification using hybrid processes of selective laser cladding and milling, *Journal of Materials Processing Technology* 110, pp. 98-103.
- [80] Kerschbaumer, M., Ernst, G., 2004. Hybrid manufacturing process for rapid high performance tooling combining high speed milling and laser cladding, *Proceedings of 23rd International Congress on Applications of Lasers & Electro-Optics*.

- [81] Fessler, J.R., Merz, R., Nickel, A.H., Prinz, F.B., Weiss, L.E., 1996. Laser deposition of metals for shape deposition manufacturing, Solid Freeform Fabrication Symposium, Austin, Texas, pp. 117-124.
- [82] Ichimura, M., Urushisaki, Y., Amaya, K., Chappell, S., Honnami, M., Mochizuki, M., Chung, U., 2014. Medical Implant Manufacture using the Hybrid Metal Laser Sintering with Machining Process, 15th International Conference on Precision Engineering (ICPE), Kanazawa, Japan, pp. 1-2.
- [83] Akula, S., Karunakaran, K.P., 2006. Hybrid adaptive layer manufacturing: An Intelligent art of direct metal rapid tooling process, Robotics and Computer-Integrated Manufacturing 22, pp. 113-123.
- [84] Karunakaran, K.P., Shanmuganathan, P.V., Jadhav, S.J., Bhadauria, P., Pandey, A., 2000. Rapid prototyping of metallic parts and moulds, Journal of Materials Processing Technology 105, pp. 371-381.
- [85] Karunakaran, K.P., Suryakumar, S., Pushpa, V., Akula, S., 2010. Low cost integration of additive and subtractive processes for hybrid layered manufacturing, Robotics and Computer-Integrated Manufacturing 26, pp. 490-499.
- [86] Karunakaran, K.P., Sreenathbabu, A., Pushpa, V., 2004. Hybrid layered manufacturing: Direct rapid metal tool-making process, Proceedings of the Institution of Mechanical Engineers, Part B: Journal of Engineering Manufacture 218, pp. 1657-1665.
- [87] Xinhong, X., Haiou, Z., Guilan, W., Guoxian, W., 2010. Hybrid plasma deposition and milling for an aeroengine double helix integral impeller made of superalloy, Robotics and Computer-Integrated Manufacturing 26, pp. 291-295.
- [88] Xiong, X., Zhang, H., Wang, G., 2009. Metal direct prototyping by using hybrid plasma deposition and milling, Journal of Materials Processing Technology 209, pp. 124-130.
- [89] Amon, C.H., Beuth, J.L., Weiss, L.E., Merz, R., Prinz, F.B., 1998. Shape Deposition Manufacturing With Microcasting: Processing, Thermal and Mechanical Issues 120, pp. 653-665.
- [90] Friel, R.J., Harris, R.A., 2013. Ultrasonic Additive Manufacturing – A Hybrid Production Process for Novel Functional Products, Procedia CIRP 6, pp. 35-40.
- [91] Schwope, L., Friel, R.J., Johnson, K.E., Harris, R.A., 2009. Field repair and replacement part fabrication of military components using ultrasonic consolidation cold metal deposition, NATO Science and Technology Organization NATO;RTO-MP-AVT-163.

- [92] Mizukami, Y., Osakada, K., 2002. Three-Dimensional Fabrication of Metallic Parts and Molds Using Hybrid Process of Powder Layer Compaction and Milling, Solid Freeform Fabrication Symposium, Austin, Texas, pp. 474-481.
- [93] Sreenathbabu, A., K.P. Karunakaran, Amarnath, C., 2005. Statistical process design for hybrid adaptive layer manufacturing, Rapid Prototyping Journal 11, pp. 235-248.
- [94] Yasa, E., Kruth, J.P., 2010. Investigation of laser and process parameters for Selective Laser Erosion, Precision Engineering 34, pp. 101-112.
- [95] Shiomi, M., Osakada, K., Nakamura, K., Yamashita, T., Abe, F., 2004. Residual Stress within Metallic Model Made by Selective Laser Melting Process, CIRP Annals - Manufacturing Technology 53, pp. 195-198.
- [96] Achutan, A., Gale, J., 2017. Application of ultrasonic peening during DMLS production of 316L stainless steel and its effect on material behavior, Rapid Prototyping Journal 23, pp. 1185-1194.
- [97] AlMangour, B., Yang, J., 2016. Improving the surface quality and mechanical properties by shot-peening of 17-4 stainless steel fabricated by additive manufacturing, Materials & Design 110, pp. 914-924.
- [98] Salvati, E., Lunt, A.J.G., Ying, S., Sui, T., Zhang, H.J., Heason, C., Baxter, G., Korsunsky, A.M., 2017. Eigenstrain reconstruction of residual strains in an additively manufactured and shot peened nickel superalloy compressor blade, Computer Methods in Applied Mechanics and Engineering 320, pp. 335-351.
- [99] Kanger, C., Hadidi, H., Akula, S., Sandman, S., Quint, J., Alsunni, M., Underwood, R.P., Slafter, C., Sonderup, J., Spilinek, M., Casias, J., Rao, P., Sealy, M.P., 2017. Effect of Process Parameters and Shot Peening on Mechanical Behaviour of ABS Parts Manufactured by Fused Filament Fabrication (FFF), Solid Freeform Fabrication Symposium, Austin, Texas, pp. 444-458.
- [100] Madireddy, G., Montazeri, M., Curtis, E., Underwood, N., Berger, J., Al Khayari, Y., Marth, B., Smith, B., Christy, S., Krueger, K., Sealy, M.P., Rao, P., 2017. Effect of Process Parameters and Shot Peening on the Tensile Strength and Deflection of Polymer Parts Made using Mask Image Projection Stereolithography (MIP-SLA), Solid Freeform Fabrication Symposium, Austin, Texas, pp. 1761-1770.
- [101] Book, T.A., Sangid, M.D., 2016. Evaluation of Select Surface Processing Techniques for In Situ Application During the Additive Manufacturing Build Process, JOM 68, pp. 1780-1792.
- [102] Gibson, I., Rosen, D.W., Stucker, B., 2015. Additive Manufacturing Technologies: 3D Printing, Rapid Prototyping, and Direct Digital Manufacturing, 2nd ed., Springer, pp. 1-498.

- [103] Lunney, J.G., 1995. Pulsed laser deposition of metal and metal multilayer films, *Applied Surface Science* 86, pp. 79-85.
- [104] Boyd, I.W., 1996. Thin film growth by pulsed laser deposition. *Ceramics International* 22, pp. 429-434.
- [105] Morgan, R., Sutcliffe, C., O'Neill, W., 2001. Experimental investigation of nanosecond pulsed Nd:YAG laser re-melted pre-placed powder beds, *Rapid Prototyping Journal* 7, pp. 159-172.
- [106] Zhou, Y.C., Yang, Z.Y., Zheng, X.J., 2003. Residual stress in PZT thin films prepared by pulsed laser deposition, *Surface and Coatings Technology* 162, pp. 202-211.
- [107] Palanivel, S., Nelaturu, P., Glass, B., Mishra, R.S., 2015. Friction stir additive manufacturing for high structural performance through microstructural control in an Mg based WE43 alloy, *Materials & Design* 65, pp. 934-952.
- [108] Francis, R., Newkirk, J.W., Liou, F., 2014. Investigation of Forged-Like Microstructure Produced by a Hybrid Manufacturing Process, *Solid Freeform Fabrication Symposium*, Austin, Texas, pp. 484-499.
- [109] Ding, K., Ye, L., 2006. *Laser Shock Peening: Performance and process simulation*, Woodhead publishing Limited, Cambridge, England.
- [110] Sealy, M.P., Guo, Y.B., 2010. Surface integrity and process mechanics of laser shock peening of novel biodegradable magnesium–calcium (Mg–Ca) alloy, *Journal of the Mechanical Behavior of Biomedical Materials* 3, pp. 488-496.
- [111] Guo, Y., Sealy, M.P., Guo, C., 2012. Significant improvement of corrosion resistance of biodegradable metallic implants processed by laser shock peening, *CIRP Annals* 61, pp. 583-586.
- [112] Sano, Y., Mukai, N., Okazaki, K., Obata, M., 1997. Residual stress improvement in metal surface by underwater laser irradiation, *Nuclear Instruments and Methods in Physics Research Section B: Beam Interactions with Materials and Atoms* 121, pp. 432-436.
- [113] Groover, M.P., 1996. *Fundamentals of Modern Manufacturing: Materials, Processes, and Systems*, Printice-Hall, New Jersey.
- [114] Peyre, P., Fabbro, R., Merrien, P., Lieurade, H.P., 1996. Laser shock processing of aluminium alloys. Application to high cycle fatigue behaviour, *Materials Science and Engineering: A* 210, pp. 102-113.

- [115] Salimianrizi, A., Foroozmehr, E., Badrossamay, M., Farrokhpour, H., 2016. Effect of Laser Shock Peening on surface properties and residual stress of Al6061-T6, *Optics and Lasers in Engineering* 77, pp. 112-117.
- [116] Nalla, R.K., Altenberger, I., Noster, U., Liu, G.Y., Scholtes, B., Ritchie, R.O., 2003. On the influence of mechanical surface treatments—deep rolling and laser shock peening—on the fatigue behavior of Ti–6Al–4V at ambient and elevated temperatures, *Materials Science and Engineering: A* 355, pp. 216-230.
- [117] Maawad, E., Sano, Y., Wagner, L., Brokmeier, H.-., Genzel, C., 2012. Investigation of laser shock peening effects on residual stress state and fatigue performance of titanium alloys, *Materials Science and Engineering: A* 536, pp. 82-91.
- [118] Zhang, X.C., Zhang, Y.K., Lu, J.Z., Xuan, F.Z., Wang, Z.D., Tu, S.T., 2010. Improvement of fatigue life of Ti–6Al–4V alloy by laser shock peening, *Materials Science and Engineering: A* 527, pp. 3411-3415.
- [119] Hu, Y., Yao, Z., 2008. Overlapping rate effect on laser shock processing of 1045 steel by small spots with Nd:YAG pulsed laser, *Surface and Coatings Technology* 202, pp. 1517-1525.
- [120] Caralapatti, V.K., Narayanswamy, S., 2017. Effect of high repetition laser shock peening on biocompatibility and corrosion resistance of magnesium, *Optics & Laser Technology* 88, pp. 75-84.
- [121] Lu, J.Z., Qi, H., Luo, K.Y., Luo, M., Cheng, X.N., 2014. Corrosion behaviour of AISI 304 stainless steel subjected to massive laser shock peening impacts with different pulse energies, *Corrosion Science* 80, pp. 53-59.
- [122] Braisted, W., Brockman, R., 1999. Finite element simulation of laser shock peening, *International Journal of Fatigue* 21, pp. 719-724.
- [123] Hu, Y., Yao, Z., Hu, J., 2006. 3-D FEM simulation of laser shock processing, *Surface and Coatings Technology* 201, pp. 1426-1435.
- [124] Bammann, D.J., Chiesa, M.L., Horstemeyer, M.F., Weingarten, L.I., 1993. Failure in Ductile Materials Using Finite Element Methods, *Structural Crashworthiness and Failure*, pp. 1-54.
- [125] Bammann, D.J., Chiesa, M.L., Johnson, G.C., 1996. Modeling Large Deformation and Failure in Manufacturing Process, *Theoretical Applied Mechanics*, pp. 359-376.
- [126] Horstemeyer, M.F., Lathrop, J., Gokhale, A.M., Dighe, M., 2000. Modeling stress state dependent damage evolution in a cast Al–Si–Mg aluminum alloy, *Theoretical and Applied Fracture Mechanics* 33, pp. 31-47.

- [127] Zhang, W., Yao, Y.L., 2002. Micro Scale Shock Processing of Metallic Components, *Journal of Manufacturing Science and Engineering* 124, pp. 369-378.
- [128] Sealy, M.P., Guo, Y.B., 2009. Fabrication and Finite Element Simulation of Micro-Laser Shock Peening for Micro Dents, *International Journal for Computational Methods in Engineering Science and Mechanics* 10, pp. 134-142.
- [129] Peyre, P., Berthe, L., Scherpereel, X., Fabbro, R., Bartnicki, E., 1998. Experimental Study of Laser-driven shock waves in stainless steel, *Journal of Applied Physics*, pp. 5985-5992.
- [130] Devaux, D., Fabbro, R., Tollier, L., Bartnicki, E., 1993. Generation of shock waves by laser-induced plasma in confined geometry, *Journal of Applied Physics* 74, pp. 2268-2273.
- [131] Berthe, L., Fabbro, R., Peyre, P., Tollier, L., Bartnicki, E., 1997. Shock waves from a water-confined laser-generated plasma, *Journal of Applied Physics* 82, pp. 2826-2832.
- [132] Fabbro, R., Fournier, J., Ballard, P., Devaux, D., Virmont, J., 1990. Physical study of laser-produced plasma in confined geometry, *Journal of Applied Physics* 68, pp. 775-784.
- [133] Wu, B., Shin, Y.C., 2005. A self-closed thermal model for laser shock peening under the water confinement regime configuration and comparisons to experiments, *Journal of Applied Physics* 97, pp. 113517:1-11.
- [134] Voothaluru, R., Richard Liu, C., Cheng, G.J., 2012. Finite Element Analysis of the Variation in Residual Stress Distribution in Laser Shock Peening of Steels, *Journal of Manufacturing Science and Engineering* 134, pp. 061010-061010.
- [135] Sealy, M.P., Madireddy, G., Williams, R.E., Rao, P., Toursangsaraki, M., 2018. Hybrid Processes in Additive Manufacturing, *Journal of Manufacturing Science and Engineering* 140, pp. 060801-13.
- [136] Keicher, D.M., Romero, J.A., Atwood, C.L., Smugeresky, J.E., Griffith, M.L., Jeantette, F.P., Harwell, L., Greene, D., 1996. Laser engineered net shaping (LENSTM) for additive component processing, *Proceedings of Rapid Prototyping and Manufacturing*. United States.
- [137] Manvatkar, V.D., Gokhale, A.A., Jagan Reddy, G., Venkataramana, A., De, A., 2011. Estimation of Melt Pool Dimensions, Thermal Cycle, and Hardness Distribution in the Laser-Engineered Net Shaping Process of Austenitic Stainless Steel, *Metallurgical and Materials Transactions A* 42, pp. 4080-4087.

- [138] Wang, L., Felicelli, S., 2006. Analysis of thermal phenomena in LENS™ deposition, *Materials Science and Engineering: A* 435–436, pp. 625-631.
- [139] Heigel, J.C., Michaleris, P., Reutzel, E.W., 2015. Thermo-mechanical model development and validation of directed energy deposition additive manufacturing of Ti–6Al–4V, *Additive Manufacturing* 5, pp. 9-19.
- [140] Wang, L., Felicelli, S.D., Pratt, P., 2008. Residual stresses in LENS-deposited AISI 410 stainless steel plates, *Materials Science and Engineering: A* 496, pp. 234-241.
- [141] Wang, Q., Li, J., Gouge, M., Nassar, A.R., (Pan) Michaleris, P., Reutzel, E.W., 2016. Physics-Based Multivariable Modeling and Feedback Linearization Control of Melt-Pool Geometry and Temperature in Directed Energy Deposition, *Journal of Manufacturing Science and Engineering* 139, pp. 021013-021013-12.
- [142] Ye, R., Smugeresky, J.E., Zheng, B., Zhou, Y., Lavernia, E.J., 2006. Numerical modeling of the thermal behavior during the LENS® process, *Materials Science and Engineering: A* 428, pp. 47-53.
- [143] Chiumenti, M., Lin, X., Cervera, M., Lei, W., Zheng, Y., Huang, W., 2017. Numerical simulation and experimental calibration of additive manufacturing by blown powder technology. Part I: thermal analysis, *Rapid Prototyping Journal* 23, pp. 448-463.
- [144] Vasinonta, A., Beuth, J.L., Griffith, M., 2006. Process Maps for Predicting Residual Stress and Melt Pool Size in the Laser-Based Fabrication of Thin-Walled Structures, *Journal of Manufacturing Science and Engineering* 129, pp. 101-109.
- [145] Neela, V., De, A., 2009. Three-dimensional heat transfer analysis of LENS™ process using finite element method, *The International Journal of Advanced Manufacturing Technology* 45, pp. 935.
- [146] Peyre, P., Aubry, P., Fabbro, R., Neveu, R., Longuet, A., 2008. Analytical and numerical modeling of direct metal deposition laser process, *Journal of Physics D: Applied Physics* 41, pp. 1-10.
- [147] Zecovic, S., Dwivedi, R., Kovacevic, R., 2005. Thermo-Mechanical Finite Element Analysis of Direct Laser Metal Deposited Thin-Walled Structures, *Solid Freeform Fabrication Symposium, Austin, Texas*, pp. 338-355.
- [148] Anca, A., Fachinotti, V.D., Escobar-Palafox, G., Cardona, A., 2011. Computational modelling of shaped metal deposition, *International Journal for Numerical Methods in Engineering* 85, pp. 84-106.
- [149] Chiumenti, M., Cervera, M., Salmi, A., Agelet de Saracibar, C., Dialami, N., Matsui, K., 2010. Finite element modeling of multi-pass welding and shaped metal

- deposition processes, *Computer Methods in Applied Mechanics and Engineering* 199, pp. 2343-2359.
- [150] Jendrzewski, R., Śliwiński, G., Krawczuk, M., Ostachowicz, W., 2004. Temperature and stress fields induced during laser cladding, *Computers & Structures* 82, pp. 653-658.
- [151] Plati, A., Tan, J., Golosnoy, I., Persoons, R., van Acker, K., Clyne, T., 2006. Residual Stress Generation during Laser Cladding of Steel with a Particulate Metal Matrix Composite, *Advanced Engineering Materials* 8, pp. 619-624.
- [152] Qi, H., Mazumder, J., Ki, H., 2006. Numerical simulation of heat transfer and fluid flow in coaxial laser cladding process for direct metal deposition, *Journal of Applied Physics* 100, pp. 024903.
- [153] Goldak, J., Chakravarti, A., Bibby, M., June 1984. A new finite element model for welding heat sources, *Metallurgical Transactions B* 15, pp. 299-305.
- [154] Costa, L., Vilar, R., Reti, T., Deus, A.M., 2005. Rapid tooling by laser powder deposition: Process simulation using finite element analysis, *Acta Materialia* 53, pp. 3987-3999.
- [155] Labudovic, M., Hu, D., Kovacevic, R., 2003. A three dimensional model for direct laser metal powder deposition and rapid prototyping, *Journal of Materials Science* 38, pp. 35-49.
- [156] Denlinger, E.R., Heigel, J.C., Michaleris, P., 2015. Residual stress and distortion modeling of electron beam direct manufacturing Ti-6Al-4V, *Proceedings of the IMechE* 229, pp. 1803-1813.
- [157] Yang, Y., Babu, S.S., 2010. An Integrated Model to Simulate Laser Cladding Manufacturing Process for Engine Repair Applications, *Welding in the World* 54, pp. R298-R307.
- [158] Marimuthu, S., Clark, D., Allen, J., Kamara, A.M., Mativenga, P., Li, L., Scudamore, R., 2013. Finite element modelling of substrate thermal distortion in direct laser additive manufacture of an aero-engine component, *Proceedings of the IMechE* 227, pp. 1987-1999.
- [159] Ghosh, S., Choi, J., 2005. Three-dimensional transient finite element analysis for residual stresses in the laser aided direct metal/material deposition process, *Journal of laser applications* 17, pp. 144-158.
- [160] Aggarangsi, P., Beuth, J.L., Griffith, M., 2003. Melt pool size and stress control for laser-based deposition near a free edge, *Solid Freeform Fabrication Symposium*, Austin, Texas, pp. 196-207.

- [161] Yongkang, Z., Shuyi, Z., Xiaorong, Z., Lan, C., Jichang, Y., Naifei, R., 1997. Investigation of the surface qualities of laser shock-processed zones and the effect on fatigue life of aluminum alloy, *Surface and Coatings Technology* 92, pp. 104-109.
- [162] Mercelis, P., Jean-Pierre Kruth, 2006. Residual stresses in selective laser sintering and selective laser melting, *Rapid Prototyping Journal* 12, pp. 254-265.
- [163] Fu, C.H., Guo, Y.B., 2014. 3-Dimensional Finite Element Modeling of Selective Laser Melting Ti-6Al-4V Alloy, 2014 Annual International Solid Freeform Fabrication Symposium, pp. 1129-1144.
- [164] Boivineau, M., Cagran, C., Doytier, D., Eyraud, V., Nadal, M.-., Wilthan, B., Pottlacher, G., 2006. Thermophysical Properties of Solid and Liquid Ti-6Al-4V (TA6V) Alloy, *International Journal of Thermophysics* 27, pp. 507-529.
- [165] Verhaeghe, F., Craeghs, T., Heulens, J., Pandelaers, L., 2009. A pragmatic model for selective laser melting with evaporation, *Acta Materialia* 57, pp. 6006-6012.
- [166] Boyer, R., Welsch, G., Collings, E.W., 1993. *Materials Properties Handbook: Titanium Alloys*, ASM International.
- [167] Edwards, P., Ramulu, M., 2014. Fatigue performance evaluation of selective laser melted Ti-6Al-4V, *Materials Science and Engineering: A* 598, pp. 327-337.
- [168] Roberts, I.A., Wang, C.J., Esterlein, R., Stanford, M., Mynors, D.J., 2009. A three-dimensional finite element analysis of the temperature field during laser melting of metal powders in additive layer manufacturing, *International Journal of Machine Tools and Manufacture* 49, pp. 916-923.
- [169] Berthe, L., Fabbro, R., Peyre, P., Bartnicki, E., 1999. Wavelength dependent of laser shock-wave generation in the water-confinement regime, *Journal of Applied Physics* 85, pp. 7552-7555.
- [170] Clauer, A.H., 1996. Laser Shock Peening for fatigue resistance Surface Performance of Titanium, pp. 217-230.
- [171] Ramesh, A., Melkote, S.N., 2008. Modeling of white layer formation under thermally dominant conditions in orthogonal machining of hardened AISI 52100 steel, *International Journal of Machine Tools and Manufacture* 48, pp. 402-414.
- [172] Guo, Y.B., Liu, C.R., 2001. Mechanical Properties of Hardened AISI 52100 Steel in Hard Machining Processes, *Journal of Manufacturing Science and Engineering* 124, pp. 1-9.

- [173] Anurag, S., Guo, Y.B., Horstemeyer, M.F., 2009. The effect of materials testing modes on finite element simulation of hard machining via the use of internal state variable plasticity model coupled with experimental study, *Computers & Structures* 87, pp. 303-317.
- [174] Shah, S.M., Nélias, D., Zain-ul-abdein, M., Coret, M., 2012. Numerical simulation of grinding induced phase transformation and residual stresses in AISI-52100 steel, *Finite Elements in Analysis and Design* 61, pp. 1-11.